EUROPEAN COMMISSION
Community Research

RAPHAEL

Contract Number: 516508 (FI6O)

DELIVERABLE (D-ML1.2)

Specification of Test Programmes for Vessel Material Features Tests

Author(s): **Y. LEJEAIL, E. PLUYETTE**
M. BRUMOVSKÝ

Reporting period: 15/04/2005 – 14/04/2006

Date of issue of this report : 14/04/2006

Start date of project : **15/04/2005** Duration : **48 Months**

Project co-funded by the European Commission under the Euratom Research and Training Programme on Nuclear Energy within the Sixth Framework Programme (2002-2006)		
Dissemination Level (place an X in the appropriate cell)		
PU	Public	
RE	Restricted to the partners of the RAPHAEL project	
CO	Confidential, only for specific distribution list defined on this document	X

RAPHAEL ***(ReActor for Process heat, Hydrogen And ELectricity generation)***

Distribution list

Person and organisation name and/or group	Comments
RAPHAEL SP ML Work Package 1 participants	
Panagiotis Manolatos (EC DG RTD)	
Sylvie Casalta (EC DG RTD)	
Edgar Bogusch (AREVA NP)	
Vincent Chauvet (STEP)	

ReActor for Process heat, Hydrogen And ELectricity generation (RAPHAEL)		
Sub-project: SP-ML **Work package:** 1	**RAPHAEL document no:** RAPHAEL-0604-D-ML1-2	**Document type:** D=Deliverable / M=Minute / P=Progress report / S=Support
Issued by: CEA (FR) & NRI-Rez (CZ) **Internal no.: CEA/DEN/CAD/DER/SESI/LCSI/NT DO 13** 16/03/06 **NRI-Rez**		**Document status:** Final

Document title

Specification of Test Programmes

Abstract

This document summarizes the work performed both in CEA and NRI-Rez to propose an experimental programme for the study of creep on specimens representative of HTR's and VHTR's large structures. The different materials and loading conditions of these reactors have been reviewed, pointing out that the steel parts will sustain very high temperatures, in normal or transient conditions. There are already laboratory experiments to understand the creep behaviour of base metal and welds inside the Raphael project. But as explained in the present work, it is necessary to study the creep phenomenon on so-called large specimens (and to define the meaning of large). CEA intends to perform creep tests on 9Cr1Mo mod tubes, and NRI-Rez propose to realize tests on plate geometries. In any case the welds will be done by FRAMATOME-ANP. Experiments on large specimens are not common, so that they are interesting to carryout. In addition, with the Large Scale Tests, it is expected a global validation of the Finite Element creep models identified on laboratory creep tests, which models could be used in the future to define accurate Weld Creep Factor within design codes.

Revisions

Rev.	Date	Short description	Author	WP Leader	SP Leader	Coordinator
00	15/04/2006	First issue	Y. LEJEAIL CEA M. BRUMOVSKÝ NRI-Rez	H. HEGEMANN NRG *Signature*	Derek Buckthorpe NNC	Edgar Bogusch, Areva NP
01						

The Very High Temperature Reactors (VHTR) of the Generation IV international project are characterized by some common features:

- graphite fuel assemblies or pebbles;
- helium coolant with high inlet and outlet temperatures;
- fuel with low power density;
- metallic pressure vessel.

Therefore, they are considered as inherently safe, even in the case of a depressurization transient, since the reactor residual power should be removed by conduction through the vessel and transferred by radiation. The NRI-Rez document "Materials Under Enhanced Operational Parameters of Advanced Nuclear Power Plants" from Milan Brumovský, is given in Appendix 1, and describes the loading parameters and the different possible materials that could be used inside a VHTR.

As the gas coolant is at high temperature, the vessel itself could be at a mean temperature up to 420°C during nominal conditions. That is the reason why advanced martensitic steel could be chosen for the vessel (P91 or T91, i.e. 9Cr1Mo mod). This steel has high mechanical design stress (S_m), and can be welded even in high thickness. But the creep strength, aging and irradiation resistance of this metal must be investigated, especially by experimental tests.

In the framework of RAPHAEL-IP project, which is part of the 6^{th} FWP, the materials are studied in the SP-ML material Sub Project. It is planned to focus on irradiation, creep and creep/fatigue damages, inside the WP1 Work Package. Finally, the task 2 deals with creep damages and is the subject of this document (Deliverable ML1.2 of [1]).

First the problem of Weld Joint Factor for Design Codes is discussed in the CEA document "Large scale tests on 9Cr1Mo mod tubes with circumferential welds in creep regime. Specification of the experimental programme and parametric finite element calculations. Deliverable ML1.2 of Raphael-IP SP4/WP1/TASK 2", included in Appendix 2, pointing out the interest to use numerical methods in order to understand the behaviour of these complex assemblies.

Then, some practical aspects of the validation tests are given, concerning the experimental rig, the material procurement, the instrumentation of the specimens, and the planning of the programme.

Finally, a unified model for creep flow and damage representation is also described. It was first applied by V. Gaffard [2] on 9Cr1Mo mod steel at 625°C. Some parametric calculations have been performed with this model to investigate the effect of vessel and weld dimensions, and the results are shown in this report. The equivalent stress that must be used for creep design has been also studied. The numerical results allow us to propose an experimental creep test for the validation of the approach.

[1] 6th Framework Programme, RAPHAEL-IP, Annex 1 – « Description of Work », Euratom call Nuchtech-2004.3.4.1.1-1

[2] V. Gaffard, « Experimental Study and Modelling of High Temperature Creep Flow and Damage Behaviour of 9Cr1Mo-NbV Steel Weldments », Ph.D Thesis of the Ecole des Mines de Paris, December 13th, 2004

Appendix 1

Ústav jaderného výzkumu Řež a.s.

Materials Under Enhanced Operational Parameters of Advanced Nuclear Power Plants

Milan Brumovský

Nuclear Research Institute Řež, plc.
March 2006

Ústav jaderného výzkumu Řež a.s.

Content:

Ústav jaderného výzkumu Řež a.s.

Abstract

NRI Rez, plc, created this report as a contribution to the D-ML-1-2 project: Specification of test programme for vessel features tests in the context of RAPHAEL project, WP-ML1: Vessel Material.

The report summarizes results of projects, analyses of particular materials used for main components of GEN IV reactor types, especially for reactor vessels. The report also focuses on the results of possible special materials used on experimental works (mechanical tests including non-irradiated and irradiated state).

1. Introduction

Parameters of advanced nuclear power plants (NPPs), especially reactor pressure vessels are generally higher, than in the case of existing NPPs, whether considering power-pressure reactor type, boiling-water reactor type, fast reactor type or gas-cooled reactor type.

There are three types of new generation reactors GEN IV under consideration:

1 High-temperature gas-cooled reactor,
2 Super-critical water reactor,
3 Fast reactor with the coolant on the base of Pb-Bi (or based on similar metals).

This report, above all will be focused on materials for reactors working with thermal neutrons for their parameters considerably differing from already existing operated reactors types PWR/BWR or GCR. And for which realization will be necessary to complete selection and wide-broad experimental & technological works.

2. Main parameters of GEN IV reactor types

Main reactor types, which are defining operational conditions and parameters, are summarized in the following Table 2.1.

Table 2.1: Overview of considered reactors for GEN IV

	Acronym	Coolant	Neutron
Gas-Cooled Fast Reactor (Medium, Long Term)	*GFR*	*Gas*	*Fast*
Lead-Cooled Reactor (Medium, Long Term)	*LFR*	*Liquid Metal*	*Fast*
Molten Salt Reactor (Low, Long Term)	*MSR*	*Molten Salt*	*Thermal*
Sodium-Cooled Reactor (Low, Long Term)	*SFR*	*Liquid Metal*	*Fast*
Supercritical Water-Cooled Reactor (Medium, Long Term)	*SCWR*	*Water*	*Thermal – (Fast)*
Very High Temperature Reactor (High, Mid Term)	*VHTR –NGNP–*	*Gas*	*Thermal*

Following main operational parameters are ensuing from above-mentioned reactor projects. Table 2.2 is summarizing these parameters.

Table 2.2: Main operational parameters of reactors for GEN IV

Reactor	Coolant	Operating Temp. (°C)	Off-Normal Temp/Time. (°C)	Operating Pressure (MPa)	Neutron Spectrum	Dose (dpa)
NGNP	Helium	400-500	520-610/50h	7.4-8.0	Thermal	0.008
SCWR	Supercritical Water	280	280	25	Thermal	0.05
GFR[a]	Helium	300-850	800-1100	7-21	Fast	<40
LFR[b]	Lead or Pb/Bi	Near:<550 Long:<800	??	Atmos-pheric	Fast	15-40

[a] Temperatures and pressures dependent on specific design: He direct, He/Supercritical CO_2, Supercritical CO_2

[b] Temperatures dependent on specific design: Near-term w/ outlet temp of 550°C and long-term w/outlet temp of 800°C. RPV temperature equal to inlet temperature.

Legend:

NGNP High-temperature gas-cooled reactor

SCWR Super-critical water reactor

GFR Gas-cooled fast reactor

LFR Lead-cooled fast reactor

Considering operational parameters, reactor types and experience with similar reactor types in Czech Republic, the main focus will be concentrated in next to the following two-types of reactors – NGNP = VHTR and SCWR. These two reactor projects are very close to experimental and technological base in Czech Republic.

3. VHTR = NGNP Reactor Type

This part will be addressed to main components of the VHTR reactor type and to main candidate materials, for which some data are known or which seems to be perspective in point of their characteristics and composition.

3.1 PRESSURE VESSELS

Reactor pressure boundary is practically compact arrangement of three pressure vessels:

1. Reactor pressure vessel,
2. Cross vessel,
3. Power conversion vessel.

Typical scheme with comparison of present PWR reactor dimensions of reactor vessels is shown in Figure 3.1.

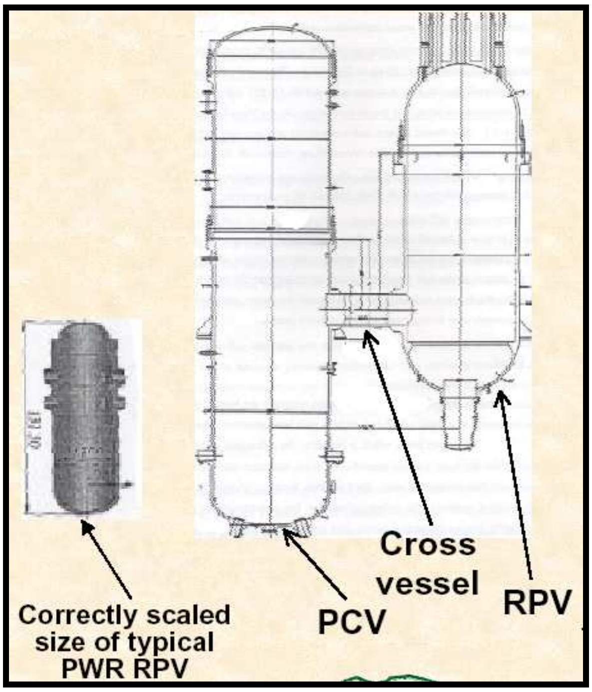

Figure 3.1: Scheme of present PWR reactor dimensions of reactor vessels

3.1.1 PRESSURE VESSEL OF THE REACTOR

Scheme of the reactor pressure vessel is shown in Figure 3.2. The main parameters given by designers are summarized in Table 3.1.

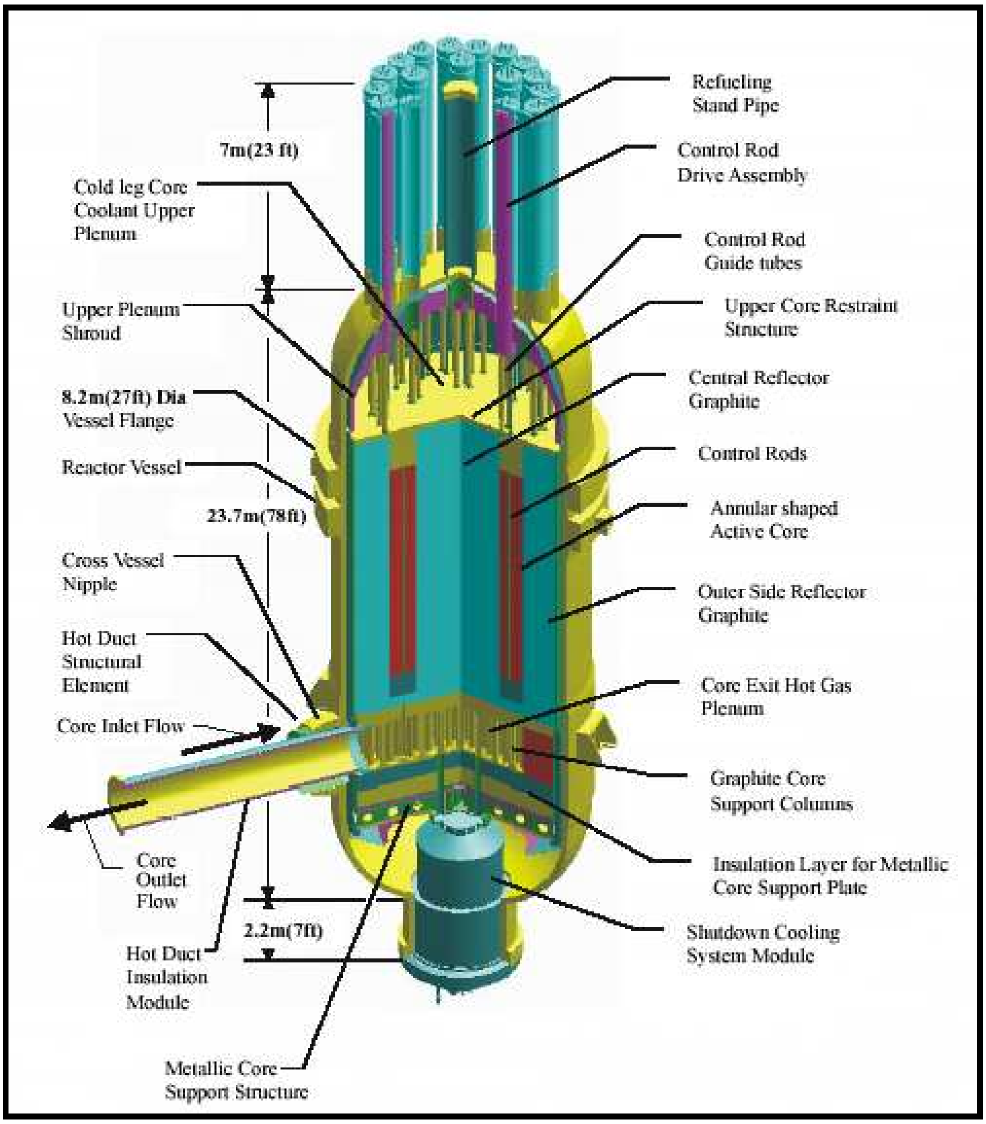

Figure 3.2: Scheme of the pressure vessel of the VHTR=NGNP reactor type

Table 3.1: Comparison of reactor pressure vessels parameters and dimensions according to different projects

RPV Parameter	GT-MHR [6]	GA-Prismatic [9]	Prismatic NGNP [7]	PBMR [10]	NGNP PBR [7]
Nominal Gas Outlet Temperature (°C)	850	950	1000	900	1000
Nominal Gas Inlet Temperature (°C)	491	590	490	482	490 [c]
RPV Normal Operating Temperature (°C)	495	350	470 [d]	300	465 [e]
RPV Worst Case Accident Temperature (°C)	565	530	560 [7], [f]	506	560 [g]
Inlet Gas Pressure (MPa)	7.07	7.07	7.07	8.9	7
Outlet Gas Pressure (MPa)	7.02	7.02	7.02	8.6	6.5?
RPV External Diameter (meters)	8.2	8.2	8.2	7.02	7.06
RPV Nominal Wall Thickness (mm)	100-300	100-300	100-300	120-220	120-220
RPV Nominal Height (meters)	23.7	23.7	24	22	19
Maximum Radiation Fast Fluence in the RPV in the RPV over 60 years (n/cm^2)	3×10^{18} [11]		1×10^{19} [7], [h]	4.5×10^{19} [7]	3.0×10^{19}

After comparison of above-mentioned reactor pressure vessels parameters with parameters of operated pressure vessels of PWR/VVER reactor types, it can be stated that operational temperatures are significantly higher (up to 495 °C) than it is in the case of PWR/VVER reactors (up to 320 °C). This increased parameter will lay emphasis on materials with higher thermal stability, especially against creep and thermal aging. Increased diameters of vessels and so dimensions of ingots will require next technological research in the field of metallurgy, mechanical working and also welding.

3.1.2 CROSS-VESSEL

Scheme of the vessel is shown in Figure 3.3. Outer diameter of the vessel is considered about 2.5 m and thickness about 100 mm. The temperature seems to be the critical parameter of the vessel – temperature of helium at the reactor output will be c. 1000 °C and temperature of the cross-vessel will depend on its construction, i.e. on fixation of its insulation. It is assumed the use of ceramic materials to ensure that the temperature will be close to temperature of helium at the reactor input, i.e. 490 °C. It is estimated, that the temperature will culminate in the range 550 °C - 490 °C.

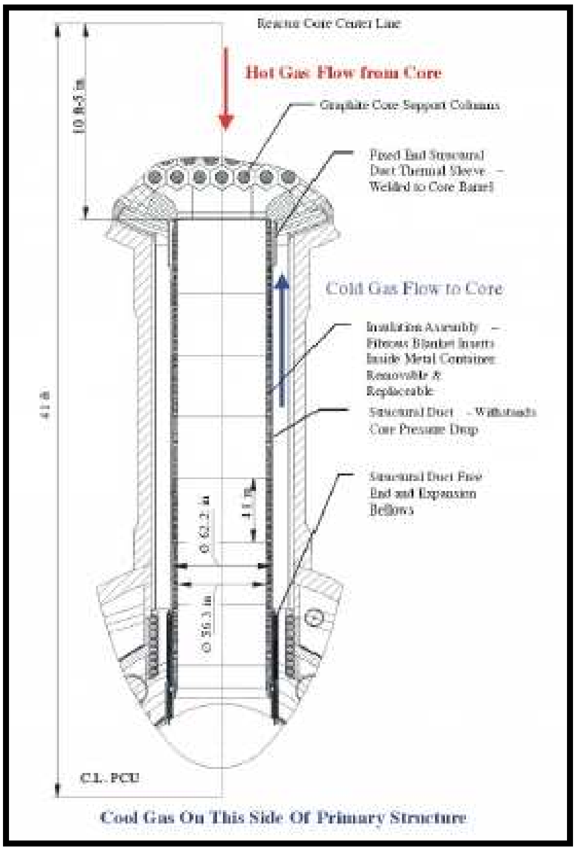

Figure 3.3: Scheme of the cross-vessel

3.2 SECONDARY VESSEL

This secondary vessel contains turbine, turbogenerator and heat exchangers needed to ensure parameters of helium, heated-up to 490 °C and pressurized between 7.4 and 8.0 MPa. Vessel height will be c. 34 m and its thickness from 100 to 300 mm. The temperature should culminate around 200 °C in the case of emergency modes around 300 °C. Scheme of the vessel is presented in Figure 3.4.

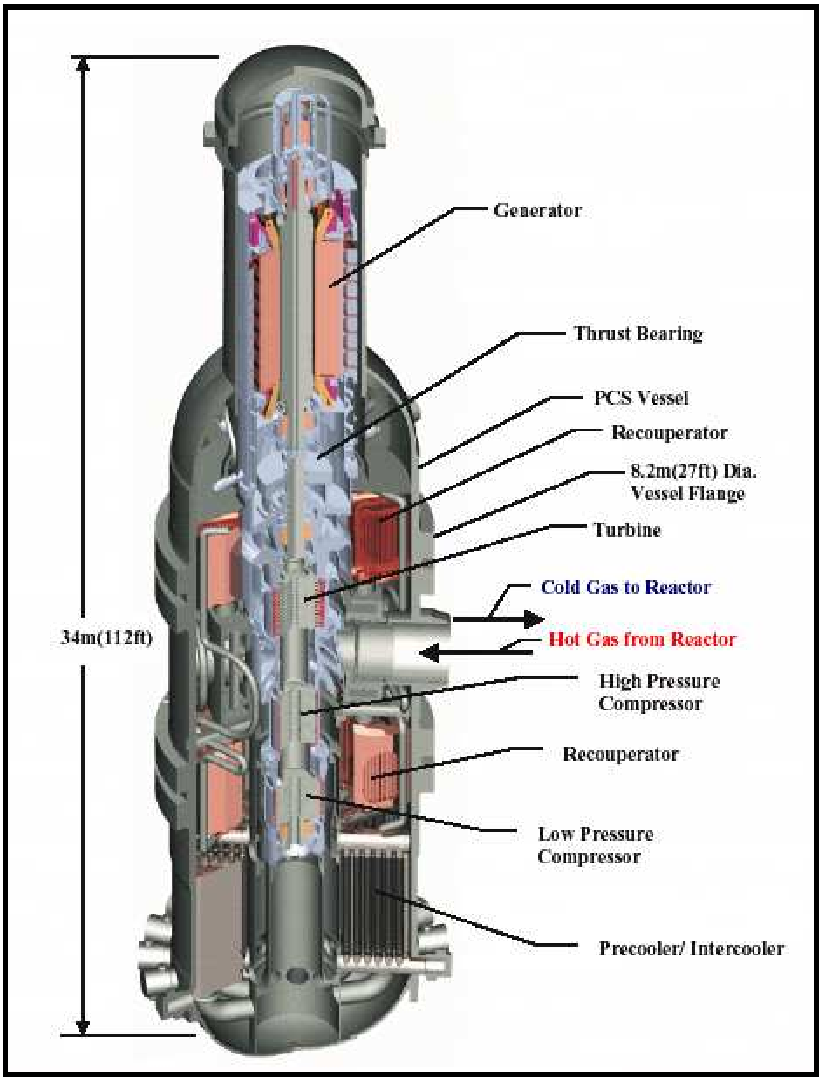

Figure 3.4: Scheme of the secondary vessel

3.3 OPERATIONAL PARAMETERS OF PARTICULAR VESSELS

Operational parameters of particular vessels are summarized in following Table 3.2.

Table 3.2: Main parameters of pressure vessels of the primary circuit (pressure boundary)

Component	Normal VHTR System Operating Conditions: Temp. [°C] Pressure [MPa]	Normal VHTR System Operating Conditions: Neutron Fluence, E>0.1 MeV (dpa)	Abnormal Conditions	Estimated Component Size
Reactor Pressure Vessel (RPV)* [7], k	300-500 °C [1] [7.4-8.0 MPa]	1×10^{19} n/cm^{-2} per 60 years (0.077 dpa)	≈560 °C at 1 atm for 200 hours	Diameter: >9m, Thickness: 100-300mm, Height: >24m
Cross Vessel (CV) [7], k	300-500 °C [7.4-8.0 MPa]	1×10^{19} n/cm^{-2} per 60 years (0.077 dpa)	300 to 560 °C for 200 h [7.4-8.0 MPa]	Diameter: >2.5m, Thickness: >100mm Length: 4-5m
Secondary Vessel [22]	300 °C [5.0-6.0 MPa]	Negligible 3×10^{14} n/cm^{-2} per 60 years	300 °C [5.0-6.0 MPa]	Diameter: 7-9m, Thickness: 100-200mm Height: • 35m
Closure Bolting [7], k	550 °C	1×10^{19} n/cm^{-2} per 60 years (0.077 dpa)	≈560 °C at 1 atm.	

After comparison of these parameters with existing parameters for pressure vessels of the for example PWR reactor type, it can be stated, that:

- fluences of neutrons are comparable or lower than present PWRs
- operational temperatures are higher than present PWRs
- operational pressures are lower than at PWRs, close to BWRs
- dimensions of pressure vessels are generally higher than at PWRs

3.4 PROSPECTIVE MATERIALS

Selection of suitable materials depends on actual state of standards, which are giving maximal permissible operational temperatures for particular materials - based on existing database of mechanical characteristics including short-term characteristics as tension characteristics, ductile fractures and long-term characteristics as creep, fatigue (synergism).

Actual state of maximal permissible operational times and temperatures, explicit in the ASME code, subsection NH, is shown in Table 3.3.

Table 3.3: Maximal permissible operational times and temperatures for particular materials according to ASME code, Subsection NH

Material	Temperature (°C) [b]	
	Primary stress limits and ratcheting rules	Fatigue curves
304 stainless steel	816	704
316 stainless steel	816	704
2 1/4 Cr – 1 Mo steel	593b	593
Alloy 800 H	760	760
Modified 9 Cr – 1Mo steel (Grade 91)	593b	538

a. Allowable stresses extend to 300,000 h (34 years) unless otherwise noted.
b. Temperatures up to 649 °C are allowed for not more than 1000 h.

It can be concluded from this review that none of above-mentioned materials meet the requirements to be a suitable material. It is necessary to put more effort on research of new prospective materials between which the following materials belong in particular: 9Cr-1MoVNb, 7-9Cr2WV, 12Cr-1MoWV, 2.75Cr-1MoV, 2.25Cr-1Mo, austenitic materials.

3.4.1 The 9Cr-1MoVNb TYPE

This class of materials is used at present and it has a large material database. For example 9Cr-1Mo-V (grade91) is allowed to be used up to 649 °C for components of classes 2 and 3 in accordance with ASME code, Section III and finishing the approval for components of class 1 in Subsection NH.

Concurrently, there are limits for the use from the point of temperatures, thickness of semi-finished products, etc.

It is possible to consider modifications in the frame of this material type, as 9Cr-1MoWV (grade 911, 92). Temporary results show increased strength under high-temperature conditions.

Notched bar toughness of these steels is quite bit worse than at present reactor pressure vessels as seen in Figure 3.5.

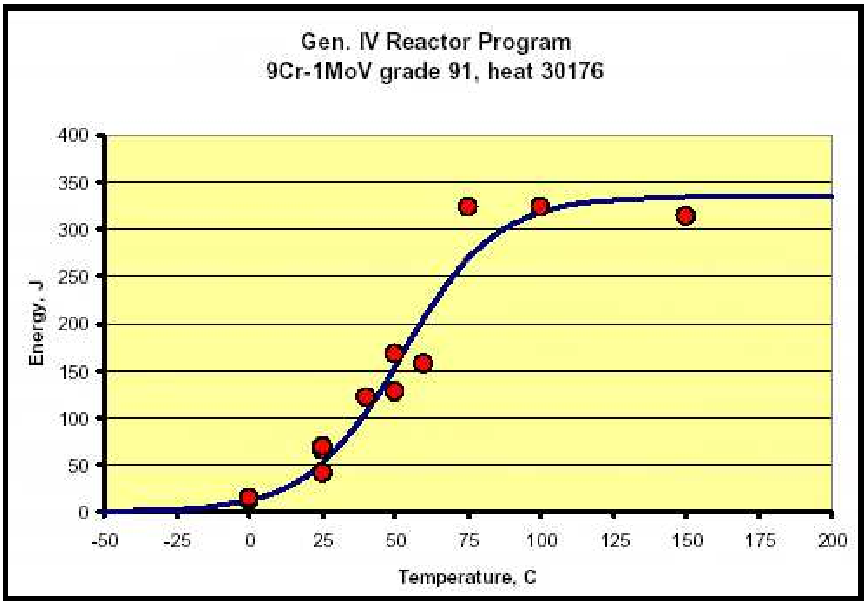

Figure 3.5: Thermal dependence of notched bar toughness of the 9Cr-1MoV steel type with transient temperature c. 20 °C

Results of fracture toughness tests of the same material with evaluation according to Master Curve conception are summarized in Figure 3.6.

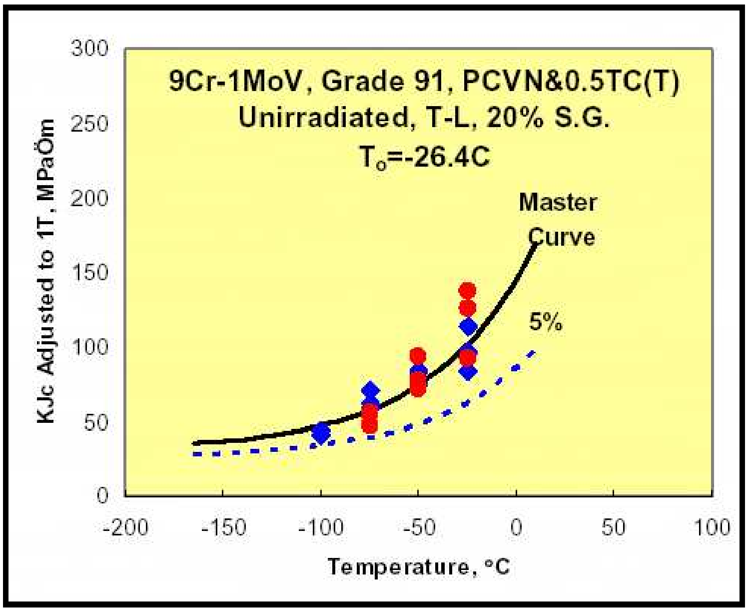

Figure 3.6: Results of fracture toughness of the same material as presented in Figure 3.5

Notched bar tests results of similar material - 9Cr-1Mo type after irradiation by fluence 13 dpa are shown in Figure 3.7. It is essential to note that radiation embrittlement (characterized by transient temperature difference) was greater during temperatures under 450 °C in the range of the irradiation temperature 390 - 550 °C:

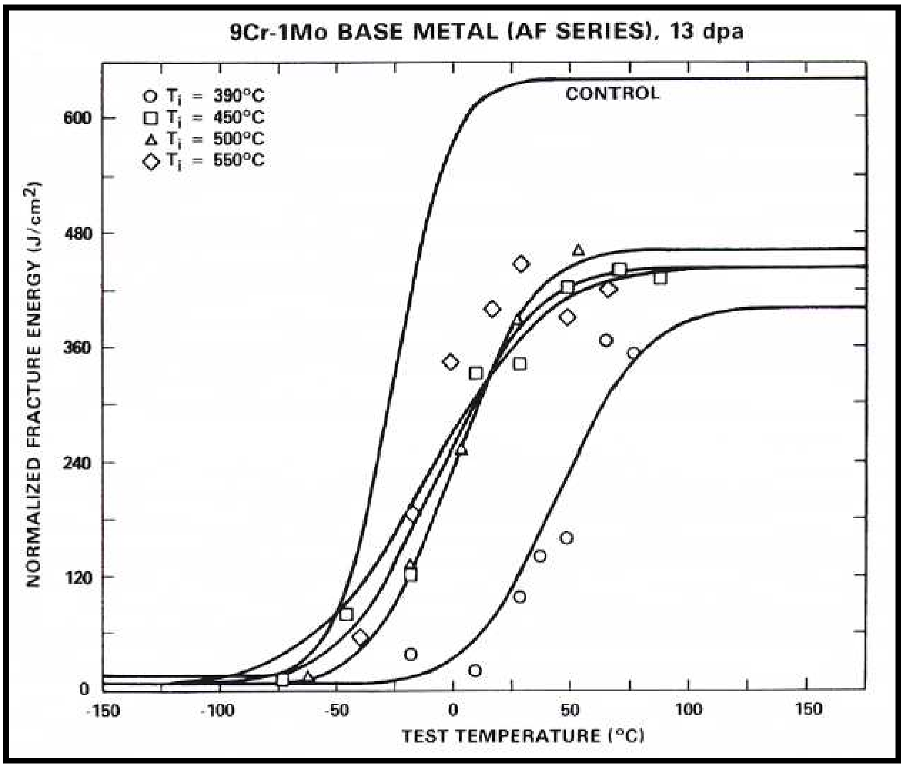

Figure 3.7: Thermal dependences of notched bar toughness of 9Cr-1Mo material type after irradiation by fluence 13 dpa in the range of temperatures 390 - 550 °C

3.5.2 The 7-9Cr2WV TYPE

Alloys of this type are developed in the frame of fusion programs. So far a small database of their characteristics exists, but some of them extend higher strength properties. Steels F82H (7,5Cr2WV), JLF1 and EUROFER (9Cr2WV) are good example of this type.

The advantage of these materials is the fact, that they have been developed with the aim of low-induced activity during the operation, which is a significant advantage during reactor shutdowns and decommissioning (dismantling).

Typical results of fracture toughness tests are shown in Figure 3.8. The transient temperature T_0 is considerably lower according to Master Curve conception than it is in the case of previous material – 9Cr-1MoV.

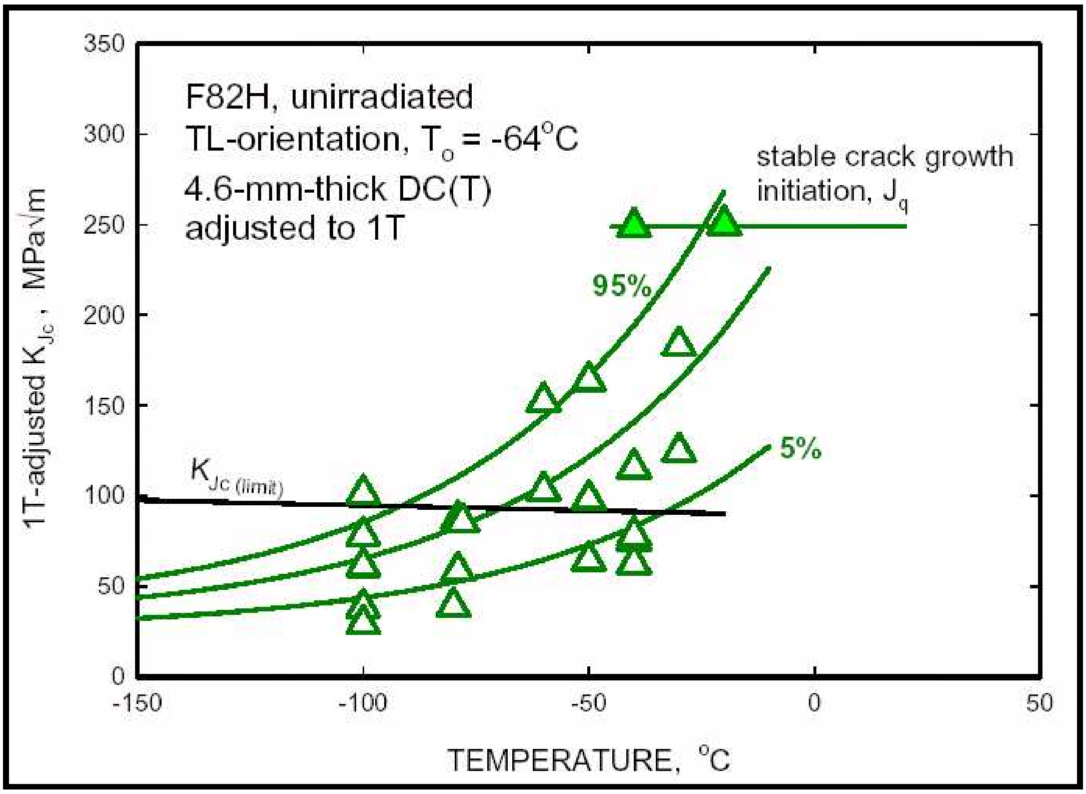

Figure 3.8: Thermal dependence of fracture toughness of the material type - F82H = 7,5Cr2WV

Irradiation results of this material show relatively small transient temperature shift during the irradiation temperature 377 °C, but significantly greater shift during the irradiation temperature 250 °C as can be seen in Figure 3.9.

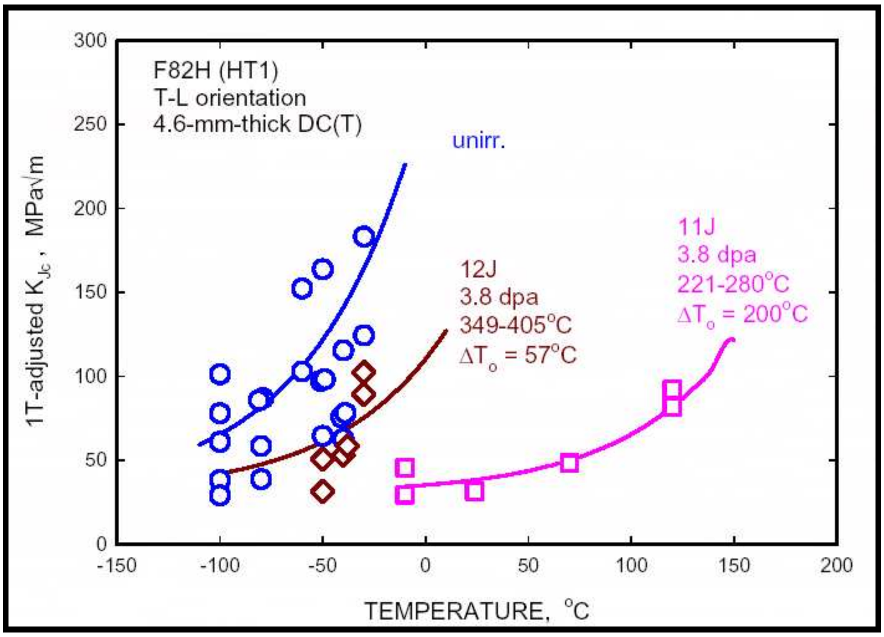

Figure 3.9: Thermal dependence of fracture toughness of non-irradiated and irradiated material type F82H = 7,5Cr2WV.

Results of irradiated tests are at same time show that changes of mechanical properties (transient temperature shift and yield strength growth) are in accordance with results of ferritic steels tests for pressure vessels of the PWR/BWR reactor types, as seen in Figure 3.10.

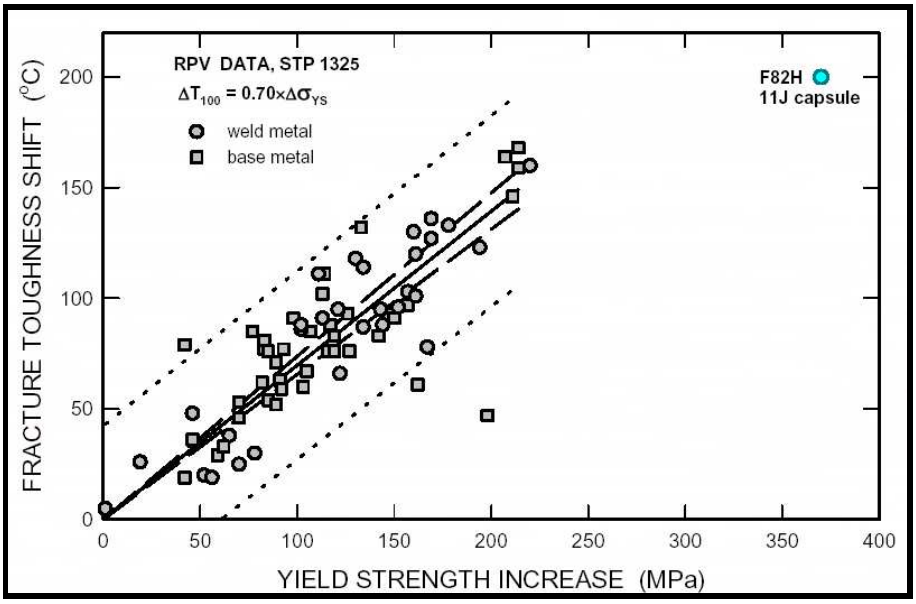

Figure 3.10: Correlation between yield strength growth and transient temperature shift for materials of reactor pressure vessels.

3.5.3 The 2.75Cr-1MoWV TYPE

This type of material shows good strength properties under high temperature conditions. However, it is a new material and only a small database of its properties exists. It has practically two times higher strength characteristics than steels SA 508 Grade 3 (at present used as RPV material for LWR) under consideration of same thickness of semi-finished products.

Present works show that there will be no needs to realize thermal processing of welded joints after welding.

The 2.75Cr-1MoV material type is developed in Russia in the frame of this class.

3.5.4. The 12Cr-1MoWV TYPE

This material is also marked as HT9. It is the oldest one from the 12Cr-1MoWV material group. A large database of characteristics exists, but this type of material has worse properties than 9Cr-1MoVNb.

There are next modifications of this alloy based on 12Cr, which have better properties than HT9. For example, HT12A has a good database and ASME, Code Case 2189 allows its use up to temperature 649 °C for applications according to Sections I a VIII. The same material is marked as SAVE12 with good strength characteristics under high-temperature in Japan.

The 12YWT alloy type can be considered in the same material group. It is an dispersion strengthened material with oxides of the Y_20_3 type 12Cr-3W-0,4Ti+0,2 Y_20_3. This alloy has enhanced strength characteristics, as shown in Figure 3.11.

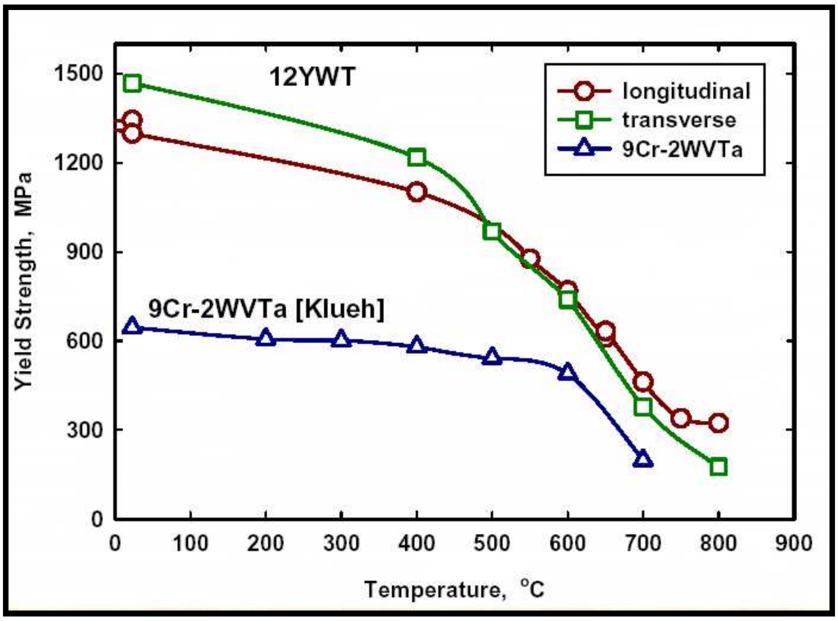

Figure 3.11: Comparison of the yield point thermal dependence of 12YWT and 9Cr-2WTa material types

This material shows considerably better resistance against fragile damage characterized by transient temperature of fracture toughness as can be seen in Figure 3.12.

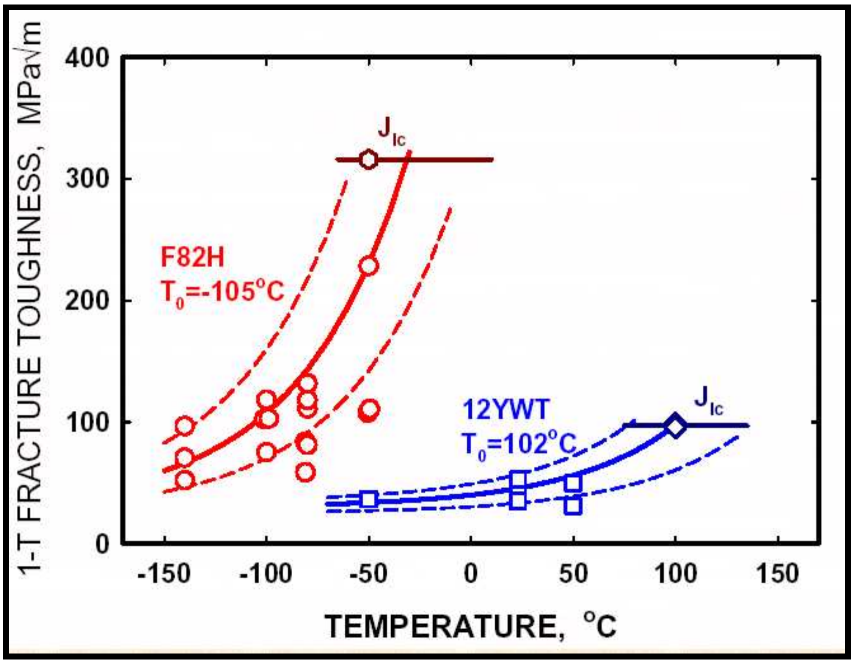

Figure 3.12: Temperature dependence of fracture toughness of materials F82H and 12YWT.

3.5.5 The 2.25Cr-1Mo TYPE

This type of material is widely used and a large database of its mechanical characteristics exists. However, it would require reduction of the operational temperature, because its high-temperature strength characteristics are under previously mentioned materials. Materials of this type can be applied to reactor vessels operated under lower temperatures, as for example HTTR (High Temperature Test Reactor) in JAERI.

3.5.6 CLASS OF AUSTENITIC MATERIALS

A large database of material characteristics for this type of steels including behavior in helium environment with different impurities already exists. Strong experience also exists with fabrication and operation of these materials under different environment and radiation.

Its strength properties are lower than at previous ferritic-martensitic steels, but they do not decrease rapidly with temperature increase. Its strength under the temperature 650 °C is lower than it is required, but the advantage of these materials is their metallurgy stability under high temperatures including abnormal conditions.

Generally, austenitic steels have great resistance against oxidation and corrosion in many environments, but they are not immune against degradation in some usual environments.

4. Conclusion

Present state of knowledge about project assumptions and project parameters of GEN IV reactor types supported the selection of candidate materials for particular main components of GEN IV reactors.

Research and development of suitable materials will require strong effort to obtain sufficient database of high-temperature properties and to continue in the technological development – fabrication of big ingots and forgings, their consecutive welding and thermal processing.

Overview of main parameters for particular reactor types and candidate materials is shown in following Table 5.1.

Table 5.1: Overview of requirements for components GEN IV

REACTOR TYPE	**COOLANT TEMPERATURE T_{in}/T_{out} [°C]**	**REPREZENTATIVE COMPONENTS AND CANDIDATE MATERIALS**
NGNP – VHTR	650/1000	9Cr(9Cr-1Mo) or 12Cr steels for RPV, Ni-alloys for components with high temperature of gas
GFR	490/850	9Cr or 12Cr martensitic steels or 2 ¼ Cr- 1Mo steels for RPV, Ni-alloys, AISI 316 or 9Cr ODS for components with high temperature of gas
SCWR	280/500	SA508 Grade 3 or higher SA508 Grade 4N or developed 3Cr-3WV steels for RPVwith insulating vessel neck 9Cr-1Mo steels or austenitic steels or their modifications for non-insulating vessels and for high-temperature steam piping
LFR	-/550 (coolant Pb-Bi) -/750-800 (cooled by pure Pb)	AISI 304 3126 austenitic steels or their modifications for reactor vessels, 2 ¼ Cr-1 Mo or 9Cr-1Mo for heat-exchangers, improved austenitic steels or ferritic-martensitic steels for inner parts of the reactor; high-temperature alloys for vessels and heat-exchangers, possibly high-temperature metals or ceramics for inner parts of the reactor

Appendix 2

CEA/DEN/CAD/DER/SESI/LCSI/NT
DO 13 16/03/06

06PPBV000013

DIRECTION DE L'ÉNERGIE NUCLÉAIRE
DIRECTION DU CENTRE DE CADARACHE
DÉPARTEMENT D'ÉTUDES DES RÉACTEURS
SERVICE D'ÉTUDES DES SYSTÈMES INNOVANTS
LABORATOIRE DE CONCEPTION DES SYSTÈMES INNOVANTS

NT	CEA/DEN/CAD/DER/SESI/LCSI/NT DO 13 16/03/06	0	5H62	A-RCGMA-02-02	DDIN/TC/RCGMA	1/54
NATURE	CHRONO UNITÉ	INDICE	UNITÉ	ÉLÉMENT D'OTP	CLASSEMENT UNITÉ	PAGE

Note Technique

TITLE : **LARGE SCALE TESTS ON 9Cr1Mo MOD TUBES WITH CIRCUMFERENTIAL WELDS IN CREEP REGIME. SPECIFICATION OF THE EXPERIMENTAL PROGRAMME AND PARAMETRIC FINITE ELEMENT CALCULATIONS. DELIVERABLE ML1.2 OF RAPHAEL-IP SP4/WP1/TASK 2.**

ESSAIS A GRANDE ECHELLE SUR TUBES EN ACIER 9Cr1Mo MOD AVEC SOUDURE CIRCONFERENTIELLE DANS LE DOMAINE DU FLUAGE. SPECIFICATION D'UN PROGRAMME D'ESSAIS ET CALCULS PARAMETRIQUES PAR ELEMENTS FINIS. LIVRABLE ML1.2 DU PROJET RAPHAEL-IP SP4/WP1/TASK 2.

AUTHOR(S) : Y. LEJEAIL, E. PLUYETTE

SUMMARY : This document is the specification for Large Scale Tests (LST) which will be performed on 9Cr1Mo mod tubes with circumferential weld, submitted to internal pressure, at 625°C (i.e. in the creep regime). The objective is to demonstrate experimentally a size effect for this kind of material: small specimens having rupture time similar to the weakest zone (the Heat Affected Zone), and big components being as strong as the Base Metal alone. The parameters of the LST have been determined, and it has been demonstrated by Finite Element calculations that we could reach a rupture time of 1230h, which is much higher than the creep life obtained from cross-weld small laboratory specimens (145h). The material supply, the experimental rig, the instrumentation,... are also briefly described in this note. The second objective of the LST is to validate a Finite Element model identified by ENSMP (*) that could be used to build simple formulas to determine the creep life of welded structures. An extension of the model of V. Gaffard is thus proposed for tubular geometries, depending on the width of HAZ, on the thickness and radius of the component.

RESUME : Ce document est la spécification pour les essais à grande échelle (LST ou CJF) qui seront réalisés sur des tubes en acier 9Cr1Mo mod avec une soudure circonférentielle, et soumis à une pression interne, à 625°C (c.-à-d. dans le régime de fluage). L'objectif est de démontrer expérimentalement un effet de taille pour ce type de matériau: les petites éprouvettes ayant des temps à rupture semblables à ceux de la zone la plus faible (la Zone Affectée Thermiquement), et les grands composants étant aussi résistants que le métal de base seul. Les paramètres des essais LST ont été déterminés, et il a été démontré par des calculs aux Eléments Finis que l'on pourrait atteindre un temps à rupture de 1230h, beaucoup plus élevé que la durée de vie en fluage obtenue à partir d'éprouvettes de laboratoire de type cross-weld (145h). L'approvisionnement en matériau, l'installation expérimentale, l'instrumentation... sont également brièvement décrits dans cette note. Le deuxième objectif des essais LST est de valider un modèle de comportement et d'endommagement identifié par l'ENSMP (*). Il pourrait être employé pour établir des formules simples qui serviraient à déterminer la durée de vie en fluage des structures soudées. On propose ainsi une extension du modèle de V. Gaffard pour les géometries tubulaires, dépendant de la largeur de la ZAT, de l'épaisseur et du diamètre du composant.

(*) Ecole Nationale Supérieure des Mines de Paris

KEYWORDS : MOTS CLES : LARGE SCALE TEST – CREEP – WELD – 9CR1MO – FINITE ELEMENT MODEL – RAPHAEL-IP

(04/02 - JA-Document30)

	Rédacteur	Vérificateur	Vérificateur Qualité	Approbateur
Fonction visa NOM	Ingénieur Yves LEJEAIL	Ingénieur Marie-Thérèse CABRILLAT	IQ du SESI Florence JOYER	Le Chef du SESI/LCSI Patrick DUMAZ
Date	27/03/06	27/03/06	13/04/06	13/04/2006

Propriété Industrielle	Cadre de réalisation	Classification					Qualité
En l'absence d'accord ou de contrat, la diffusion des informations contenues dans ce document auprès d'un organisme tiers extérieur au CEA est soumise à l'accord du Chef de Département.	DOB .... DDIN Domaine .... TC Projet .... RCGMA Contrat .. RAPHAEL-IP SP4/WP1/TASK 2	DR	CC	CD	SD	Ss X	AFAQ VERSION 2000

Indice	OBJET DES REVISIONS	DATE	RÉFÉRENCE GCAO
0	Emission initiale	13/04/06	CEA/DEN/CAD/DER/SESI/LCSI/NT DO 13 16/03/06

PLAN

1. INTRODUCTION

The Very High Temperature Reactors (VHTR) of the Generation IV international project are characterized by some common features:

- graphite fuel assemblies or pebbles;
- helium coolant with high inlet and outlet temperatures;
- fuel with low power density;
- metallic pressure vessel.

Therefore, they are considered as inherently safe, even in the case of a depressurization transient, since the reactor residual power should be removed by conduction through the vessel and transferred by radiation.
As the gas coolant is at high temperature, the vessel itself could be at a mean temperature up to 420°C during nominal conditions. That is the reason why advanced martensitic steel could be chosen for the vessel (P91 or T91, i.e. 9Cr1Mo mod). This steel has high mechanical design stress (S_m), and can be welded even in high thickness. But the creep strength, aging and irradiation resistance of this metal must be investigated, especially by experimental tests.
In the framework of RAPHAEL-IP project, which is part of the 6^{th} FWP, the materials are studied in the SP-ML material Sub Project. It is planned to focus on irradiation, creep and creep/fatigue damages, inside the WP1 Work Package. Finally, the task 2 deals with creep damages and is the subject of this document (Deliverable ML1.2 of [1]).
First the problem of Weld Joint Factor for Design Codes is discussed, pointing out the interest to use numerical methods in order to understand the behaviour of these complex assemblies.
Then, some practical aspects of the validation tests are given, concerning the experimental rig, the material procurement, the instrumentation of the specimens, and the planning of the programme.
Finally, a unified model for creep flow and damage representation is described. It was first applied by V. Gaffard [2] on 9Cr1Mo mod steel at 625°C. Some parametric calculations have been performed with this model to investigate the effect of vessel and weld dimensions, and the results are shown in this report. The equivalent stress that must be used for creep design has been also studied. The numerical results allow us to propose an experimental creep test for the validation of the approach.

2. THE PROBLEM OF WELD JOINT CREEP STRENGTH

Usually, the creep strength of welded joints is assessed directly by using the results of creep tests performed on small-scale laboratory specimens, machined from a full weld, or from a Heat Affected Zone simulated material. As reported thereafter, this kind of approach is often very conservative, since it has been shown that there are some effects of the size of the specimens, especially when the different materials inside the weld (i.e. the Weld Metal, Heat Affected Zone, and Base Metal) have different creep strain laws.

It is useful to begin with a short description of the Heat Affected Zone in martensitic steels that is categorized in 3 parts [2]:

- the Coarse Grain Heat Affected Zone (CGHAZ). The material was submitted to temperature far above Ac3 (temperature of end of austenitic transformation) and below the temperature of fusion. Therefore, the grains had sufficient energy to grow;
- the Fine Grain Heat Affected Zone (FGHAZ). The material was submitted to a temperature just above Ac3. The austenitic transformation is completed, but the grain size did not increase furthermore;
- the Inter Critical Heat Affected Zone (ICHAZ). The temperature reached during welding was comprised between Ac1 (beginning of austenitic transformation) and Ac3. Thus the austenitic transformation is not completed. This zone is divided into two different regions, depending on carbide dissolution, which occurs only for the upper bound of the temperature domain.

Note that the martensite is over-tempered when the temperatures reached during welding are just below Ac1. It is not surprising that some authors include this last part inside the HAZ.

After this brief description and definition of the HAZ, we detail below a few studies concerning the creep behaviour for different geometries and loading conditions, trying to point out the important parameters.
Most of the studies were done by Storesund and Tu ([5], [6]) on 1Cr0.5Mo steel at 550°C. They performed a Finite Element parametric study of an axially loaded Cross-Weld geometry, and of a longitudinal seam weld in a pipe submitted to internal pressure giving hoop stresses [6]. A model coupling creep damage and behaviour was used, even if the material properties of the different constituents were not precisely known (especially for the HAZ zone). They reported the evolution of the stresses and damage in the different zones, and found an effect of the diameter on the creep lifetime, with a minimum for Cross-Weld specimens with a diameter of 5 mm. Beyond this minimum, an increase of the creep life was obtained. It is noticed in [6] that Cross-Weld specimens lifetime could possibly better represent the rupture time of the seam weld pipe, if a diameter greater than 8 mm was used. Some experimental results of this study were shown in reference [5]. A large difference was obtained between "as welded" and "Post Weld Heat Treated" specimens: for the latter, the Cross-Weld rupture time was significantly lower than Parent Metal and a little bit lower than Weld Metal (some illustrations taken from reference [5] are given in the appendix 1). For "as welded" state, the differences between rupture time of Cross-Weld, Parent Metal and Weld Metal are not so large. This behaviour is explained by the minimum creep rates, which are higher for Cross-Weld specimens than for Base Metal, and Weld Metal with PWHT which can be considered as a soft material has minimum creep rates near those of Cross-Welds, and higher than "as Welded" Weld Metal. Some calculations of the Cross-Weld specimens by Finite Element method with a Norton creep law have been performed, using different parameters

for each constituent. The conclusions are very clear concerning the effect of the diameter: an increase will raise the creep life of the specimens (in reference [5] the creep life is determined by a correlation with an equivalent stress). This is linked to a stress decrease in the HAZ, especially for the case of the PWHT. A decrease in the width of the HAZ has the same effect according to the calculations, so that the welding heat input should have an effect on the creep life of Cross-Weld and real components. No effect of the weld width has been reported. Due to the creep strain mismatch between the different zones, it is shown that the initial uniaxial stress becomes multiaxial: the effect of multiaxiality is found to follow the rule of peak rupture stress, which is a combination of Von Mises equivalent $J(\tilde{\sigma})$ and of the maximum principal stress Σ_1:

$$\sigma_{peak} = \alpha\Sigma_1 + (1-\alpha)J(\tilde{\sigma}) \qquad (1)$$

Both in [5] and [6], the coefficient $\alpha = 0.43$ has been applied, without any experimental data, to the 1Cr0.5Mo steel. This value has been successfully applied for other similar steels, like 0.5CrMoV and 2.25Cr1Mo [7]. It is recognized that when creep damage corresponds to cavitation, crack initiation and propagation, the above correlation may be applied.

Payten and Law ([3], [4]) have studied this effect numerically. They used the same models and material constituents as Storesund and Tu, with the same Cross-Weld geometries, and focused on the effect of the angle and the difference between 3D and 2D axisymmetric models. Only small differences were found on the stress levels, for weld angles between 0 and 45°. The axisymmetric model has given a very good approximation of the 3D stresses. The effect of radius was also investigated and said to create a maximum of stress enhancement when the width of the HAZ is equal to the radius of the Cross-Weld specimens (for 2 and 4 mm HAZ width).

M. Prager [8] has also reported an increase of a factor 2 on the life of large specimens, compared to conventional sizes, for Cr-Mo steels with weldment.

Finally, V. Gaffard [2] also demonstrated by Finite Element calculations, for 9Cr1Mo mod martensitic steel, that both a decrease of the width of HAZ and an increase of the radius of Cross-Weld specimens led to an increase of the assembly creep life. He proposed a variation of the specimen creep life with $\frac{L_{HAZ}}{D}$, L_{HAZ} being the width of Heat Affected Zone, and D the diameter. He has also applied the peak rupture stress to take into account the multiaxiality effect in the case of calculations on pipe structures with circumferential weld submitted to internal pressure. As the present study is based on his Ph. D. work, we describe his methodology thereafter.

Some first conclusions can be drawn from these few references. First, it seems that an effect of size exists in the creep life of low-alloyed chromium steels with welds. This effect is due to a creep properties mismatch between the different zones (BM, HAZ, WM). The most detrimental case appears to arise when the HAZ is a soft material, due to the temperatures and to the strains reached during welding inside the material, and during the PWHT. Concerning the effect of the Weld Metal, it can be said that there should be no effect of this part, if the steel undergoes martensitic transformation during welding and recovers high hardness values at room temperature.
This size effect will depend on the width of the HAZ and on the diameter of the specimens or components; but it is important to improve the knowledge about the latter, since there are far less calculations and experimentations on "Large Scale" components than on small laboratory specimens. Finally, it seems that the peak rupture stress will fit several stress state in the creep domain. The purpose of this report is thus to present a proposition of Large Scale creep Tests, to

be performed at CEA on 9Cr1Mo mod steel with a weld realized by FRAMATOME Chalon. These tests will constitute a further validation of V. Gaffard creep models, which should be used in order to define the most accurate Creep Joint Factors.

3. EXPERIMENTAL CHARACTERISTICS OF THE LARGE SCALE TESTS

3.1 GENERAL OVERVIEW

The Large Scale Tests will consist in large diameter pipes submitted to both high temperature and internal pressure during a long time. Due to the internal pressure and to the closure of the gas circuit, there will be an axial force applied to the pipe, the corresponding axial stress being equal to half the hoop stress. More practical details on the future experiments are given in the chapter 3.3, whereas some first analytical calculations to explain the choice of load, geometry, and temperature are shown in chapter 3.2. There will be one thermal mock-up, one base metal pressurized pipe test, and two tests of pressurized pipes with circumferential welds. The welds will be realized by FRAMATOME Chalon with the Gas Tungsten Arc Welding process, using a Narrow Gap chamfer.

3.2 DETERMINATION OF THE MAIN EXPERIMENTAL PARAMETERS

The influence of the pressure, diameter and thickness of the tube, temperature, and of the equivalent stress criteria has been studied by analytical calculations, in order to make a choice among all the parameters: there are some practical limitations imposed by the experimental rigs, so that it is necessary to limit the pressure, diameter and duration of the tests. More detailed simulations are described in chapter 4.

Here we simply assume that the initial stress tensor due to the internal pressure is given by the formula for long thin tubes, of thickness e, internal diameter D, and pressure p:

$$\tilde{\sigma}_{(r,\theta,z)} = \begin{pmatrix} -\frac{p}{2} & & \\ & \frac{pD}{2e} & \\ & & \frac{pD}{4e} \end{pmatrix} \tag{2}$$

The mean value of the radial stress in the thickness has been chosen here. Thus the trace of the stress tensor (by definition the sum of the diagonal terms) is equal to:

$$tr(\tilde{\sigma}) = \frac{p}{2}\left(\frac{3D}{2e} - 1\right) \tag{3}$$

The second invariant of stress tensor, i.e. the Von Mises equivalent stress, may be expressed as:

$$J(\tilde{\sigma}) = \frac{p}{2}\sqrt{1 + \frac{3D}{2e} + \frac{3}{4}\left(\frac{D}{e}\right)^2} \tag{4}$$

It can be seen in this equation than the term $(D/e)^2$ is the most important one inside the root term; neglecting the other terms when D/e >> 1, we obtain the well known $J(\tilde{\sigma}) = \frac{\sqrt{3}}{2}\frac{pD}{2e}$.

An other very interesting equivalent stress to represent the time to rupture is the Maximum Strain Energy (MSE), which can be calculated from the elastic strain energy inside a volume [9]:

$$\sigma_{MSE} = \sqrt{\frac{2}{3}(1+\nu)\left(J(\tilde{\sigma})\right)^2 + \frac{1-2\nu}{3}\left(tr(\tilde{\sigma})\right)^2} \qquad (5)$$

By means of equations (1) and (4), it is possible to evaluate the peak rupture stress for the pipe under internal pressure with axial end pressure effect:

$$\sigma_{peak} = \frac{p}{2}\left[(1-\alpha)\sqrt{1+\frac{3D}{e}+\frac{3}{4}\left(\frac{D}{e}\right)^2} + \alpha\frac{D}{e}\right] \qquad (6)$$

								base metal	weld		base metal	weld		base metal	weld		base metal	weld
n°	p (bar)	Di (mm)	e (mm)	β (/mm)	10/β (mm)	Tmoy (°C)	$\sigma_{\theta\theta}$ (MPa)	tr(h)	tr(h)	$J(\sigma)$ (MPa)	tr(h)	tr(h)	σ_{MSE} (MPa)	tr(h)	tr(h)	σ_{peak} (MPa)	tr(h)	tr(h)
1	150	150	15	0,0383	261	625	75	29293	1518	71,5	40946	1929	76,8	24699	1344	73,0	35385	1738
2	180	150	15	0,0383	261	625	90	8024	602	85,9	11216	764	92,2	6766	533	87,6	9693	689
3	210	150	15	0,0383	261	625	105	2685	275	100,2	3753	350	107,6	2264	244	102,2	3243	315
4	240	150	15	0,0383	261	625	120	1040	140	114,5	1454	177	122,9	877	124	116,8	1256	160
5	270	150	15	0,0383	261	625	135	451	77	128,8	630	98	138,3	380	68	131,5	544	88
6	300	150	15	0,0383	261	625	150	213	45	143,1	298	57	153,6	180	40	146,1	258	52
7	150	150	15	0,0383	261	625	75	29293	1518	71,5	40946	1929	76,8	24699	1344	73,0	35385	1738
8	150	150	14	0,0397	252	625	80,4	17878	1067	76,2	26221	1403	82,0	15510	964	78,0	22183	1245
9	150	150	13	0,0412	243	625	86,5	10635	736	81,5	16196	994	88,0	9391	673	83,7	13475	872
10	150	150	12	0,0428	233	625	93,8	5982	488	87,8	9593	684	95,0	5450	456	90,4	7800	590
11	150	150	11	0,0448	223	625	102,3	3231	314	95,1	5409	454	103,3	3010	299	98,2	4314	386
12	150	150	10	0,0469	213	625	112,5	1645	194	104,0	2875	289	113,3	1567	187	107,6	2249	242
13	150	150	15	0,0383	261	625	75	29293	1518	71,5	40946	1929	76,8	24699	1344	73,0	35385	1738
14	150	200	15	0,0332	301	625	100	3797	352	93,2	6274	505	101,1	3510	333	96,1	5033	431
15	150	250	15	0,0297	337	625	125	778	114	114,8	1424	175	125,4	760	112	119,2	1091	145
16	150	300	15	0,0271	369	625	150	213	45	136,5	418	73	149,8	216	45	142,3	310	59
17	225	300	15	0,0271	369	550	225	1040	347	204,7	3010	1003	224,6	1059	353	213,4	1883	628
18	250	300	15	0,0271	369	550	250	319	106	227,4	923	308	249,6	325	108	237,1	577	192

Table 1: analytical calculations of the creep life of a 9Cr1Mo mod pipe submitted to internal pressure (with end pressure effect)

In the table 1, we present the results of 18 calculation cases, using the principal stress $\sigma_{\theta\theta}$, or the Von Mises, the Maximum Strain Energy equivalent stress, or the peak rupture stress. It allows evaluating the effect of:

- the pressure (cases 1 to 6);
- the thickness (cases 7 to 12);
- the diameter (cases 13 to 16);
- the pressure at a temperature of 550°C (cases 17 to 18).

For each case, we evaluate the time to rupture with a correlation deduced from RCC-MR [10] Sr_moy curves (mean creep rupture curves), using a Base Metal assumption (it means we assume the rupture will correspond to a seamless pipe). The RCC-MR curves are very near those obtained by V. Gaffard at 625°C for the Base Metal [2] as can be seen on figure 1. The times to rupture of small Cross-Weld specimens tested by V. Gaffard are also reported on figure 1. They are used to calculate a time to rupture for a "weld material" in the table 1, to be compared to the Base Metal one.

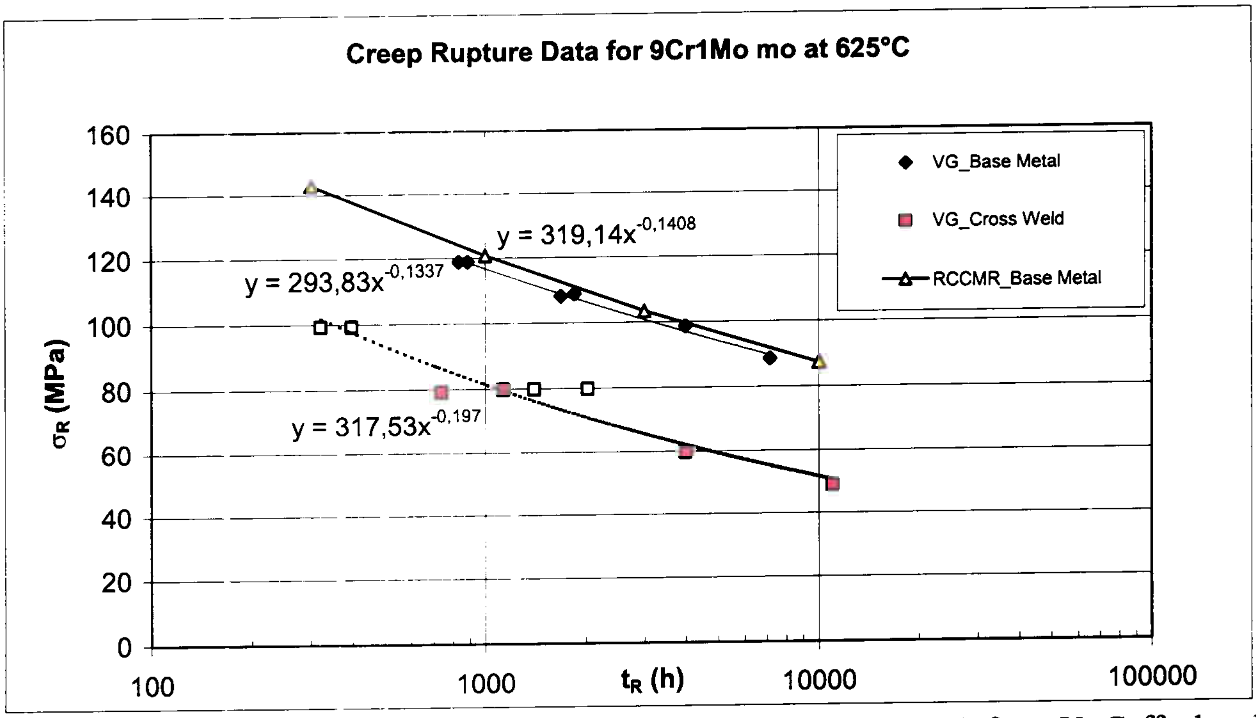

Figure 1: creep rupture characterization for 9Cr1Mo mod steel at 625°C from V. Gaffard and RCC-MR

To use these results, some additional assumptions are made, and some practical requirements are taken into account:

- the time to rupture will be close to the Base Metal one. As reported previously, for Large Scale specimens, the time to rupture is increased compared to small specimens for chromium steel with welds. This important point will be demonstrated later;
- the time to rupture must be less than 10000h; this duration is compatible with the planning of RAPHAEL-IP project;
- the pressure will be less than 200 bar. For this level we can use argon pressurized bottles which are common, cheap and easy to manipulate;
- an internal diameter of 300 mm is the maximum possible value owing to the experimental rig. Beyond 300 mm the weights of the structures are too high, and thus uneasy to handle. Also the machining prices of the different pieces become too high. Last, the internal stored energy inside the pressurised gas is proportional to the diameter, and has to be kept as low as possible. At this time the maximum tested diameter inside this experimental installation is 150 mm. During the year 2006, a security study will be carried out to confirm the feasibility to test higher diameters;
- the diameter and the thickness must be as high as possible, in order to be more representative of the real large components (pressure vessel, Cross-Vessel,…). This point must be validated by the Finite Element calculations of chapter 4.

It can be seen than case number 15 is one of the most interesting: for a pipe with 250 mm of internal diameter and 15 mm of thickness, submitted to 150 bar of pressure, we should obtain a creep life of 1091h using the peak rupture stress and the Base Metal curves at 625°C. More precise calculations are presented in chapter 4.3; they seem to confirm the interest for these test conditions. For this geometry, the table 1 gives a shell parameter $\beta = \frac{\left[12(1-\nu^2)\right]^{1/4}}{\sqrt{De}}$. This parameter permits to estimate the interaction length, i.e. the minimum length of the tube required to avoid side effects: the column $10/\beta$ of table 1 represents this minimum tube half-length. For the case 15, the minimum half-length should be equal to 337 mm. It must be noted that the true β parameter as defined by Timoshenko [13] deals with the mean diameter (and not with the internal diameter as it is defined here); nevertheless, the difference would not have any impact for this study, which is limited to thin structures (in the present chapter). Also, the interaction length 10/β is a very conservative variable compared to the π/β proposed in [13].

3.3 INSTALLATION RIG, GEOMETRY, AND SPECIMEN INSTRUMENTATION

3.3.1 General informations and experimental programme

In short, the challenge is to carry out creep tests on large tubular specimens under representative conditions by integrating the principal experimental parameters: the sample size, internal diameter of 250 mm, thickness of 15 mm and length of 600 mm, the temperature of about 625°C, the internal pressure of 150 bar, and the duration of an experimentation (approximately one month). Moreover, in order to provide valuable results, four experiments should be done at least. Fuller details related to these four tests experimental programme are given in the following paragraphs.

A first test, called thermal mock-up, should be performed in exactly the same conditions as the others tests, except for the internal pressure. This sample should be equipped with numerous thermocouples in order to check the temperatures in many places of the specimen, e.g. from the inner to the outer surfaces and from the top to the bottom of the component. The presence or the absence of a welding joint on the sample is unimportant regarding the temperature distribution through the thermal mock-up. So, conveniently, this first specimen should not bear any welding.
The temperature levels, the temperature distribution over the sample and of course the assessment of the thermal gradients are of great importance for creep calculations, so this experiment should provide a lot of interesting informations related to the refinement of the numerical models.
Moreover, the thermal mock-up should permit to establish the correlations that exist between inner and outer surface temperatures during operation. The three following tests should be performed with an applied internal pressure, so measurements of temperatures in the bulk of the samples then turn impossible. The only available data should derive from thermocouples located on the outer surface of the specimens, but the inner temperatures of the three latter samples should be accurately assessed by means of the results of the first one.

The second experiment, named seamless mock-up, should be carried out on a sample, which doesn't bear any weldment. The specimen should be directly machined from raw material to its final dimensions without any intermediate operation. In this case, like in the two next ones, the internal pressure should be applied. The aim of this second test is to check the base metal creep behaviour when applied to a large specimen. As previously mentioned, most of creep coefficient data bases or numerical models are stemming from the results of tests carried out in highly controlled conditions on small laboratory samples. The creep resistance of a given class of steel can be quite different from a supplier to another. It has been shown that in some cases, due to the manufacturing process, these coefficients can widely vary within the same production. Moreover, the distributions of the temperature and stress fields of a real big component can't be compared to the homogeneous case of a laboratory test. Therefore, this second experiment is very important in the frame of our study, for the size of our samples is large enough to justify a reference test on a seamless mock-up in order to characterize the base metal and prevent possible future problems regarding the interpretation of the results of the next tests carried out on welded samples.

Finally, two other experiments should be carried out on samples, which bear representative circumferential welding joints. These weldings should be both achieved by Framatome within the framework of its participation to this project.
The parameters of the welding of each specimen have not yet been fixed. TIG (GTAW) process seems to be the reference choice for the welding procedure of both samples but discussions are still going on to decide if the best solution is to realize the same welding joint on both specimens, to check the variability of the process, or if it is preferable to make out two different geometries of weldments to compare several procedures.
However, this important decision doesn't influence the planning of the handing-over on level of the installation, because the thermal mock-up and the seamless mock-up tests must be carried out first and, whatever the adopted solution is, the two other samples must be machined after welding to bring them back to the required dimensions to fit the test bench.

3.3.2 Experimental set-up

To reach this objective, an existing test rig has to be improved. This experimental set-up is divided in two main parts: the control room and the experimental caisson.
The control room is located nearby the caisson and ensures the remote control of the main test rig systems set into the caisson. The experimental caisson looks like a huge metallic cube where the sample, the support frame, the power supply, the heating device and the pressure control system are enclosed. The edge of the caisson is about 5 m and its cubic capacity is about 110 m^3. This welded structure is made of steel and is an assembly of 8 mm thick plates and 330 mm girders (see figure 2).

The samples should be heated up by Joules effect by means of a powerful device that can supply high direct currents under low voltage. This power supply consists in a three to six-phase transformer coupled with a twelve diodes rectifier that can deliver up to 35000 A/3.2V DC. The diodes are cooled down by water.
Before testing, the samples have to be prepared to fit to the test rig. Two metallic parts, named the heads, are welded by electron beams method to the ends of the tubular sample. In order to reduce the inner free volume, blocks of ceramic are stacked into the sample before the heads are welded (figure 3). This safety procedure aims at minimizing the source of the magnitude of the blast in case of bursting of the sample during operation.
Many other shields or protections have been set around the sample to limit the nasty effects of the bursting of the sample, like the ejections of small pieces of metal. The ultimate consideration from the safety point of view is that a complete destruction of the experimental means inside the caisson is tolerated until no consequence is noticed out of the caisson.

Electron beams method has been chosen to grant a good welded depth and a low deformation level in the same time. By this way, the welding joint is large enough to comply with the minimum section required to ensure the crossing of the high electrical current from the heads to the sample without any parasitic overheating generation. Moreover, due to the low induced deformations of the process compared to the other welding methods, the heads can be recovered after a test in order to be used again for the next one.

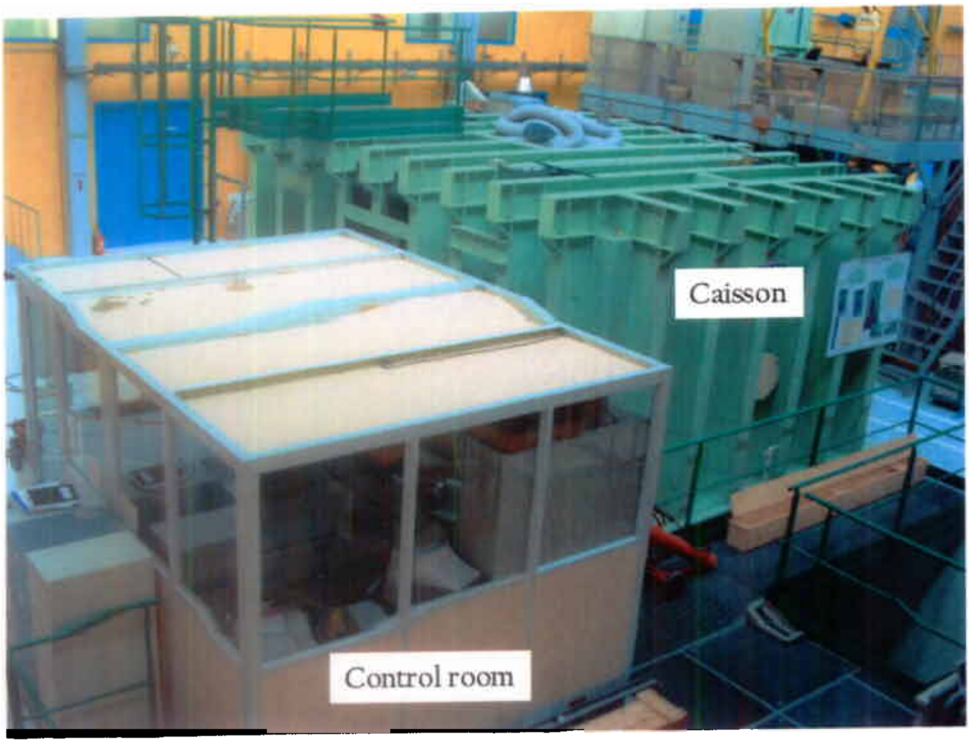

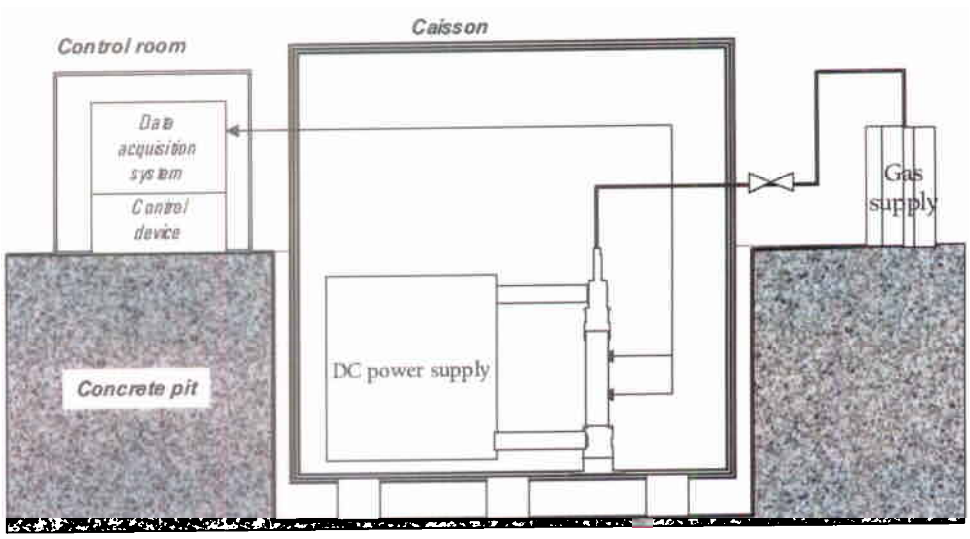

Figure2: view of the installation (up) and schematic of the test rig (down).

Once the welding of pieces has been done, the mock-up is equipped with thermocouples and other sensors.
The mock-up is then introduced into the caisson and is hung by the upper head on the support frame into the caisson. Simple guides at the level of the lower head insure that the mock-up stands in vertical position and allow free dilation of the mock-up during operation.
Massive copper bars are connected to the rectifier and the heads. The total mass of copper bars is about 700 kilograms (as illustrated on figure 4).
Gas supplying is provided by the pressure control system and is connected to the upper head. Shields and other protections are placed around the support frame.
Additional sensors, like displacement or pressure sensors, are set up. Each measurement apparatus is connected to a specific line linked to the system of data acquisition located in the control room out of the caisson.

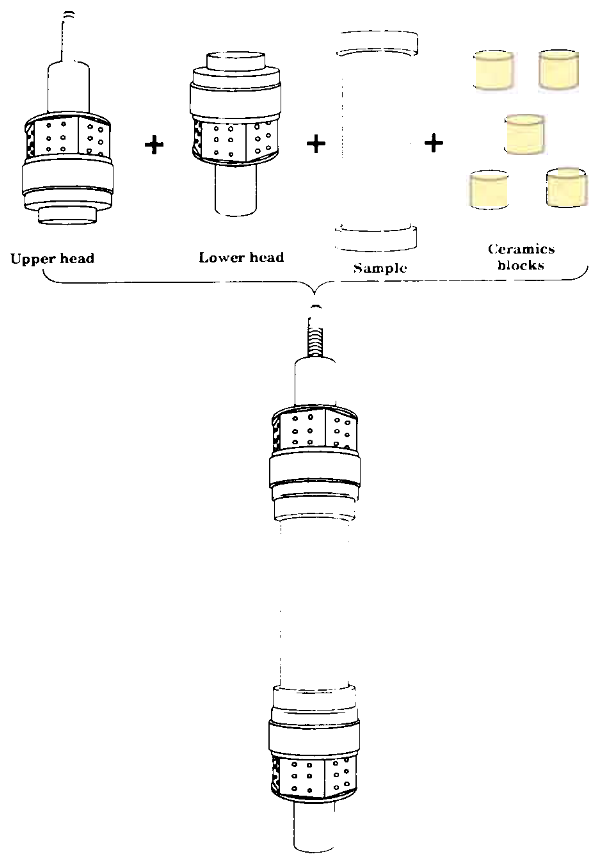

Figure 3: schematic of the assembly of the specimen

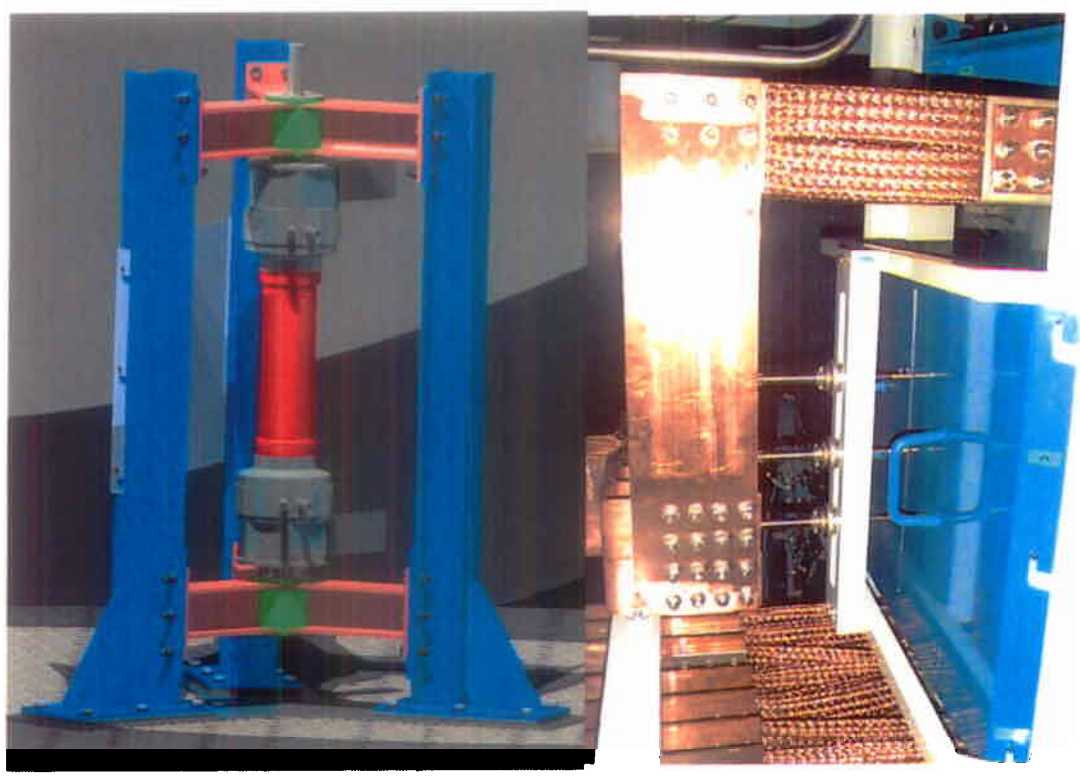

Figure 4: artistic view of the sample on its support frame (left) and view of the copper bar (right)

The door of the caisson can now be shut; the test rig is operational. Every action, like the launching of the heating phases or the control of the safety parameters, is achieved from the control room. A visual surveillance of the test rig is done by means of a video camera placed in the caisson. Safety rules imply to shut down the experiment if the door of the caisson is opened during operation.

Discussions are still going on to define if any reliable criterion can be found in order to stop the experiment before the mock-up bursts without being detrimental to the main objective of the tests. For example, calculations should be performed to define if twenty percents of radial deformations should be enough to produce creep damage that can be clearly identified and quantified by post mortem metallographic examinations.

3.3.3 Specimen instrumentation and data acquisition system

As mentioned before and except for the thermal mock-up, most of measurements achieved during experiments are related to the monitoring of the temperatures, the internal pressure and the specimen deformations (figure 5).
Most of data is collected by the real-time data acquisition system, denoted DAQ, which is controlled by computers located in the control room. This National Instrument™ product is piloted by LabView™ softwares. The evolution of measurements versus time can be seen on line on the screens of the computers and the data can be saved in files.

Temperature measurements are achieved by means of thermocouples patched to the outer surface of the specimens. The selected thermocouples, type K class 1 and 0,5 mm of diameter, are suitable for this kind of surface measurements.
More than about thirty thermocouples are set up on the sample and are spread over along one vertical generator and around three circumferences located at different levels. Each thermocouple is connected to the DAQ by means of an extension wire, except for two of them, which are directed to the heating regulator device.

Deformations are assessed by means of displacement sensors. The probes are equipped with a ceramics extension to avoid direct contact of metallic parts with the sample heated up to high temperatures. Nine sensors are spread over three levels, each level includes three sensors set at 120° around a circumference. A tenth sensor is located vertically on the bottom of the specimen to check the displacements of the lower head. Each sensor is connected to the DAQ by means of a shielded cable.

The internal pressure is controlled by a regulator, which actuates two electro-pneumatic valves located on the admission and the exit of the circuit of gas supply. One end of the circuit is connected to a group of interconnected gas cylinders filled up with argon; the other end is linked to the external atmospheric pressure through the exit line. Four pressure transducers are required by the test bench. Two of them, located in the vicinity of the valves, are necessary to ensure the regulation of the pressure, an other one grants the safety of the test rig and the last one, linked to the DAQ system, is located on the lower head of the specimens.

The thermal mock-up should be equipped with more thermocouples than the other samples. Some of them should be patched to the inner surface and some others should be brazed in holes machined at different depths in the thickness of sample. As mentioned before, this test aims at measuring temperatures everywhere in the bulk of the sample in order to achieve more accurate calculations and to assess inner temperatures by means of surface measurements for the three other pressurized tests.

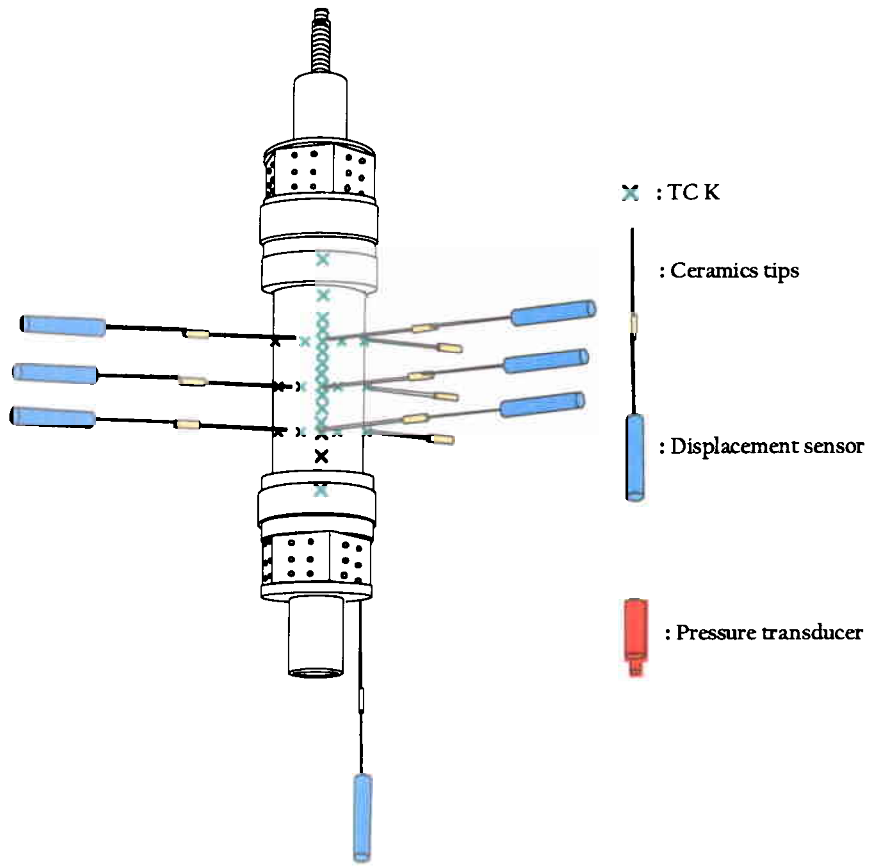

Figure 5: schematic of specimen instrumentation.

3.4 MATERIAL

Specimens must be made of 9Cr1Mo mod. (Grade 91) steel. A large tube has been supplied in order to be able to machine four samples in the same raw material. The tube was provided by Buhlmann France and was manufactured by Vallourec & Mannesmann. Its dimensions are:

- outer diameter 310 mm;
- thickness 50 mm;
- length 5,4 m.

The main informations reported in the EN 1020 4/3.1 certificate provided by the manufacturer are complying with EU and RCCMR 2002 specifications.

The main results are summarized as following:

Tube S/S X 10 Cr Mo VN B 9.1 DIN 2448/17175 A/SA 335 P91, Heat n°: 74513, Certificate V&M (D) N°61439.
Inspection certificate N° 6023/99/0012. Probe N° 2021
Tensile test/round specimen: $R_{p0.2\%}$ = 510 N/mm², R_m = 682 N/mm², A% = 25, ratio $R_{p0.2\%}/R_m$=0,75.
Impact test (transverse direction): 184 J at room temperature.
Hardness (HB): 206, 208, 210, 205.

Chemical composition (%):

Heat N°	C	SI	MN	P	S	AL	CR	NI	MO	V	NB
74513	0.11	0.32	0.45	0.016	0.002	0.019	8.54	0.28	0.93	0.203	0.075

The other results are:
Heat treatment: Normalized 45 minutes 1060°C air
Tempered 120 minutes 760°C air
US tests and hydrostatic test: satisfactory.

A view of the tube is reported figure 6.

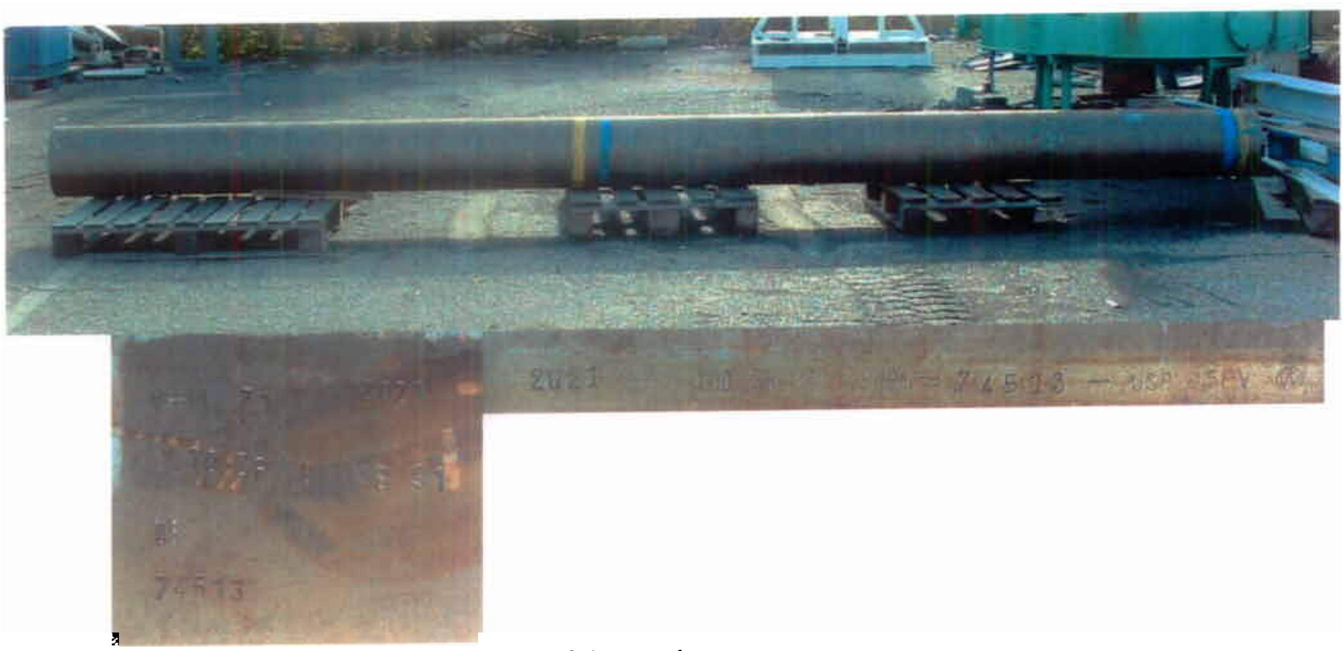

Figure 6: view of the T91 tube and zoom of the marks.

3.5 PLANNING

Four creep tests on large tubular specimen are scheduled on 2006 - 2008:

The thermal mock-up
The seamless mock-up
Two welded mock-ups.

The planning is as following:

- 2006. Test bench enhancements + thermal mock-up test;
- 2007. Seamless mock-up + 2 welded mock-ups;
- beginning of 2008. End of tests + tests report.

The test conditions are reported in the Table 1 (case 15). For the second test on welded specimen, the conditions could be revised according to the result of the first one.

4. DESCRIPTION OF A UNIFIED CONSTITUTIVE MODEL FOR DAMAGE AND STRAIN

A phenomenological model is required for the Finite Element calculations. As in the studies from the literature, V. Gaffard has identified the creep strain behaviour and the creep damage of the different zones of 9cr1Mo mod weldments (i.e. the Base Metal, the HAZ, and the Weld Metal). The HAZ zone has been assumed to be of the soft material type (it means like the ICHAZ): this is one weak point of the model, since it does not represent the gradient of material in this zone. Also, it does not take into account the strain, stress and hardening history of the metal during welding: this is in fact almost the same criticism compared to the previous one. In any case, the model is validated for two precise welding techniques:

- Gas Tungsten Arc Welding of two plates of 150 mm in thickness, with 45 runs. The electrode had a velocity of 1.8 mm/s, the energy per length was between 1700 J/mm and 2150 J/mm: the interpass temperature was below 225°C. The PWHT has been done at 750°C during 15 hours and 18 minutes;
- Gas Metal Arc Welding of two pipes of 55 mm in thickness and 295 mm in outer diameter, in 17 passes (the first being done with GTAW). The heat input was around 1300 J/mm, the pre-heat temperature was of 200°C. The PWHT was done at 760°C during 2 hours.

For the TIG (or GTAW) process, the heat input is relatively high compared to the common practice. But the total width of HAZ was measured to be around 4.4 mm for GMAW and 3.5 mm for GTAW. In both cases, the ICHAZ was found to have a lower Vickers hardness value compared to the initial Base Metal (before PWHT). The CGHAZ had a higher hardness compared to this Base Metal initial value, but also to the Weld Metal. It is reported in [2] that the creep behaviour was found to be the same for the two welding process.

In the next paragraph we detail the equations of the model, and we give the parameters identified for the different zones at 625°C by V. Gaffard.

4.1 EQUATIONS OF THE MODEL

It has been considered that the total and local mechanical strain rate is divided into an elastic part and three inelastic components:

$$\dot{\varepsilon}_t = \dot{\varepsilon}_e + \dot{\varepsilon}_{qp} + \dot{\varepsilon}_{vp} + \dot{\varepsilon}_d \quad (7)$$

In equation (7) :

- the qp index is set for "quasi-plasticity", meaning that this term represents the plasticity occuring during monotonic tensile tests. It can handle the effect of strain rate exisiting at high temperatures. Therefore it can be treated as a viscoplastic strain rate, from a numerical point of view. At 625°C, this term is the most important one for the highest stresses;
- the vp subscript is imposed for the "viscoplastic" creep regime. This term represents the creep of the dislocations, occuring at high stress levels;
- the d subscript means "diffusion". It becomes preponderent only at the lowest stress levels.

Thus, this strain rate partition is consistent with the physical creep strain regimes first defined by Ashby.

Each inelastic term is considered as normal to the yield surface Φ_m , m being the associated flow mechanism (m=qp, or m=vp, or m=d). That means, for the uncoupled version of the model :

$$\dot{\varepsilon}_m = \dot{p}_m \frac{\partial \Phi_m}{\partial \sigma} \tag{8}$$

While for the full version there is a (1-f) factor multiplying the strain rate modulus $\dot{p}_m$, f being the porosity (and the damage).
The yield surface is set to an equivalent stress σ^*_m, which is in fact the Von Mises stress for the uncoupled model. In the full model coupling strain and damage evolution, the σ^*_m is numerically obtained by the Gurson, Tvergaad, Needleman equation (not described here).

$$\Phi_m = \sigma^*_m - R_m \tag{9}$$

The viscoplastic strain rate modulus of each mechanism is a simple power function of the yield surface (equation (10)). It can be seen as a Norton creep law with an internal stress R_m, which is in fact the isotropic hardening internal variable for the mechanism m:

$$\dot{p}_m = \left\langle \frac{\Phi_m}{K_m} \right\rangle^{n_m} \tag{10}$$

The bracket sign means that only the positive numbers are elevated to the power n_m, otherwise the strain rate modulus is equal to 0. It is thus possible to evaluate the cumulated viscoplastic strains by:

$$p_m = \int \dot{p}_m dt \tag{11}$$

There is a coupling between the quasiplastic and viscoplastic mechanisms, since they are both due to the moving of the dislocations. The diffusion creep process is due to the motion of vacancies so that it is completely independent from the two others :

$$\begin{pmatrix} \overline{p}_{qp} \\ \overline{p}_{vp} \\ \overline{p}_d \end{pmatrix} = \begin{pmatrix} 1 & 1 & 0 \\ 1 & 1 & 0 \\ 0 & 0 & 1 \end{pmatrix} \begin{pmatrix} p_{qp} \\ p_{vp} \\ p_d \end{pmatrix} \tag{12}$$

To describe this interaction, the equation (12) is used, to define three new cumulated strain which are designed by a bar sign. These cumulated strains are introduced in the calculation of the isotropic hardening :

$$R_m(\overline{p}_m) = R_{0m} + Q_{m1}(1 - \exp(-b_{m1}\overline{p}_m)) - \{Q_{m2}(1 - \exp(-b_{m2}(\overline{p}_m - p_{mc})))\} \tag{13}$$

The Q_{m1} constant gives the hardening part, while the Q_{m2} constant is a strain recovery term which is kept to zero when the cumulated strain p_m is below a critical strain p_{mc}. Note that $p_{mc} = 0$ for the quasi-plasticity. Also, there is no isotropic hardening for the diffusion creep.

At this point the creep flow is entirely described, and we can begin the presentation of the damage laws. The porosity f (or damage) evolution law is the sum of two terms, the first one being the contribution of the volume change due to compressibility (the strain rate of the full model version having a deviatoric part and a spherical part), and the second one coming from void nucleation rates $\dot{f}_m$:

$$\dot{f} = (1-f)\sum_m tr(\dot{\varepsilon}_m) + \sum_m \dot{f}_m = (1-f)^2 \sum_m \dot{p}_m tr\left(\frac{\partial \Phi_m}{\partial \sigma}\right) + \sum_m \dot{f}_m \tag{14}$$

The latter can be expressed as a function of the trace of σ, of the Von Mises, and of the viscoplastic strain rate, for each mechanism:

$$\dot{f}_m = \left(A_{m1} + A_{m2} \left(\frac{tr\,(\sigma)}{3\,J(\sigma)} \right)^{\alpha_m} \right) \dot{p}_m \tag{15}$$

The $tr(\dot{\varepsilon}_m)$ term can be also calculated as a function of $X = \dfrac{q_2\, tr(\sigma)}{2\sigma^*_m}$:

$$\dot{f} = (1-f)^2 \sum_m \dot{p}_m \frac{\left(\dfrac{3 q_2 q_1 f}{2} \sinh X \right)}{\left[1 + q_1^{\,2} f^2 - 2 q_1 f \cosh X + q_1 f X \sinh X \right]} + \sum_m \dot{f}_m \tag{16}$$

This equation allows calculating the damage evolution. For crack initiation, it has been found sufficient to use the uncoupled model; when a critical void fraction f_c is reached, crack initiation is considered to occur. The value f_c=0.1 has been selected as the best choice to define creep crack initiation for the 9Cr1Mo mod steel.

4.2 IDENTIFICATION OF THE COEFFICIENTS

The table 2 summarizes all the coefficients needed for the calculations, for each material zone, at 625°C. For the HAZ, simulated material has been created by reproducing a welding temperature transient typical of the ICHAZ. For this material only specimens of Notch Creep (NC) type can be produced.

		Weld Metal	Base Metal	ICHAZ
Young's modulus	E	145 GPa	145 GPa	145 GPa
Poisson's ratio	υ	0.3	0.3	0.3
Quasi plastic hardening at 625°C	R_{0qp}	Id.	173 MPa	Id.
	Q_{qp1}	Id.	128 MPa	Id.
	b_{qp1}	Id.	400	Id.
	Q_{qp2}	Id.	80 MPa	Id.
	b_{qp2}	Id.	7.3	Id.
Viscoplastic hardening at 625°C	R_{0vp}	0 MPa	0 MPa	0 MPa
	Q_{vp1}	40 MPa	40 MPa	40 MPa
	b_{vp1}	569	569	200
	Q_{vp2}	/	40 MPa	20 MPa
	b_{vp2}	/	75	10
	p_c	/	0.03	0.01
Quasi plastic strain rate effect at 625°C	K_{qp}		$112\ MPa.h^{-1/n_{qp}}$	
	n_{qp}		5.0	
Viscoplastic strain rate at 625°C	K_{vp}	$1233\ MPa.h^{-1/n_{vp}}$	$542\ MPa.h^{-1/n_{vp}}$	$395\ MPa.h^{-1/n_{vp}}$
	n_{vp}	3.8	5.38	4.95
Diffusion strain rate at 625°C	K_d	$0.33\ .10^9\ MPa.h^{-1/n_d}$	$0.33\ .10^9\ MPa.h^{-1/n_d}$	$0.020\ .10^9\ MPa.h^{-1/n_d}$
	n_d	1.0	1.0	1.0
GTN model	q_1	1.5	1.5	1.5
	q_2	1.0	1.0	1.0
	f_c	0.1	0.1	0.1
	δ_c	6.0	6.0	6.0
Nucleation by the viscoplastic mechanism	A_{vp1}	0.0	0.01	0.05
	A_{vp2}	0.0	0.15	0.4
	α_{vp}	0.0	2.0	2.0
Nucleation by the diffusional mechanism	A_{d1}	0.0	14.0	5
	A_{d2}	0.0	16.0	0.5
	α_d	0.0	2.0	2.0

Table 2: coefficients defined by V. Gaffard for the 9Cr1Mo mod steel, the HAZ and Weld Metal at 625°C (from reference [2]).

The procedure of identification is quite complex, and requires Finite Element calculations even for the case of creep on smooth specimens, since the dimensional effects must be also considered. This procedure could be summarized as follows:

- first, the quasi-plastic flow coefficients are identified from Smooth Tensile (ST) experimental results. With the coefficients obtained the model may predict the beginning of the monotonic tensile curves. The same coefficients are taken for each zone as the small differences which exist in the different regions should not have a large influence on creep;
- then the viscoplastic flow coefficients are determined on Smooth Creep (SC) specimens. It is experimentally observed that no creep damage exists in these geometries before the necking of the specimen, due to the absence of stress triaxiality, so that the damage can be neglected during the identification phase. For this creep mechanism, the critical strain for softening is different for Base Metal and ICHAZ (respectively 0.03 and 0.01). It must be noted that the tertiary creep dominates the creep life for this type of specimen, and in these precise conditions;
- for the diffusion regime, the coefficients of creep laws are identified from literature test results (Kloc and Sklenicka [11]). As reported previously, there is no isotropic hardening for the diffusion creep regime;

The coefficients for the damage laws are set up as explained thereafter:

- stress triaxiality exponent α_{vp} and α_d are taken from the literature (Mac Lean [12]). Their value is equal to 2;
- the A_{vp1} and A_{d1} coefficients were determined from SC specimens tertiary creep, which is due to strain softening and diameter shrinkage. These coefficients were adjusted to reach the experimental void fractions after necking;
- the A_{vp2} and A_{d2} where determined on NC specimens, since they give the effect of stress triaxiality. Several notch radii were used, allowing the determination of both the location and time to rupture. Note that the location of the rupture could only be obtained from the full model. It is also reported by the author of the study that the secondary creep regime is preponderant on this geometry, due to the notch strain constraint.

A few creep tests have been performed on Compact Tension (CT) specimens, and on Plate Notched (PN) specimens. In both cases, 3D Finite Element calculations have been realized. For the PN specimens, the elongation versus time was very closely reproduced, while for the CT specimens, the opening versus time and also the crack growth rate were found satisfactorily estimated.

Finally, it is interesting to point out some features or remaining questions about the model. First of all, most of the time, the diffusion creep regime may not be reached experimentally, since it corresponds to low stress levels and very large time to rupture. This kind of model shows that the stress triaxiality decreases the time to rupture, so that notched specimens can be seen as experimental ways to enhance the diffusion creep, and to obtain indirect measurement of this phenomenon. Although the enhancement of the mechanism could lead to misinterpretations, by short-circuiting metallurgical strengthening mechanisms which are time dependent (i.e. precipitations). So that it is necessary to perform true long-term tests, in order to really know the creep behaviour at low stress regime. This question is particularly important since the diffusion creep becomes preponderant for design time durations, and this point is not discussed inside design codes.
Coefficients at 550°C are also given in reference [2], but this temperature has been far less studied compared to 625°C. Most of the coefficients are extrapolated, or derived from the literature. As there are less experimental validations at 550°C, the confidence is lower for the coefficients. This is the reason why further works are needed concerning this domain of temperature that is more consistent with the normal operating temperatures of 9Cr1Mo mod structures in the nuclear industry. A Ph. D. study has just started at the Ecole des Mines de Paris on this subject. The temperature of 625°C is a little bit above the temperature reached during some transients on a HTR (like blackout).

At this point, we describe a parametric study on tubular structures with circumferential welds submitted to creep at 625°C.

4.3 PARAMETRIC CALCULATIONS

There are several points that could be studied by Finite Element methods:
- the influence of stress triaxiality;
- the influence of the welding parameters, like weld angle, weld width, HAZ width;
- the effect of geometry, by mean of thickness and diameter.

For this study, the geometry can be simplified as shown on figure 7.

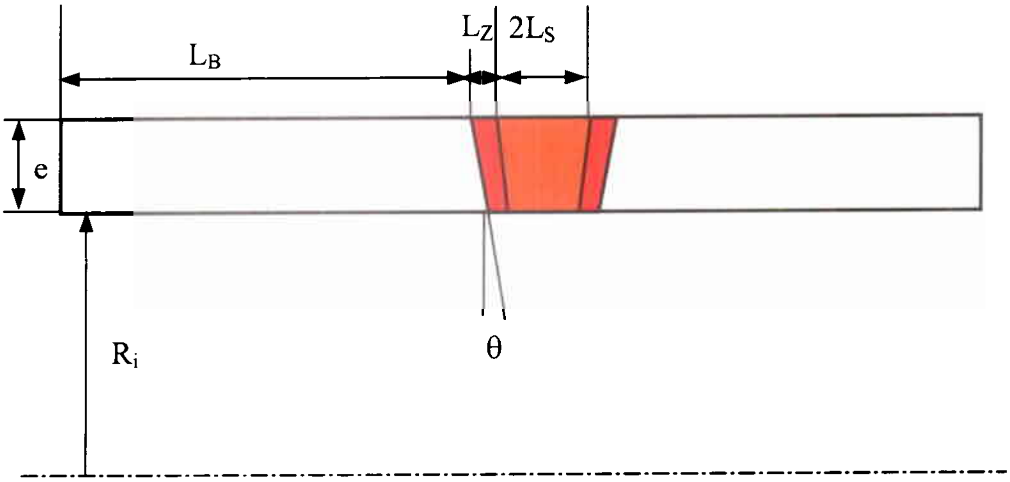

Figure 7: schema of the geometry

In the most recent calculations (performed in 2005) which are presented here, the weld angle θ is set to 2°, and the weld width $2L_s$ = 35 mm. This assumption has been chosen after the first calculation results in 2004, which have shown no influence of these parameters, for $0 < \theta < 2°$ and $20 < 2L_s < 35$ mm [12]. In this reference, 60 calculations were performed as a screening study. It permitted to define the best parameters for the present study.
The tables 3 and 4 show the values of the parameters to study respectively the effects of stress triaxiality and of the geometry.

Reference case	Angle θ (°)	HAZ width L_z (mm)	Weld width $2L_S$ (mm)	Internal radius R_i (mm)	thickness e (mm)	Hoop stress $\sigma_{\theta\theta}$ (MPa)	Axial stress σ_{zz} (MPa)
1	2	5	35	3650	190	150	0
11	2	5	35	3650	190	100	0
21	2	5	35	3650	190	0	150
31	2	5	35	3650	190	0	100
41	2	5	35	3650	190	150	75
51	2	5	35	3650	190	100	50

Table 3: calculation cases for the study of stress triaxiality

Reference case	Angle θ (°)	HAZ width L_z (mm)	Weld width $2\ L_S$ (mm)	Internal radius R_i (mm)	Thickness e (mm)	External Diameter D_e (mm)	Hoop stress $\sigma_{\theta\theta}$ (MPa)	Axial stress σ_{zz} (MPa)
lab_specimen_cas21	2	4	35	0	2,5	5	0	150
lab_specimen_cas31	2	4	35	0	2,5	5	0	100
tube_31,25_cas21	2	5	35	0,625	15	31,25	0	150
tube_31,25_cas21_thin	2	5	35	14,125	1,5	31,25	0	150
tube_31,25_cas31	2	5	35	0,625	15	31,25	0	100
tube_62,5_cas21	2	5	35	16,25	15	62,5	0	150
tube_62,5_cas31	2	5	35	16,25	15	62,5	0	100
tube_LST_cas21	2	5	35	125	15	280	0	150
tube_LST_cas31	2	5	35	125	15	280	0	100
tube_LST_cas21_thick	2	5	35	40	100	280	0	150
tube_LST_cas21_thin	2	5	35	139,85	0,15	280	0	150
tube_625_cas21	2	5	35	297,5	15	625	0	150
tube_625_cas31	2	5	35	297,5	15	625	0	100
tube_CDuct_cas21	2	5	35	1000	100	2200	0	150
tube_CDuct_cas31	2	5	35	1000	100	2200	0	100

Table 4: calculation cases for the estimation of the effect of dimension changes

It can be seen in table 3 that the structure is a very large pressure vessel, submitted to axial stress, or hoop stress due to pressure (but without axial stress), and hoop and axial stresses due to an internal pressure. The first numbers in the reference cases of table 4 refer to the outer diameter, whereas cas21 and cas31 indexes correspond to the level of the axial stresses; as the effect of triaxiality could be considered to be solved (thanks to the study described in table 3). In addition, lab_specimen means "small specimen tested in laboratory", LST means "Large Scale Tests", Cduct is set for "Cross-Duct" geometry.

The calculations and some typical results can be further detailed at this point.

4.3.1 Mesh, boundary conditions, and loads

The figure 8 shows a typical mesh (cases 1 to 51 for the pressure vessel) in a 2D axisymmetric model.

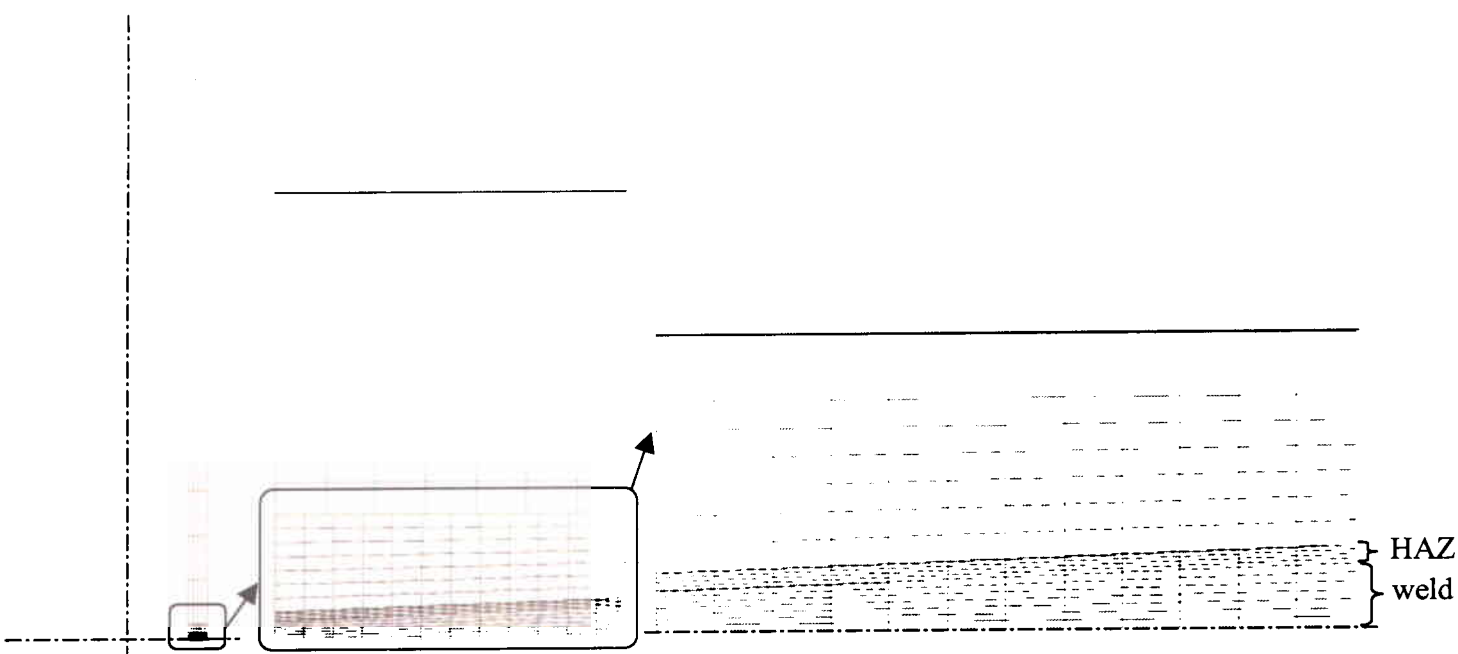

Figure 8: example of a mesh (pressure vessel case), with a detail in the weld area

For all the geometries, quadratic 8 nodes elements were used. There were always 12 elements in the thickness direction (near the weld), 7 elements in the half-width of weld, and 4 elements in the HAZ width. The number of elements in Base Metal is reduced as the distance to the centre increases. The length of base metal is calculated according to the β shell parameter, as explained in chapter 3.2. It can be seen that the thickness is increased at the extremity of the tubes; there are two reasons for this choice, which may not impact the calculated stress/strains in the weld region most of the time:

- the higher thickness is a real feature in laboratory specimens, pressure vessel components which have flanges, and the future Large Scale Tests. Otherwise, the deformations of the ends will be higher than those in the centre, for the internal pressure cases of constant thickness tubes. Such a result is not representative of the real pressurized components that are always closed geometries;
- as the temperature is constant in our calculations, it is necessary to restrain the deformation of the end of the tube. Also, for the LST, there is a temperature gradient along the tube due to the cooling heads, so that the centre has higher strains compared to the ends.

Nevertheless, some additional calculations should be performed on real geometries to verify that there are no unexpected effects, compared to the results obtained on the ideal conditions of the present study.

Half of the structures are represented, so that the weld is in the centre of the real geometry: on the symmetry line, the axial displacement is imposed to zero. The different loads are applied as follow:

- the axial stress is applied at the end of the mesh, but the level of the stress indicated in the tables 3 and 4 correspond to the initial level in the centre of the structure. This load is kept constant, so that the axial stress may increase when the accumulated strain is large;
- the hoop stress is imposed by mean of an internal pressure. Again, the level reported in the tables represent the initial hoop stress value in the centre of the mesh. The pressure is kept constant, so that the hoop stress will increase when the thickness will reduce due to the deformations;
- the internal pressure with induced end load is a combination of the two precedent cases, but the axial stress is imposed to be half the hoop stress.

4.3.2 Conditions of the calculations

Some important hypotheses have been taken:

- the large displacements option is used, meaning that the dimensions of the structure are updated at each step;
- the internal pressure is always applied normal to the elements, even in the case of very large swelling of the structure during the calculation. The influence of this option is very sensitive in the last instants of the calculations (not taking it into account can increase the calculated life by about 20%). This assumption is realistic in case of gas or liquid pressurized components;
- the uncoupled model is used here. Its accuracy has been found sufficient compared to the full model [2]. The coefficients of table 2 are used in the adequate zones.

In addition, a procedure was followed to stop the calculations: near to the rupture, the strain rates often increase drastically due to local shrinkage. So that it was necessary to restart the calculations when the strain increment became larger than 5.10^{-3}, and to refine the corresponding time step manually. The calculations were stopped when the total damage reached 0.1 somewhere in the structure, corresponding to creep crack initiation.

4.3.3 Results of parametric calculations

There are lot of results to describe; the strains, stresses, and damage have an evolution both in space and time. For this report, it is proposed to describe the particular behaviours that have been observed. Then we will try to present a synthesis of the results with a few simple curves giving the effect of stress triaxiality and structure size.

First, it is interesting to look at the stress components. The initial stresses are homogeneous and correspond to the initial loadings. Then, due to the creep strain, there are stress redistributions between the different zones: a hoop stress appears in the case of pure initial uniaxial creep (figure 9 for a thick vessel and figure 15 for a small laboratory specimen); in the case of internal pressure, the hoop stress can locally vanish (even for the so-called primary stress loadings, the hoop stress is dependent on the width of the HAZ, and it can decrease due to the different material properties). For the axial stress, there is also a big difference between thick and thin structures; for the latter, stress redistribution affects the whole thickness (figure 16), whereas for the thick vessel, the axial stress increases only very locally, at internal and external side (figure 10).

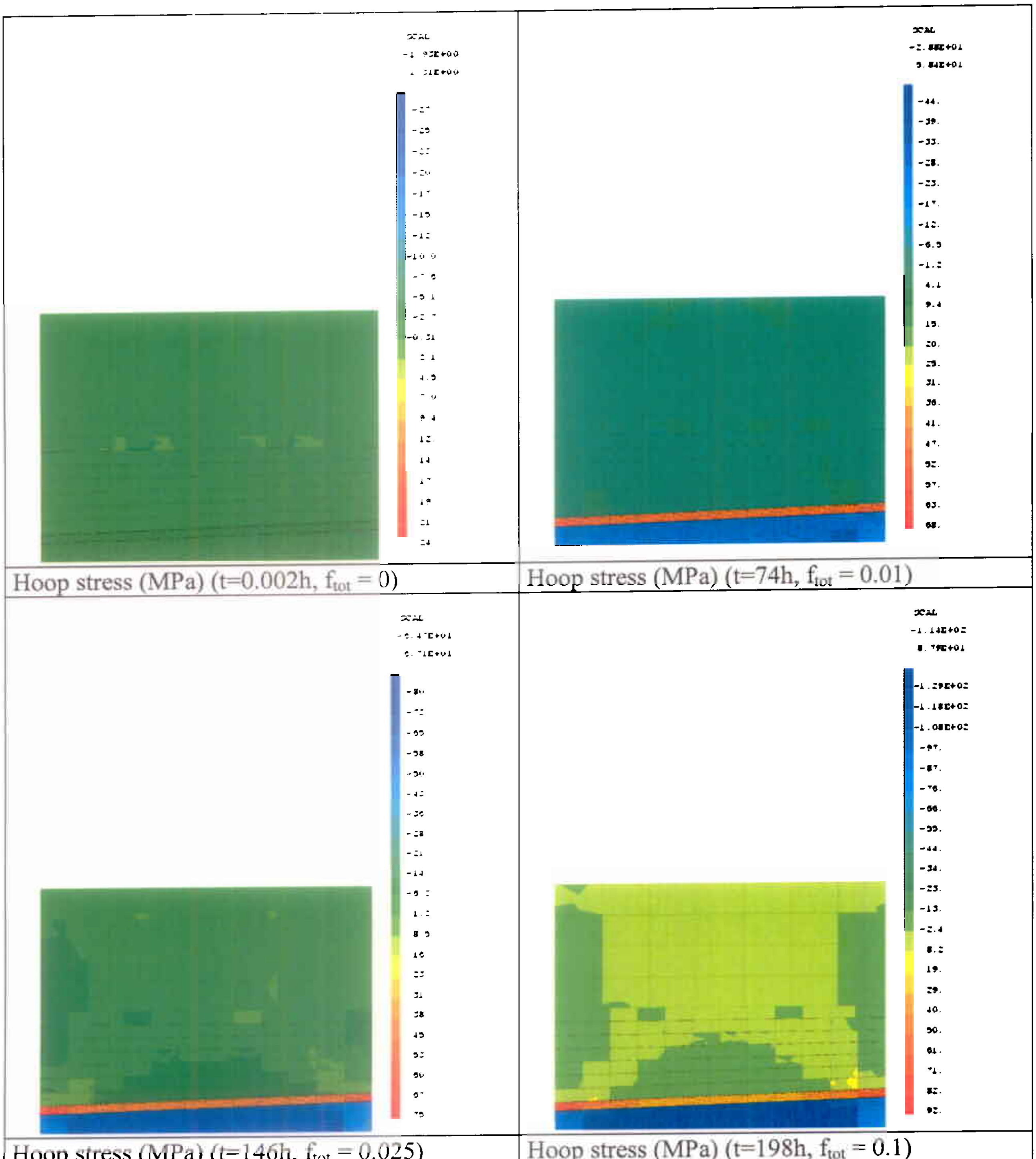

Hoop stress (MPa) (t=0.002h, f_{tot} = 0)

Hoop stress (MPa) (t=74h, f_{tot} = 0.01)

Hoop stress (MPa) (t=146h, f_{tot} = 0.025)

Hoop stress (MPa) (t=198h, f_{tot} = 0.1)

Figure 9: hoop stress evolution during axial creep of a vessel with circumferential weldment (case 21)

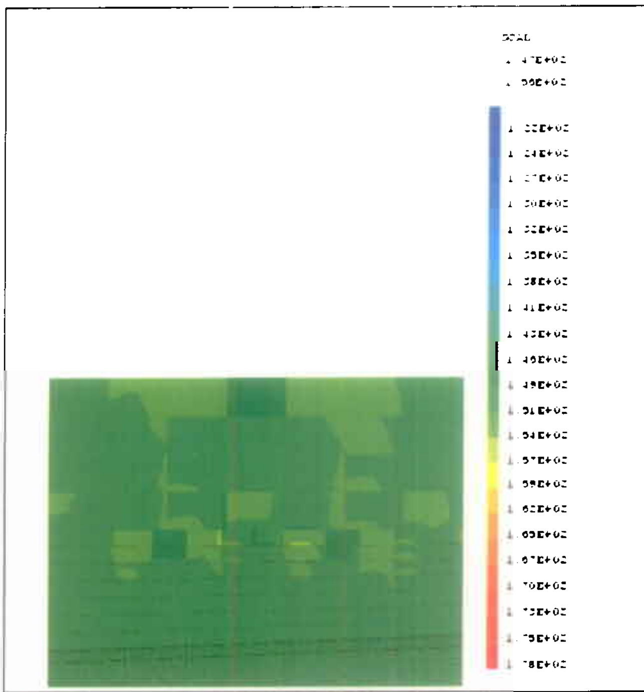

Axial stress (MPa) (t=0.002h, $f_{tot} = 0$)

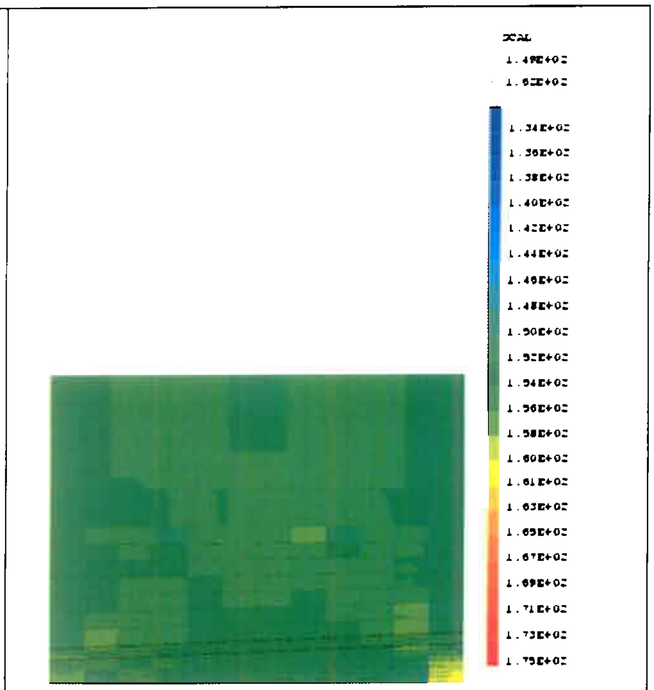

Axial stress (MPa) (t=74h, $f_{tot} = 0.01$)

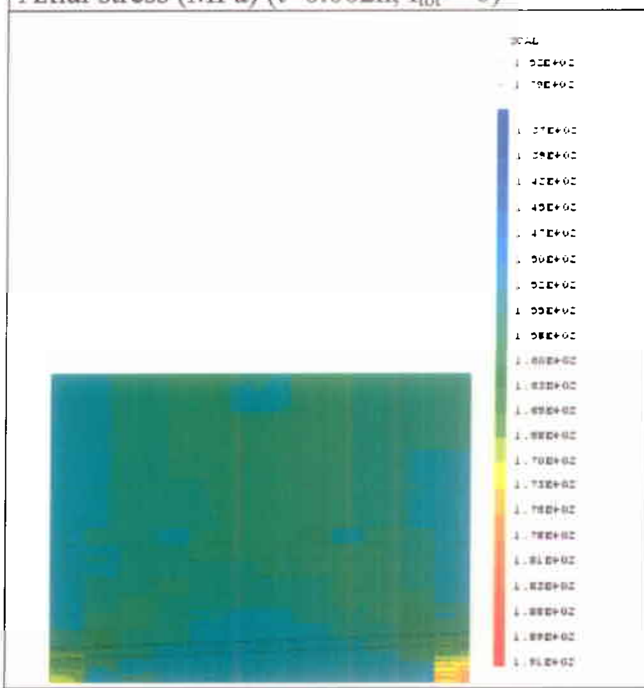

Axial stress (MPa) (t=146h, $f_{tot} = 0.025$)

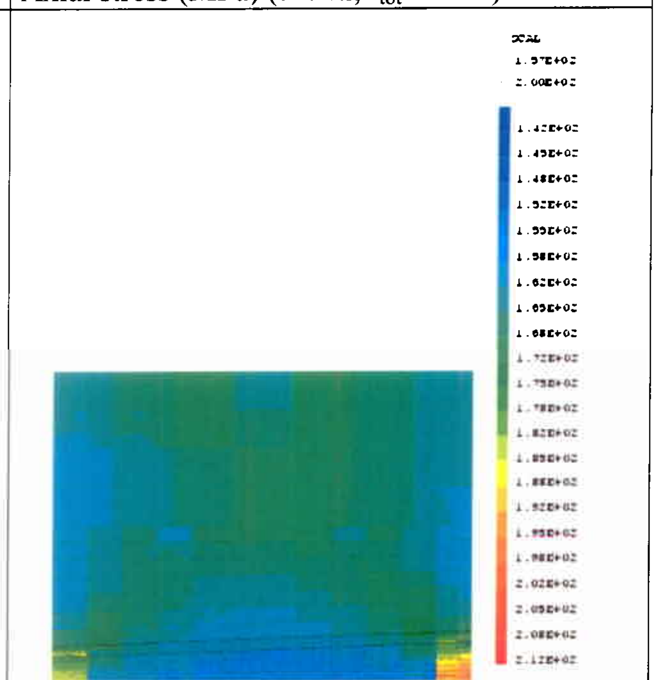

Axial stress (MPa) (t=198h, $f_{tot} = 0.1$)

Figure 10: axial stress evolution during axial creep of a vessel with circumferential weldment (case 21)

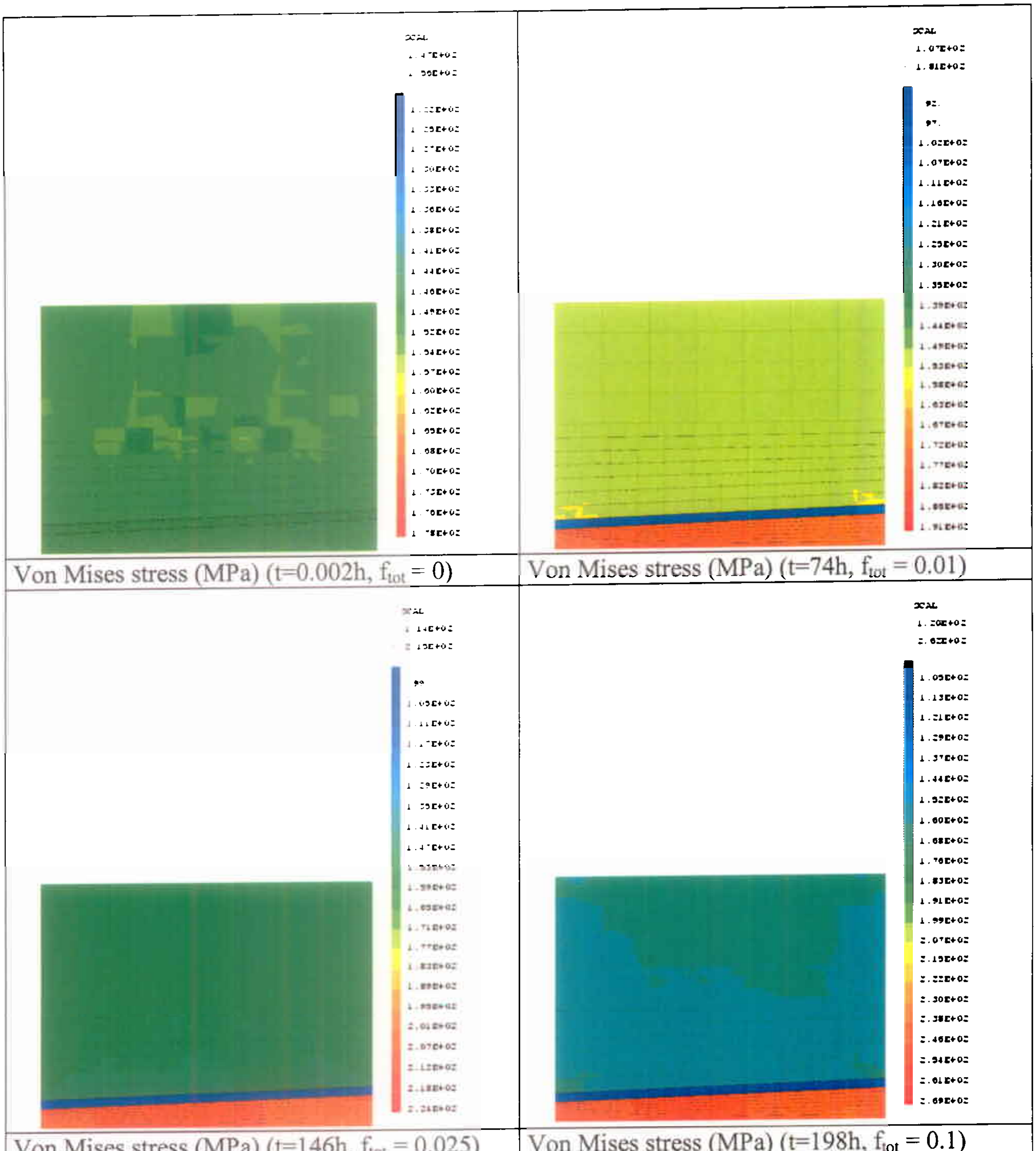

Von Mises stress (MPa) (t=0.002h, f_{tot} = 0)

Von Mises stress (MPa) (t=74h, f_{tot} = 0.01)

Von Mises stress (MPa) (t=146h, f_{tot} = 0.025)

Von Mises stress (MPa) (t=198h, f_{tot} = 0.1)

Figure 11: Von Mises stress evolution during axial creep of a vessel with circumferential weldment (case 21)

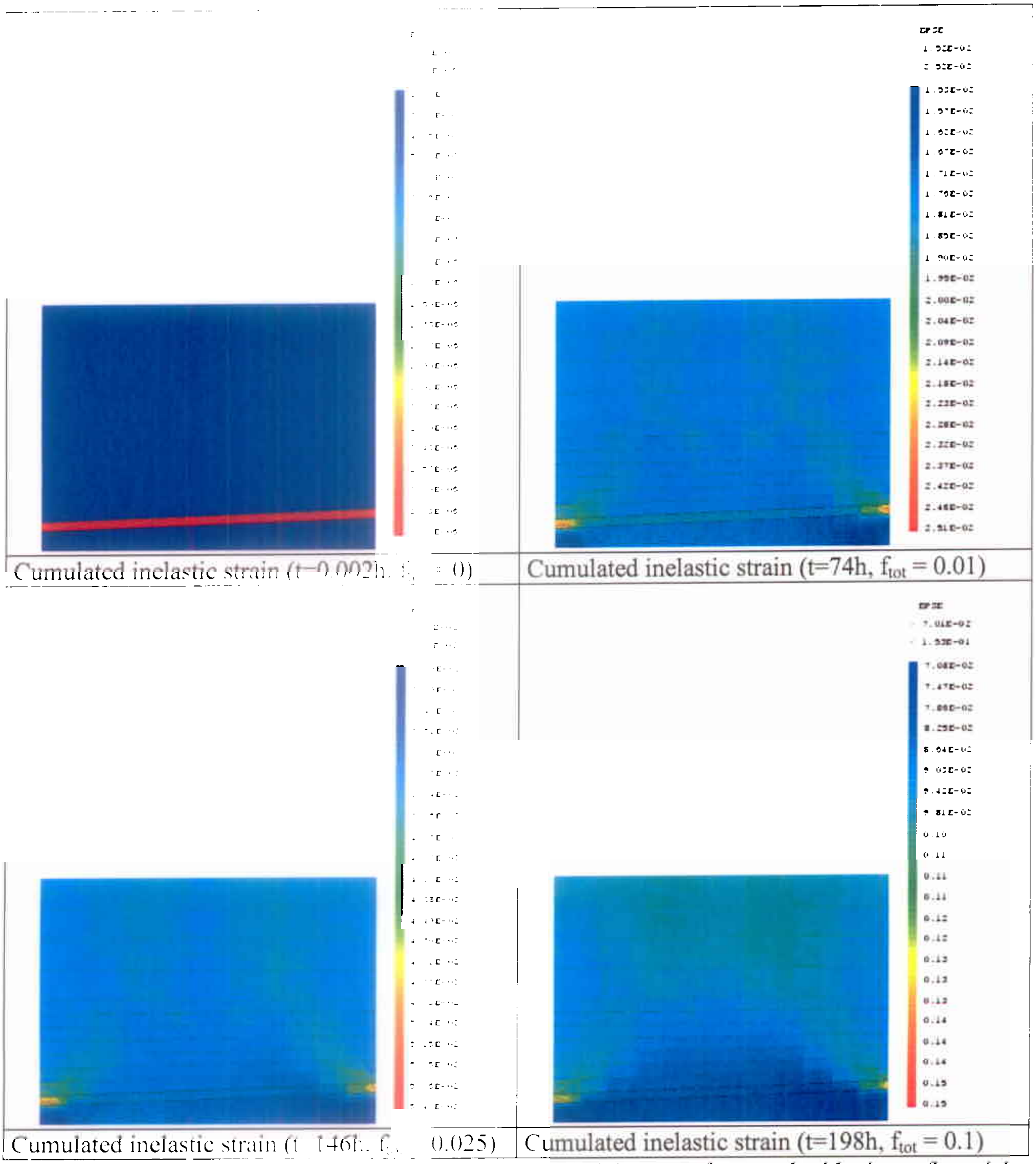

Cumulated inelastic strain ($t=0.002h$, $f_{tot} = 0$)

Cumulated inelastic strain ($t=74h$, $f_{tot} = 0.01$)

Cumulated inelastic strain ($t=146h$, $f_{tot} = 0.025$)

Cumulated inelastic strain ($t=198h$, $f_{tot} = 0.1$)

Figure 12: cumulated inelastic strain evolution during axial creep of a vessel with circumferential weldment (case 21)

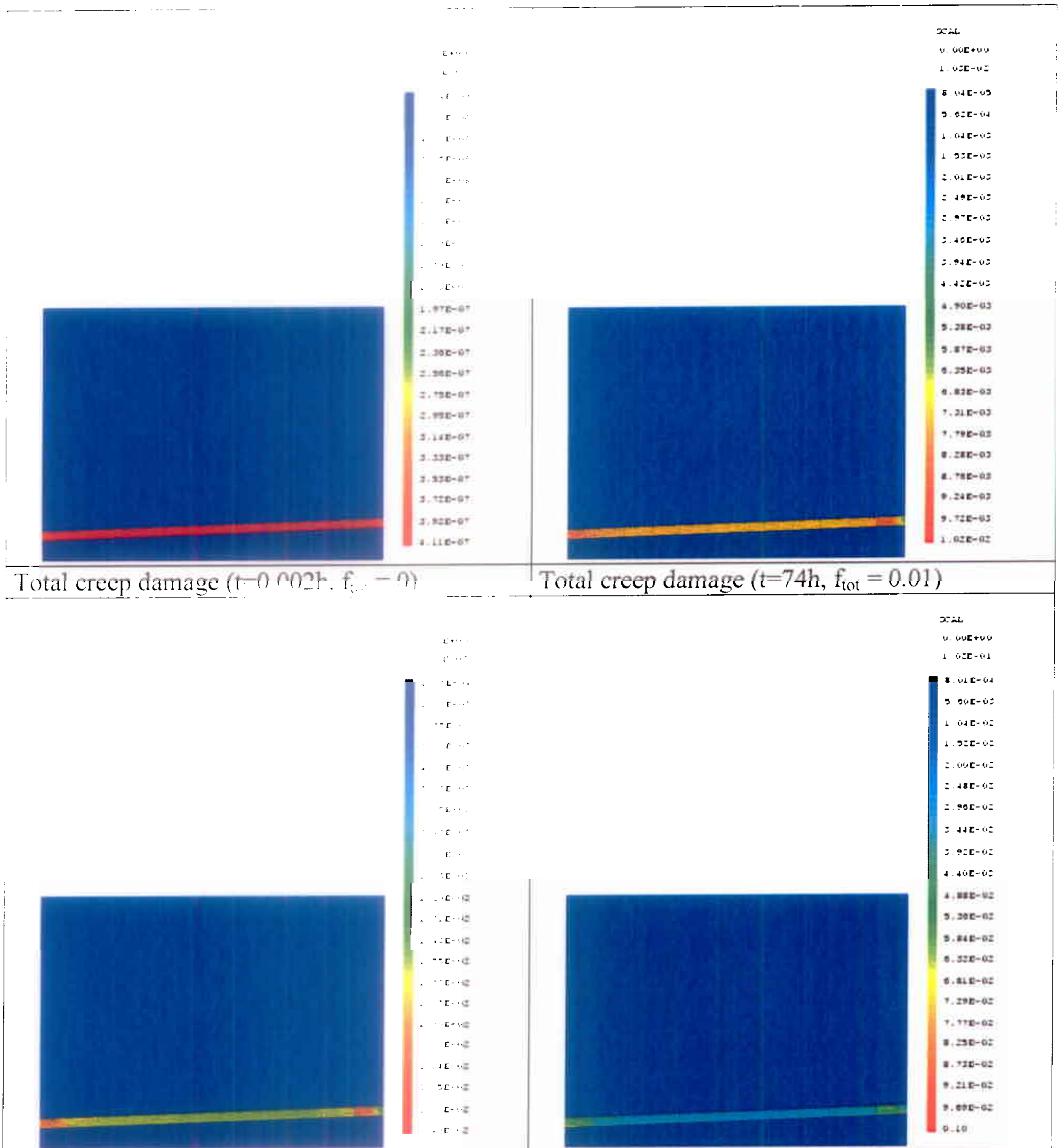

Total creep damage (t=0.002h, f_{tot} = 0) | Total creep damage (t=74h, f_{tot} = 0.01)

Total creep damage (t=146h, f_{tot} = 0.025) | Total creep damage (t=198h, f_{tot} = 0.1)

Figure 13: total creep damage evolution during axial creep of a vessel with circumferential weldment (case 21)

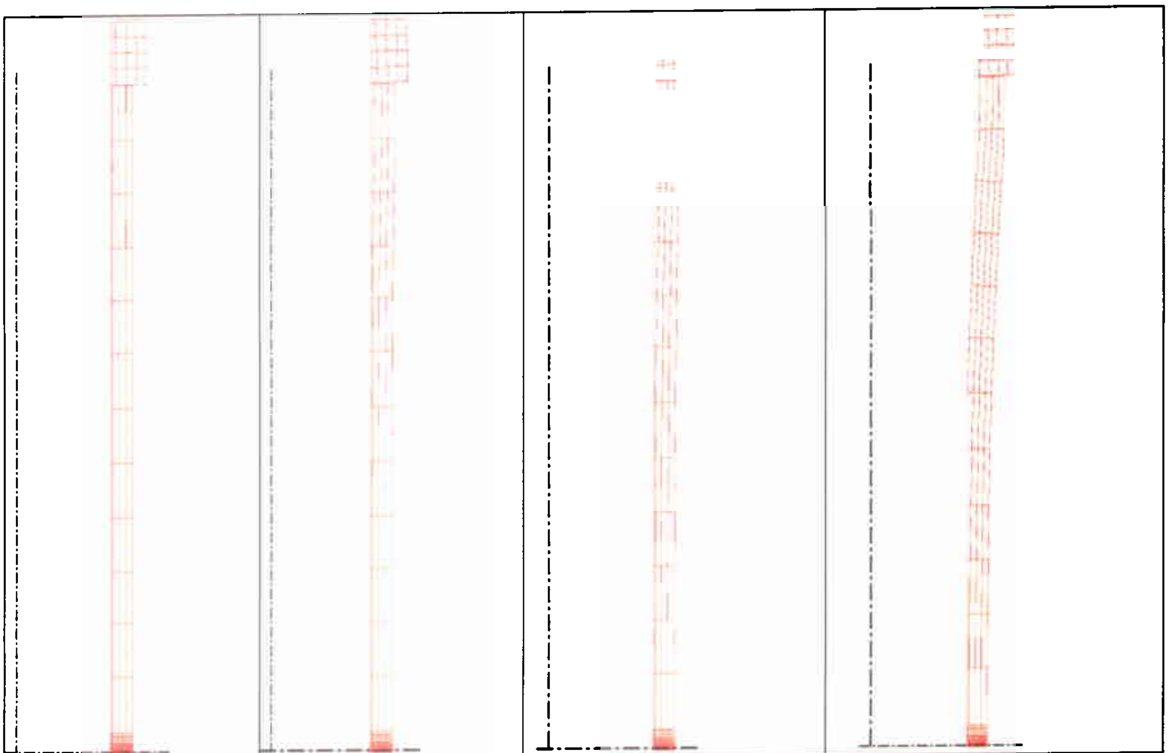

t=0.002h, f_{tot} = 0	t=74h, f_{tot} = 0.01	t=146h, f_{tot} = 0.025	t=198h, f_{tot} = 0.1

Figure 14: deformed shape evolution (x1) during axial creep of a vessel with circumferential weldment (case 21)

This particular behaviour can be explained by the link between strain and geometry: for the thick component, the deformations of the HAZ are restrained by the surrounding Base Metal (figure 12). On the contrary, for thin specimens, the width of HAZ is sufficiently important to lead to an unrestrained behaviour; the Base and Weld metals can't decrease the strain rate in HAZ. It can be seen on figure 18 that the whole thickness of HAZ in small specimens has a rather homogeneous equivalent inelastic strain. For this kind of geometries and loadings, the damage of the HAZ is located in the region corresponding to the highest cumulated inelastic strains and also to the highest stress components (figure 13 and 19). It must be noted that the mesh shown on the isovalues is just a part of the whole geometry (as can be seen by comparison on the deformed shape of figures 14 and 20).

The figures 9 to 13 for the thick vessel, and 15 to 19 for the small laboratory specimen, seem to indicate that once the stress redistribution has occurred, a stabilized strain regime is reached. Thus the stress and strain patterns do not change largely between the times associated to maximum total damage f_{tot}= 0.01 and f_{tot}= 0.1. This point can be confirmed by looking at the evolution of stresses, strains and damage with time.

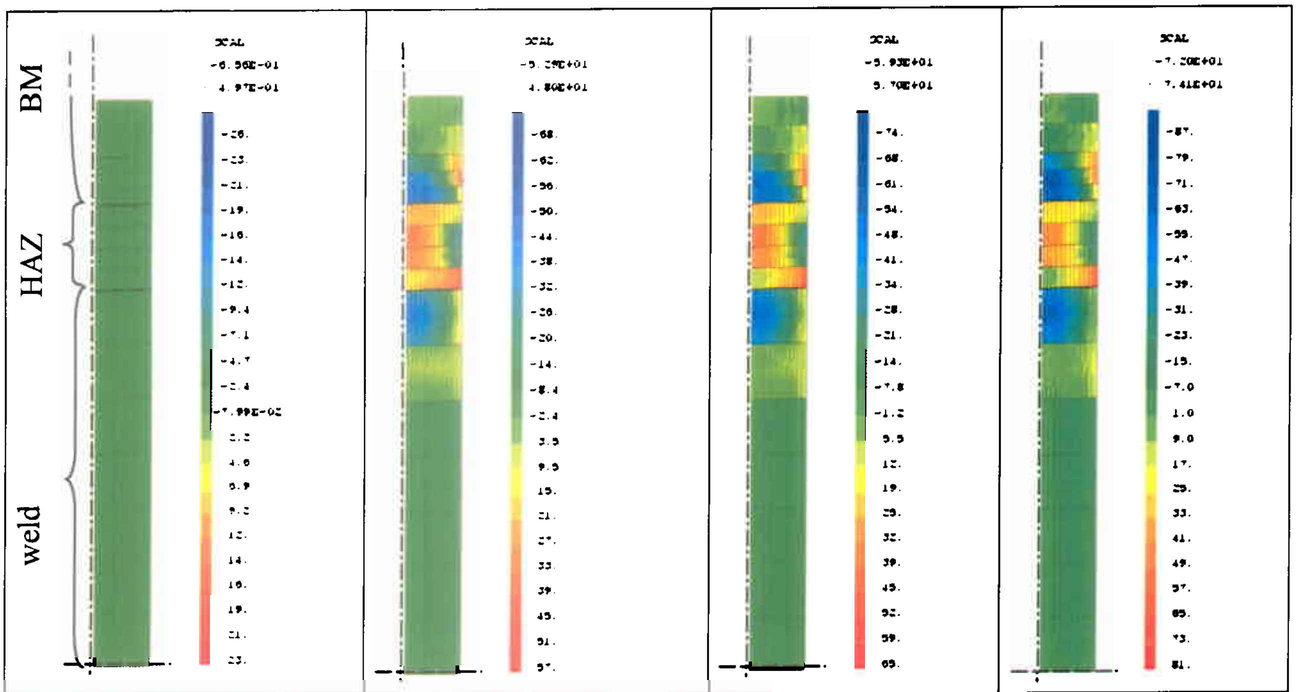

t=0.002h, $f_{tot} = 0$	t=10h, $f_{tot} = 0.01$	t=18h, $f_{tot} = 0.025$	t=33h, $f_{tot} = 0.1$

Figure 15: hoop stress evolution (MPa) during axial creep of a small cross weld specimen (lab_specimen_cas21)

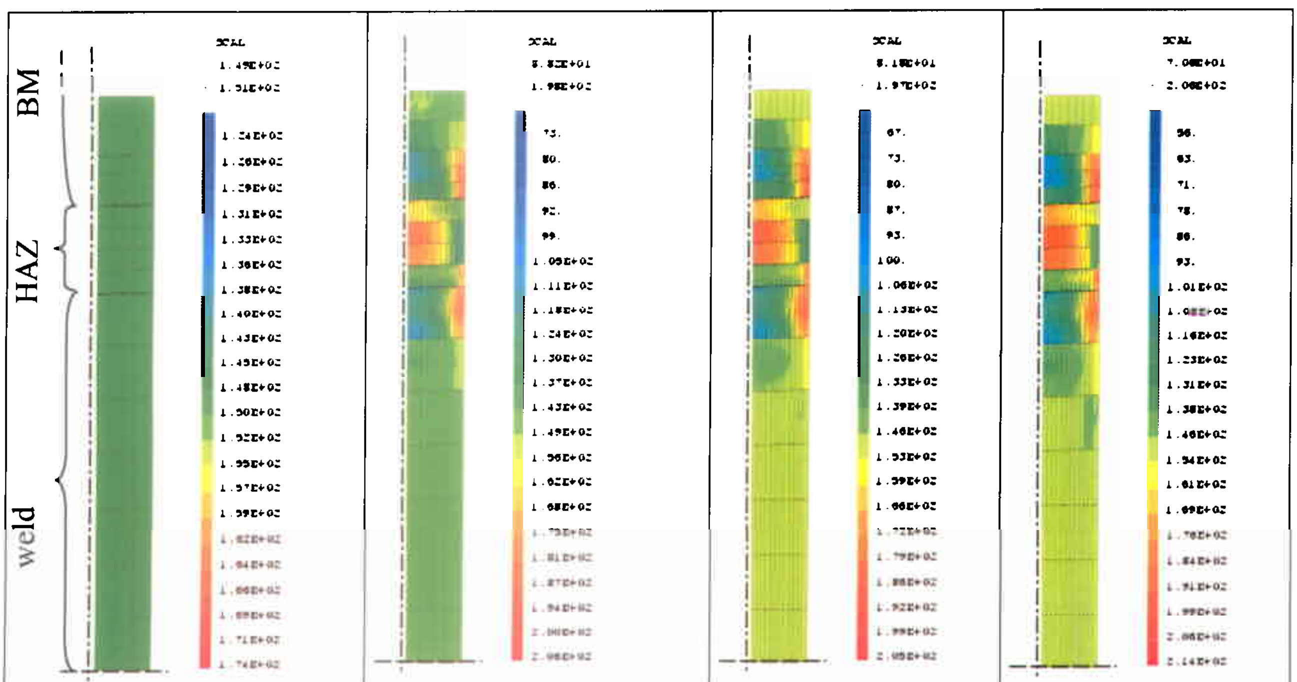

t=0.002h, $f_{tot} = 0$	t=10h, $f_{tot} = 0.01$	t=18h, $f_{tot} = 0.025$	t=33h, $f_{tot} = 0.1$

Figure 16: axial stress evolution (MPa) during axial creep of a small cross weld specimen (lab_specimen_cas21)

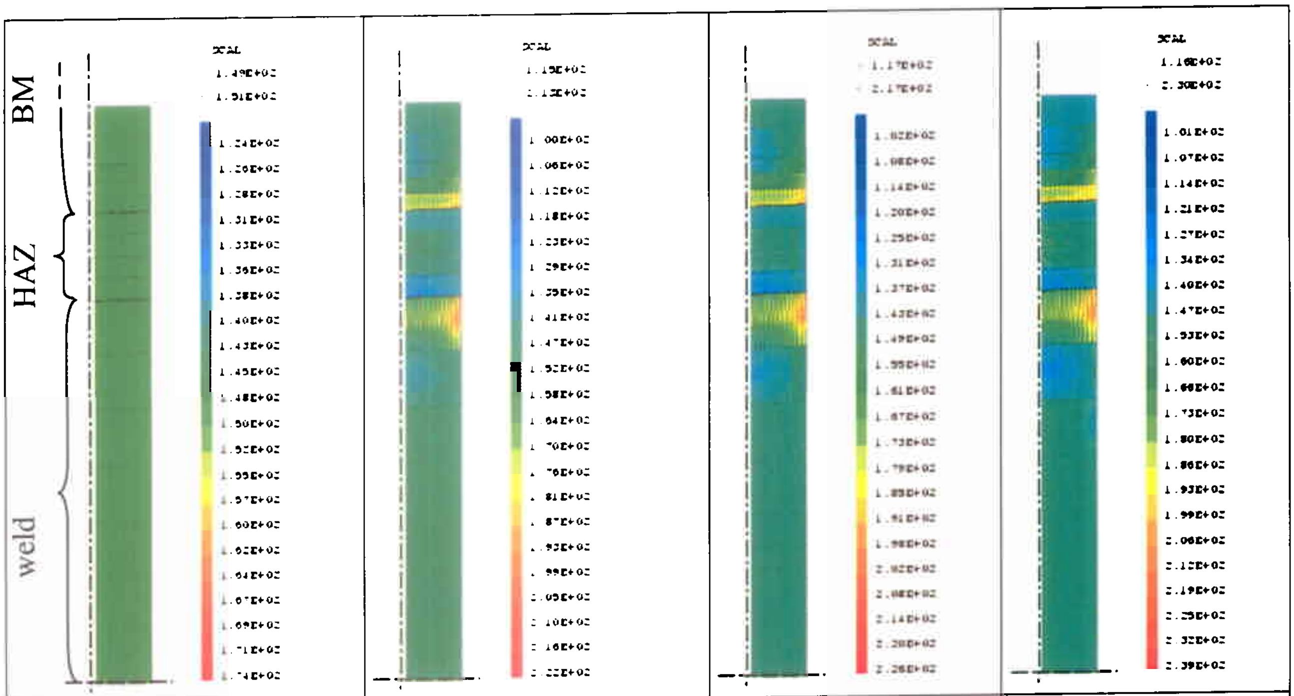

t=0.002h, $f_{tot} = 0$	t=10h, $f_{tot} = 0.01$	t=18h, $f_{tot} = 0.025$	t=33h, $f_{tot} = 0.1$

Figure 17: Von Mises stress evolution (MPa) during axial creep of a small cross weld specimen (lab_specimen_cas21)

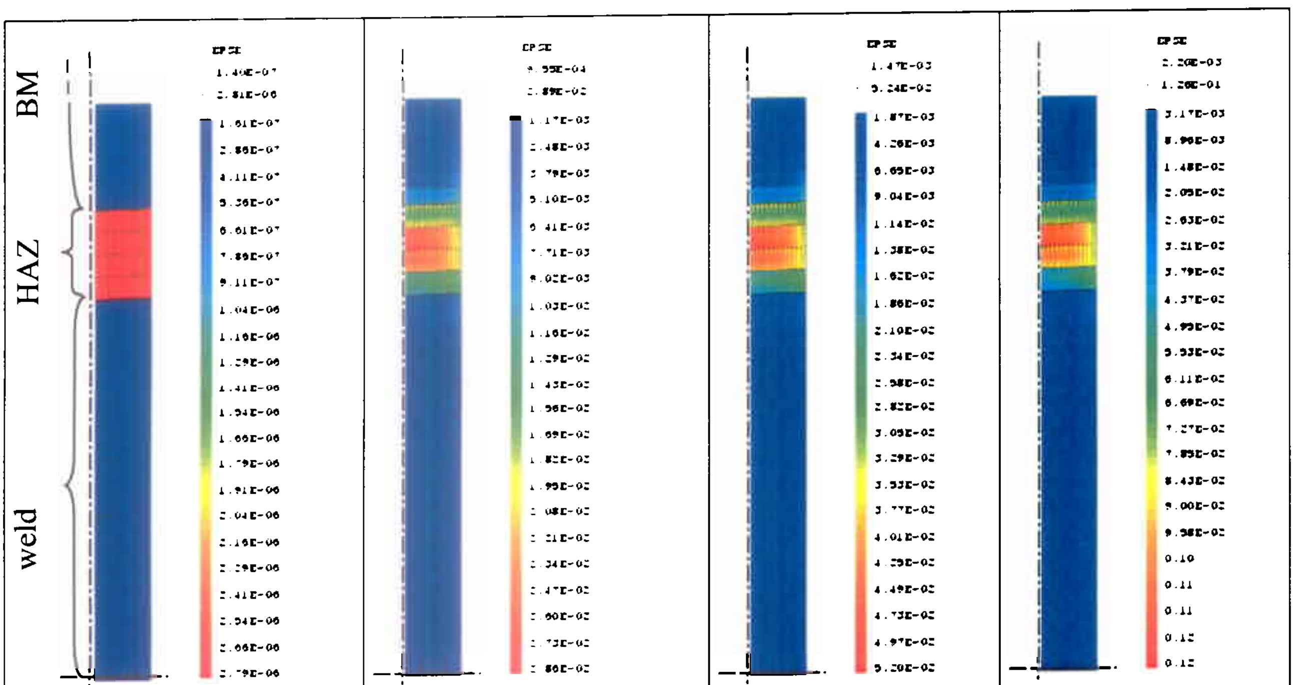

t=0.002h, $f_{tot} = 0$	t=10h, $f_{tot} = 0.01$	t=18h, $f_{tot} = 0.025$	t=33h, $f_{tot} = 0.1$

Figure 18: cumulated inelastic strain evolution during axial creep of a small cross weld specimen (lab_specimen_cas21)

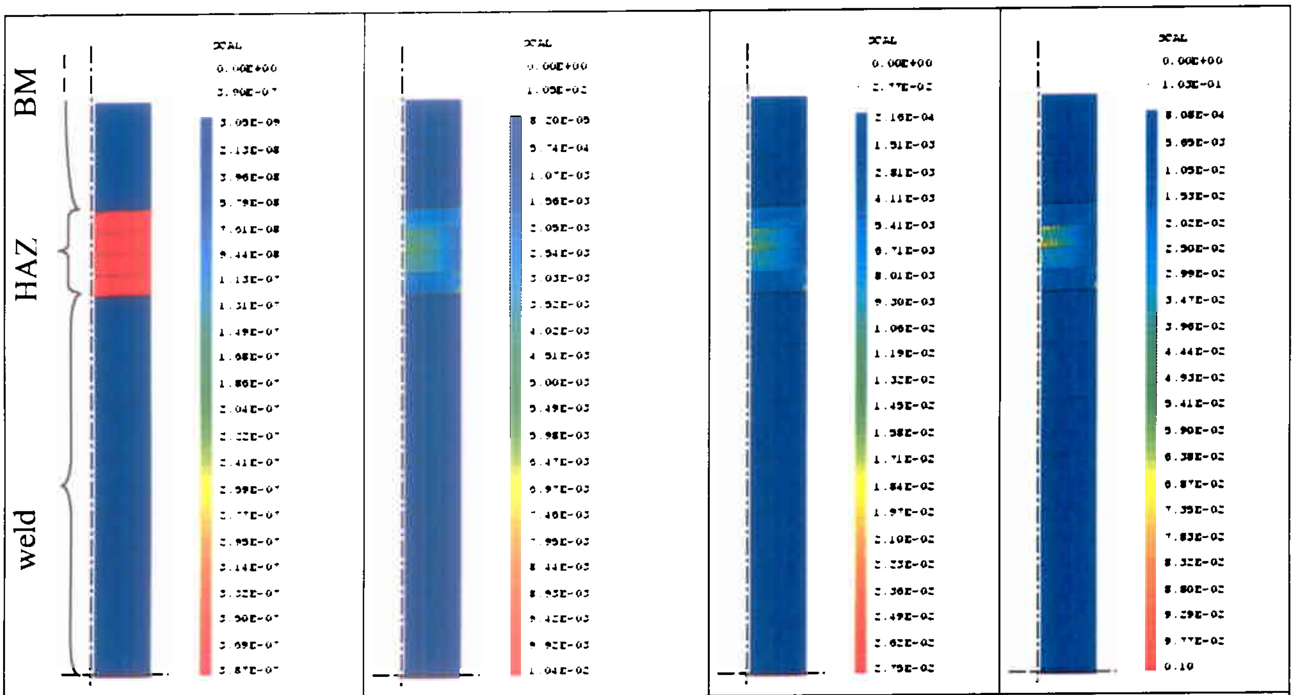

t=0.002h, f_{tot} = 0	t=10h, f_{tot} = 0.01	t=18h, f_{tot} = 0.025	t=33h, f_{tot} = 0.1

Figure 19: total creep damage evolution during axial creep of a small cross weld specimen (lab_specimen_cas21)

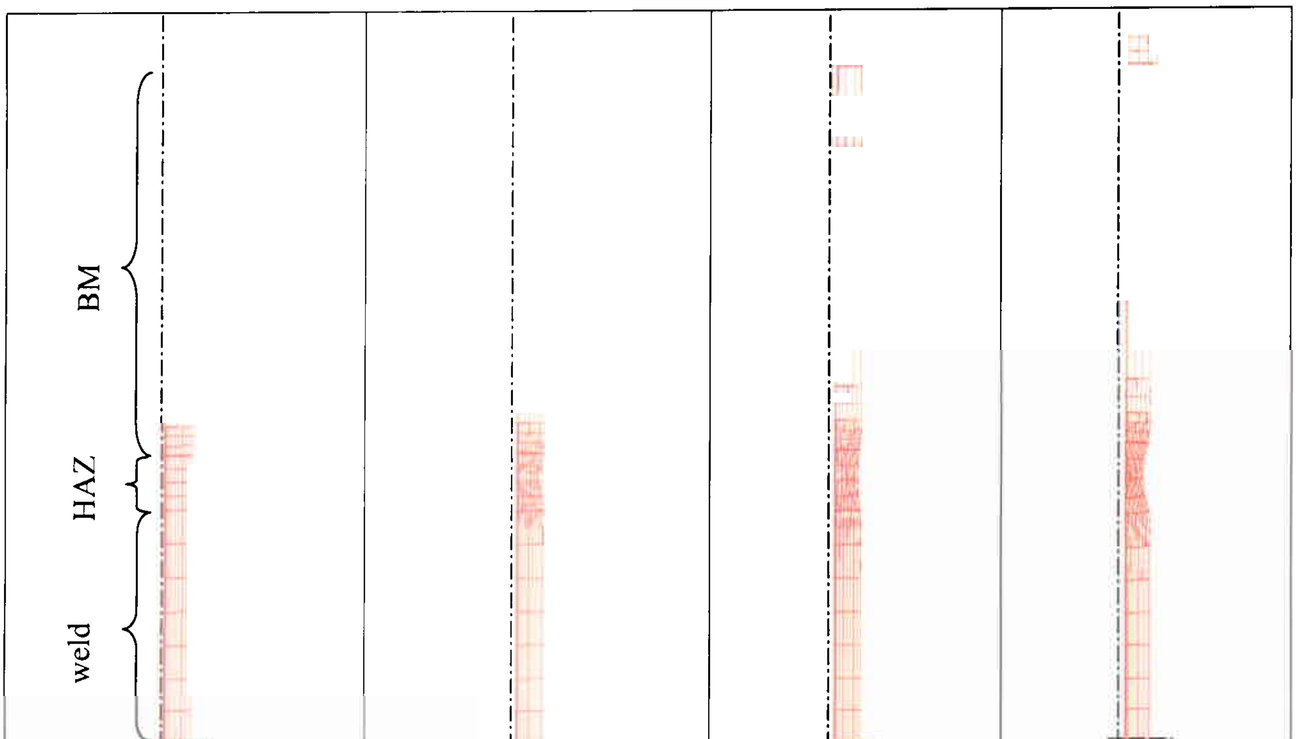

t=0.002h, f_{tot} = 0	t=10h, f_{tot} = 0.01	t=18h, f_{tot} = 0.025	t=33h, f_{tot} = 0.1

Figure 20: deformed shape evolution (x5) during axial creep of a small cross weld specimen (lab_specimen_cas21)

To ameliorate our understanding, we have calculated the creep behaviour of the model for the HAZ and the Base Metal alone. The numerical model is simplified as it takes only the viscoplastic behaviour (neglecting the diffusion). The model is able to represent the isotropic hardening and the strain recovery, but there is no stress enhancement due to the reduction of the cross section (i.e. no large displacements). So that it may underestimate the strain rates for strains higher than 3%. The coefficients that were used are those of table 2. The results have been compared to the values taken from the Finite Element Cross-Weld calculations.
For instance we can see on figures 21 and 22 that the maximum cumulated inelastic strains of HAZ and BM are:

- for thin welded structures, very similar to the HAZ alone (calculated from the simplified numerical model). This means that the strains of the base metal are increased by the deformations produced in HAZ;
- for thick welded structures, close to the Base Metal alone (calculated from the simplified model). This point confirms that the Base Metal restrains the deformations of the HAZ as reported previously.

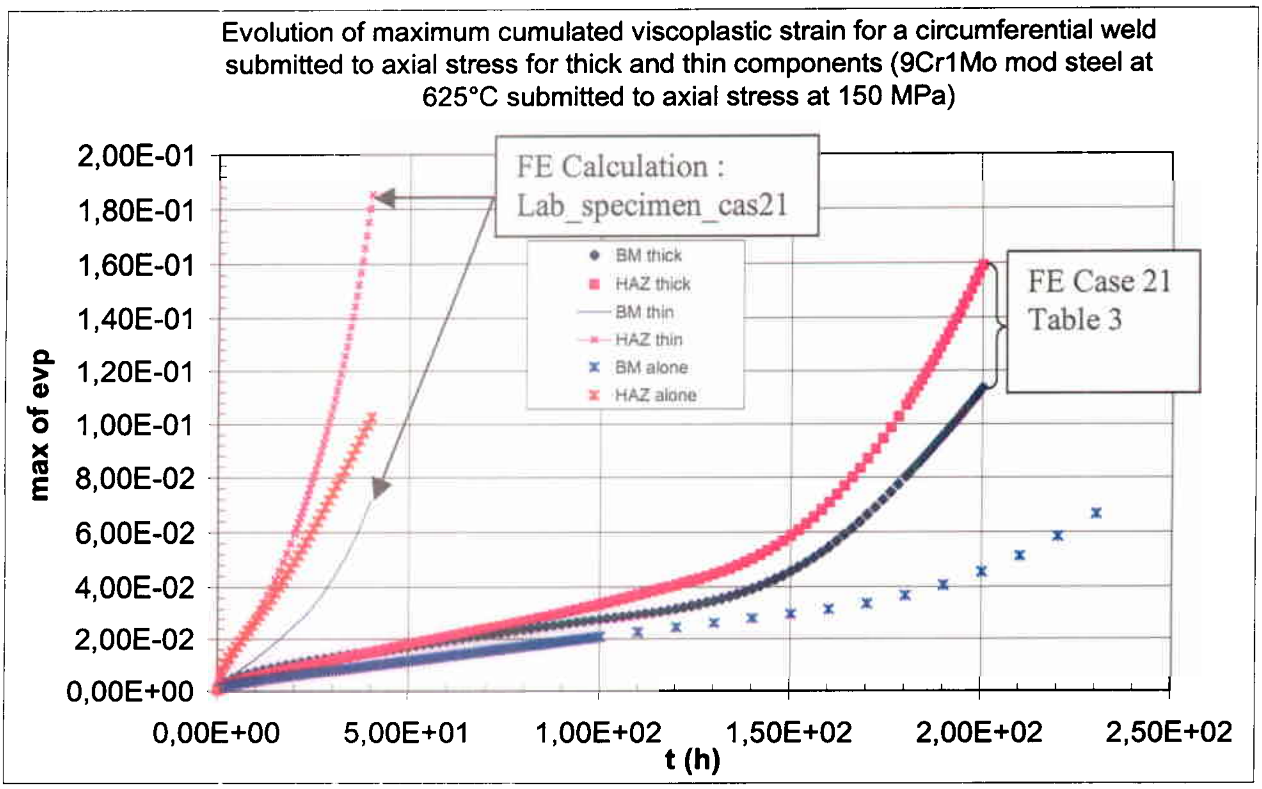

Figure 21: maximum cumulated creep strain in two Finite Element calculations simulating axial creep at a same stress level

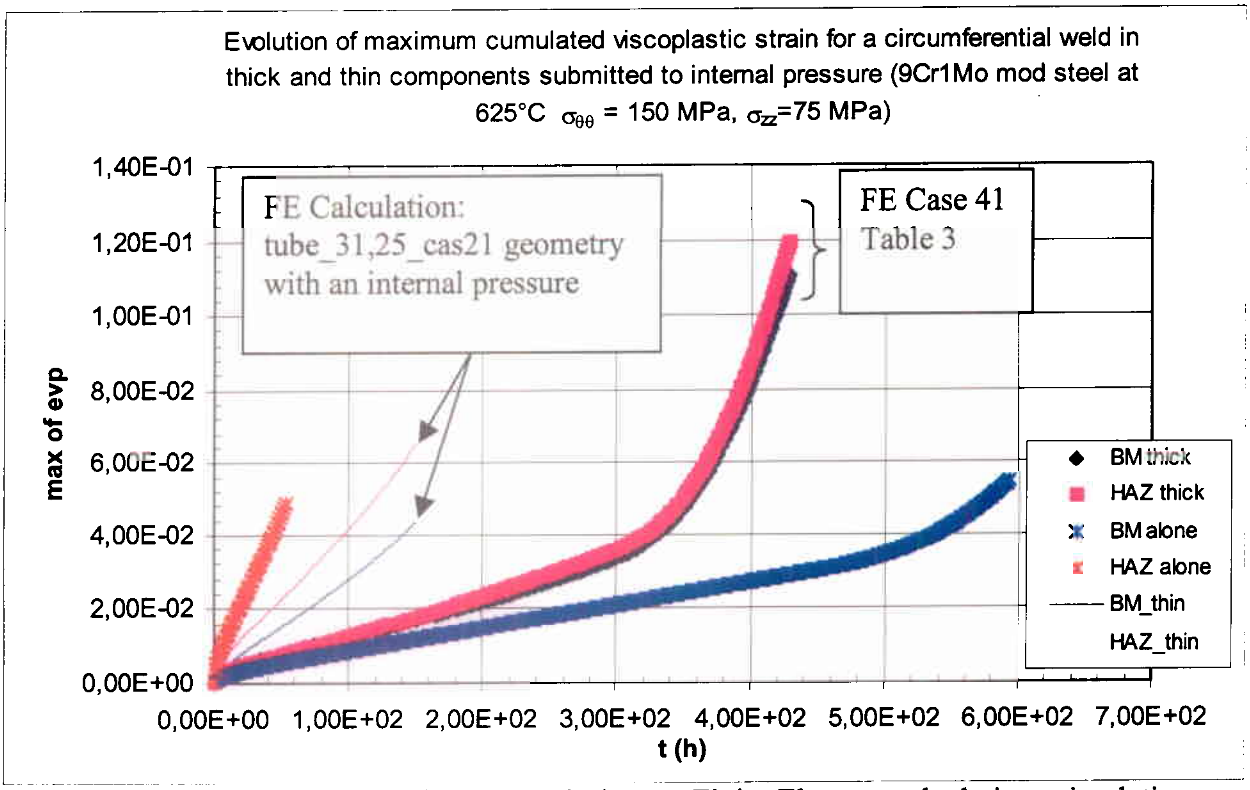

Figure 22: maximum cumulated creep strain in two Finite Element calculations simulating creep for a tube with internal pressure at a same stress level

It is also interesting to plot on figure 23 and 24 the total maximum damage in the HAZ and in the Base Metal. The damage in the HAZ is much larger than the Base Metal one (the differences coming from the strains are amplified by the damage function. Even for the same strain evolution, the HAZ damage would be greater than in BM.

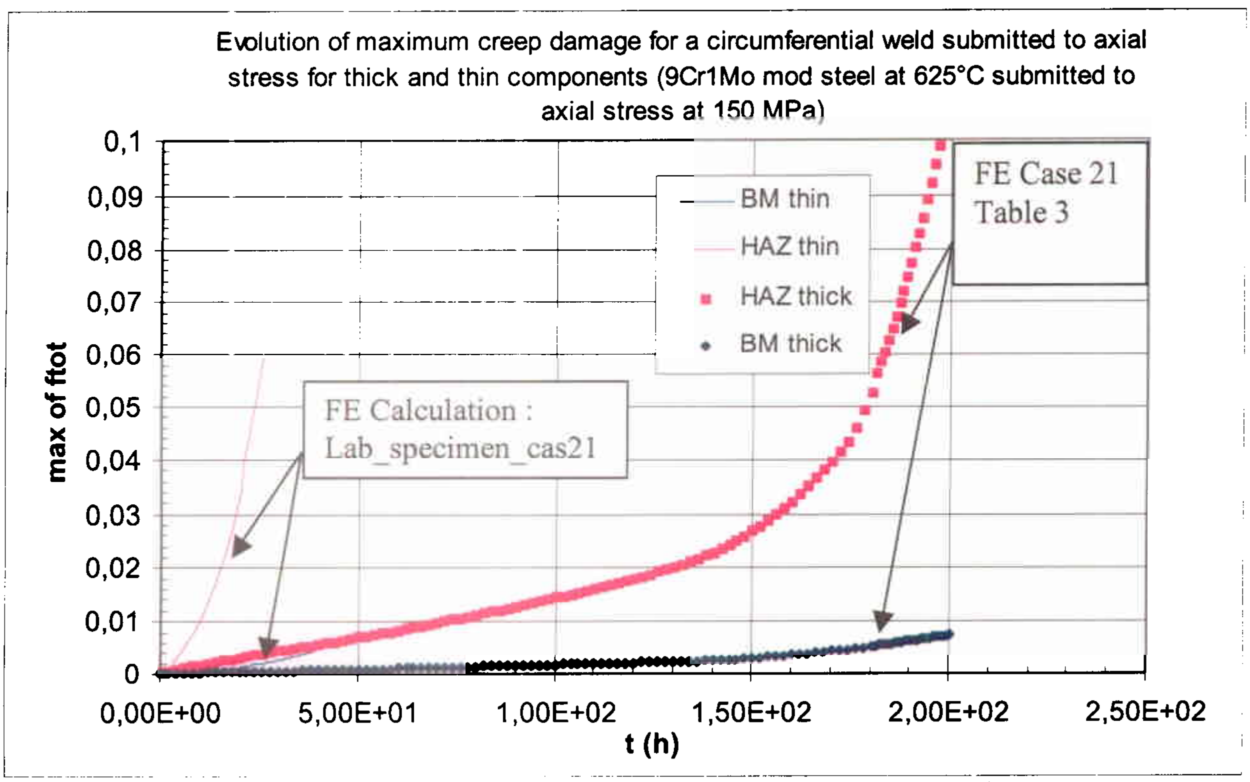

Figure 23: maximum creep damage in two Finite Element calculations (axial creep)

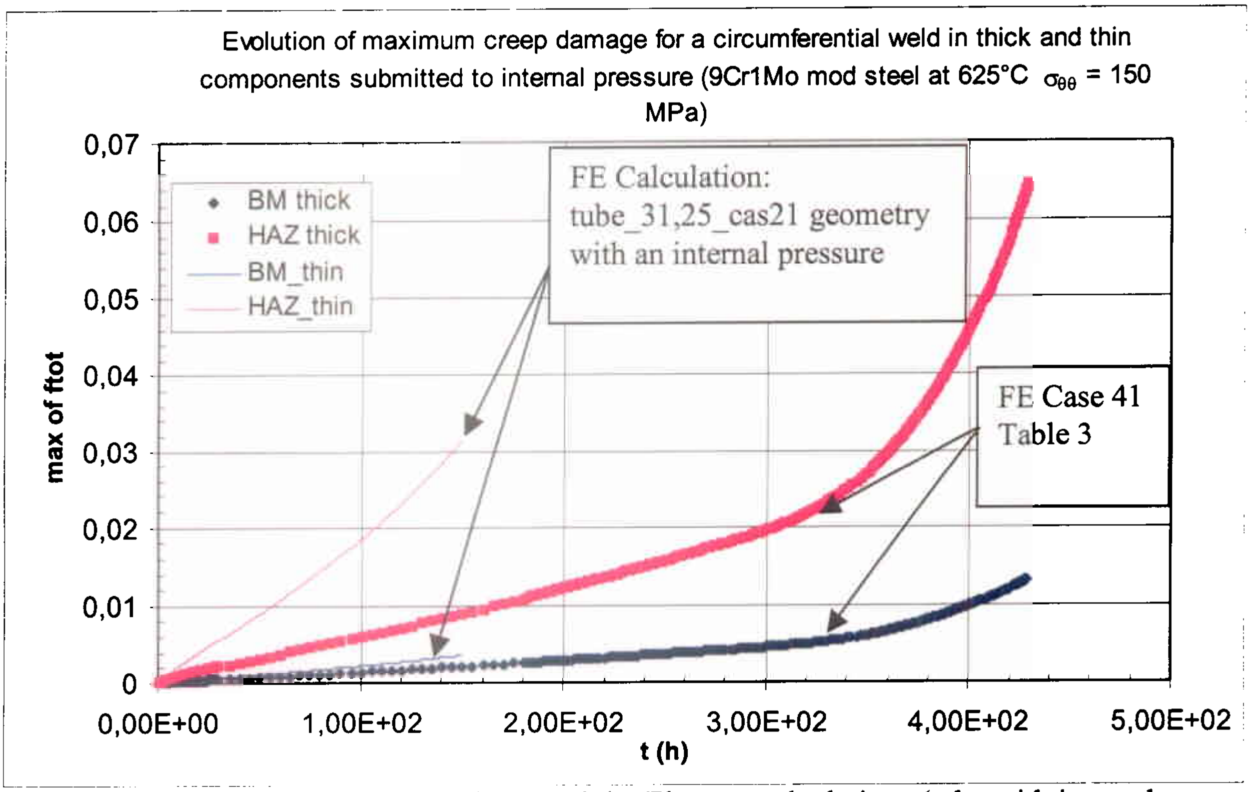

Figure 24: maximum creep damage in two Finite Element calculations (tube with internal pressure creep)

4.3.3.1 Equivalent stress representation

The creep initiation is reached when total damage $f_{tot} = 0.1$. We plot on the figure 25 the results of table 3, with the time corresponding to calculated creep initiation in abscissa, and with different equivalent stresses in ordinate (see paragraph 3.2 for more details). In fact the only case with a difference in the equivalent stresses is the internal pressure with axial effect; for the axial force, the three criteria give the same stress value (equal to the initial axial stress). For the internal pressure, the three criteria are still approximately the same. So that the maximum differences are observed for the structures submitted to internal pressure with axial effect. The stress from the Maximum Strain Energy (SMSE on figure 25) formula does not fit the three stress states, for 100 MPa, and for 150 MPa stress levels (as the SMSE slopes of the three triangle points at 100 MPa and 150 MPa are very different from the slope of the uniaxial creep tests on Base Metal (RCC-MR): the SMSE slopes are nearly constant which is close to a maximum principal stress criterion). At the opposite, the Von Mises criterion gives the lowest stress levels (rhombus points on the figure 25). Thus, the Peak Rupture stress (SPRS on the figure 25) is exactly between the two precedents, and the tendency seems to agree better with the slope of uniaxial creep tests.

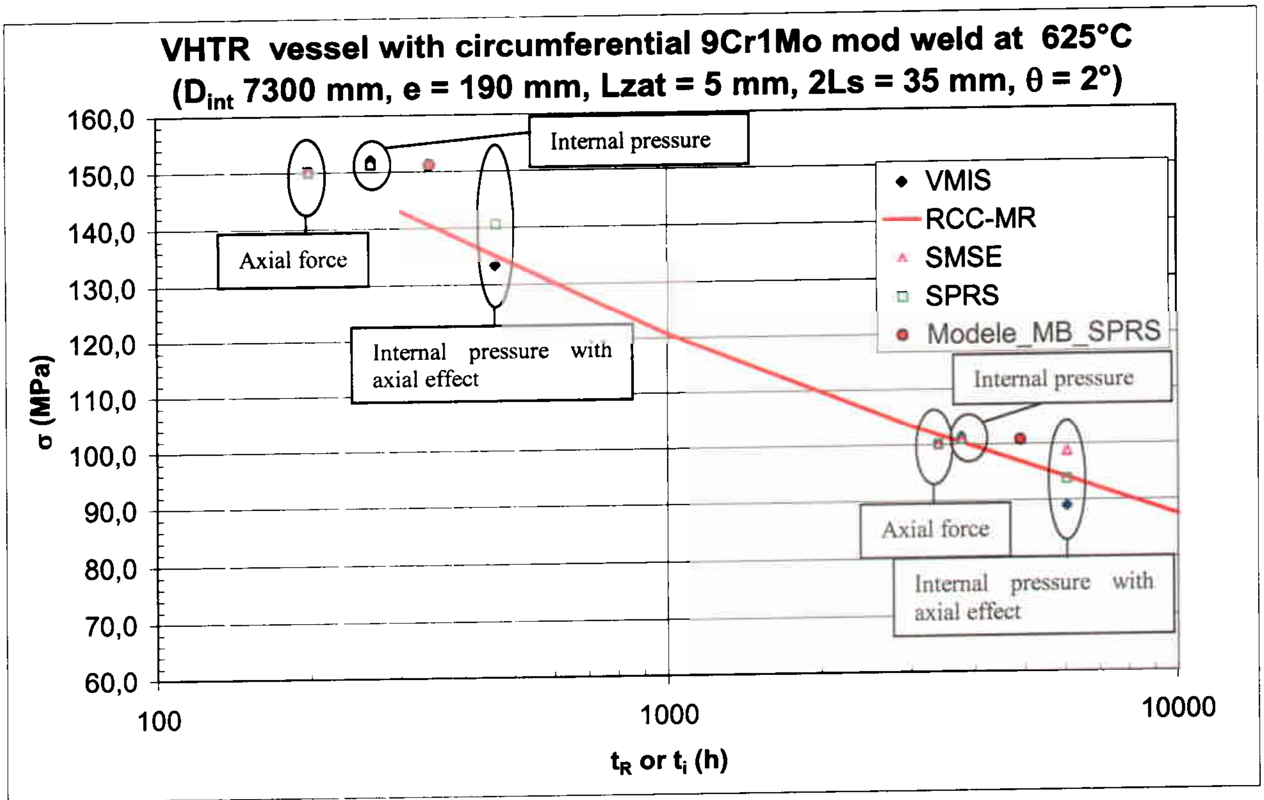

Figure 25: calculations of the creep life of a welded tube having the size of a VHTR pressure vessel, compared to experimental Base Metal creep rupture time (RCC-MR)

There are four points worth mentioning or to report here:

- the above curve should be taken as a convenient representation of multiaxial creep results. But it is in fact a drastic simplification of the real stress/strain dependence of crack initiation (for instance the stresses increase during the reduction of cross-sections, and it does not appear on this figure);
- by the way, the stress which is indicated on the figure 25 is the initial stress. The idea is interesting since the characterization creep tests are always described with the applied load;
- it was not possible to investigate the negative axial stresses in order to test further the stress triaxiality effect. The reason was the appearance of buckling in the calculated structure causing numerical instability;
- it has been shown that the uncoupled model tends to overestimate the time to crack initiation, compared to the fully coupled model. This may explain why the calculated points are above the RCC-MR mean curve. However the difference is very limited and has been found to be within a factor 2 ([2]).

The figure 25 shows also the creep initiation time calculated for the same vessel without weld, and submitted to internal pressure (two points indicated MB_SPRS). These two points have to be compared directly on the figure 25 with the "internal pressure" points for the geometry with circumferential weld. The difference is very small between the calculations: the reduction of creep life is about 24% when there is a weld inside the pressure vessel. It is thus necessary to give more details on the effect of geometry size, i.e. on the study corresponding to table 4.

4.3.3.2 *Size effect for welded structures submitted to creep*

The main results (i.e. calculated time to initiation when f_{tot}=0.1 is reached somewhere) are reported in table 5 and 6.

Reference case	HAZ width L_z (mm)	Internal radius R_i (mm)	Thickness e (mm)	External Diameter D_e (mm)	β (mm⁻¹)	BM Width L_B (mm)	β' (mm⁻¹)	$L_z\beta'$	$L_z\beta'/(L_{z\,ref}\,\beta'_{ref})$	t(h) for f_{tot}=0,1	$t(h)/t_{ref}$ (h)
lab_specimen_cas21	4	0	2,5	5		23,8	0,4	1,6	1	3,30E+01	1,00E+00
tube_31,25_cas21	5	0,625	15	31,25	0,41981	23,8	0,065319726	0,32659863	0,204124145	9,96E+01	3,02E+00
tube_31,25_cas21_thi	5	14,125	1,5	31,25	0,27925	35,8	0,206559112	1,03279556	0,645497224	5,55E+01	1,68E+00
tube_62,5_cas21	5	16,25	15	62,5	0,08233	121,5	0,046188022	0,23094011	0,144337567	1,76E+02	5,33E+00
tube_LST_cas21	5	125	15	280	0,02969	336,9	0,021821789	0,10910895	0,068193091	1,80E+02	5,45E+00
tube_LST_cas21_thick	5	40	100	280	0,02032	492,0	0,008451543	0,04225771	0,02641107	1,97E+02	5,96E+00
tube_LST_cas21_thin	5	139,85	0,15	280	0,28065	35,6	0,21821789	1,09108945	0,681930907	8,03E+01	2,43E+00
tube_625_cas21	5	297,5	15	625	0,01924	519,7	0,014605935	0,07302967	0,045643546	1,80E+02	5,45E+00
tube_CDuct_cas21	5	1000	100	2200	0,00406	2460,1	0,003015113	0,01507557	0,00942223	2,04E+02	6,18E+00

Table 5: time for creep initiation (f_{tot}=0.1) for several geometries submitted to 150 MPa initially axial creep

Reference case	HAZ width L_z (mm)	Internal radius R_i (mm)	Thickness e (mm)	External Diameter D_e (mm)	β (mm⁻¹)	BM Width L_B (mm)	β' (mm⁻¹)	$L_z\beta'$	$L_z\beta'/(L_{z\,ref}\,\beta'_{ref})$	t(h) for f_{tot}=0,1	$t(h)/t_{ref}$ (h)
lab_specimen_cas31	4	0	2,5	5		23,8	0,40000	1,60000	1,00000	4,25E+02	1,00
tube_31,25_cas31	5	0,625	15	31,25	0,41981	23,8	0,06532	0,32660	0,20412	1,30E+03	3,06
tube_62,5_cas31	5	16,25	15	62,5	0,08233	121,5	0,04619	0,23094	0,14434	2,05E+03	4,83
tube_LST_cas31	5	125	15	280	0,02969	336,9	0,02182	0,10911	0,06819	2,20E+03	5,18
tube_625_cas31	5	297,5	15	625	0,01924	519,7	0,01461	0,07303	0,04564	2,30E+03	5,42
tube_CDuct_cas31	5	1000	100	2200	0,00406	2460,1	0,00302	0,01508	0,00942	3,25E+03	7,64

Table 6: time for creep initiation (f_{tot}=0.1) for several geometries submitted to 100 MPa initially axial creep

There are several points to explain in these tables:

- the β parameter allows to calculate the width of the BM necessary to avoid side effects. As already reported at the end of 3.2, the definition adopted here is different from the literature. It may lead to noticeable effects on the MB width (L_B) for geometries with small diameters, without changing the results of the study since a conservative margin was taken on L_B;
- nevertheless, a modified parameter, called β', is used to study the size effects. With $\beta' = \frac{1}{\sqrt{eR_{ext}}}$, it is possible to calculate the parameter both for tubes and cylinders (i.e. laboratory specimens);
- the reference parameters $L_{z\,ref}$ and β'_{ref}, as well as the t_{ref} calculation result, are those from the laboratory specimens. They are used to normalize the results.

The β' parameter has been defined as above as we can see that the thickness modifies the creep initiation time, as well as the radius. Figure 26 is a plot of $t(h)/t_{ref}$ versus $L_z\,\beta'/(L_{z\,ref}\,\beta'_{ref})$, with the additional results of table 3 for the VHTR main vessel (case 21 and 31, see also figure 25).

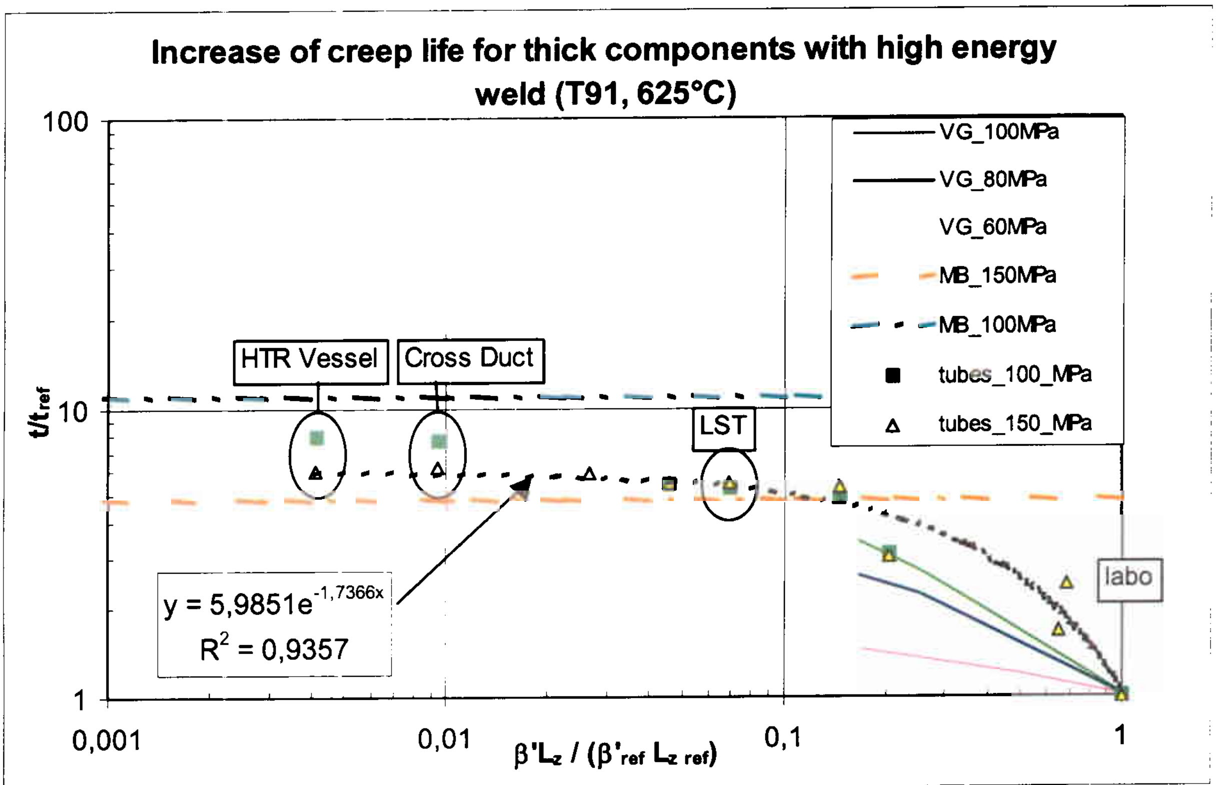

Figure 26: normalized calculated creep initiation life for 9Cr1Mo mod welded structures at 625°C, plotted versus normalized size parameter

This figure is rather complex because:

- the calculations of Vincent Gaffard [2] for "big laboratory specimens" are drawn (VG_60MPa, VG_80MPa, VG_100MPa). The curves are consistent with our results on hollow cylinders for the 100 MPa stress level (green squares). It seems that the higher is the stress, the sooner the size effect occurs with respect to the $\beta' L_z$ parameter;
- the base metal creep lives are reported for 100 and 150 MPa stress levels, as two horizontal dashed lines. Every stress level will have a different line since the ratio t/t_{ref} is not a constant. Here the ratio t/t_{ref} is determined by pure experimental results (for a given stress level, it is the time to rupture of RCC-MR mean curve divided by the time to rupture from V. Gaffard Cross-Weld specimens, see figure 1);
- the t/t_{ref} from the calculations are as explained previously for table 5 and 6 explanations, pure calculations results. This leads to a small difference with experimental asymptotes. For a full consistency, calculated asymptotes could be used here;
- as the base metal line are asymptotes, we have adjusted an exponential function to the 150 MPa results of table 5 (yellow triangles). It seems that the Large Scale Test (LST) geometry is very near the HTR vessel, and thus to the Base Metal creep life. By the way, every stress level would have a different exponential function;
- the "High Energy" term in the title qualifies the energies used for the welds of this study (the values are recalled inside chapter 4).

So that for the geometry of Large Scale Tests, a lower diameter or a lower thickness would result in a significant decrease in creep life. **Last, no investigation has been made on plate geometries at the time; it is intended to reproduce a similar size effect than in cylinders, but would require 3D calculations for accurate results.**

Let us describe now the Finite Element calculations corresponding to this proposed test, firstly reported in chapter 3.2.

4.4 PROPOSITION OF INDUSTRIAL SCALE VALIDATION TESTS FOR THE APPROACH

The calculation of the future Large Scale Test condition (chapter 3.2) gives further information about stresses, strains and damage distributions and evolutions. We have applied the same procedure as in 4.3 to describe the results, looking at the time corresponding to a total damage of 0 (i.e. at end of loading), 0.01, 0.025, and 0.1 (which gives the crack initiation).

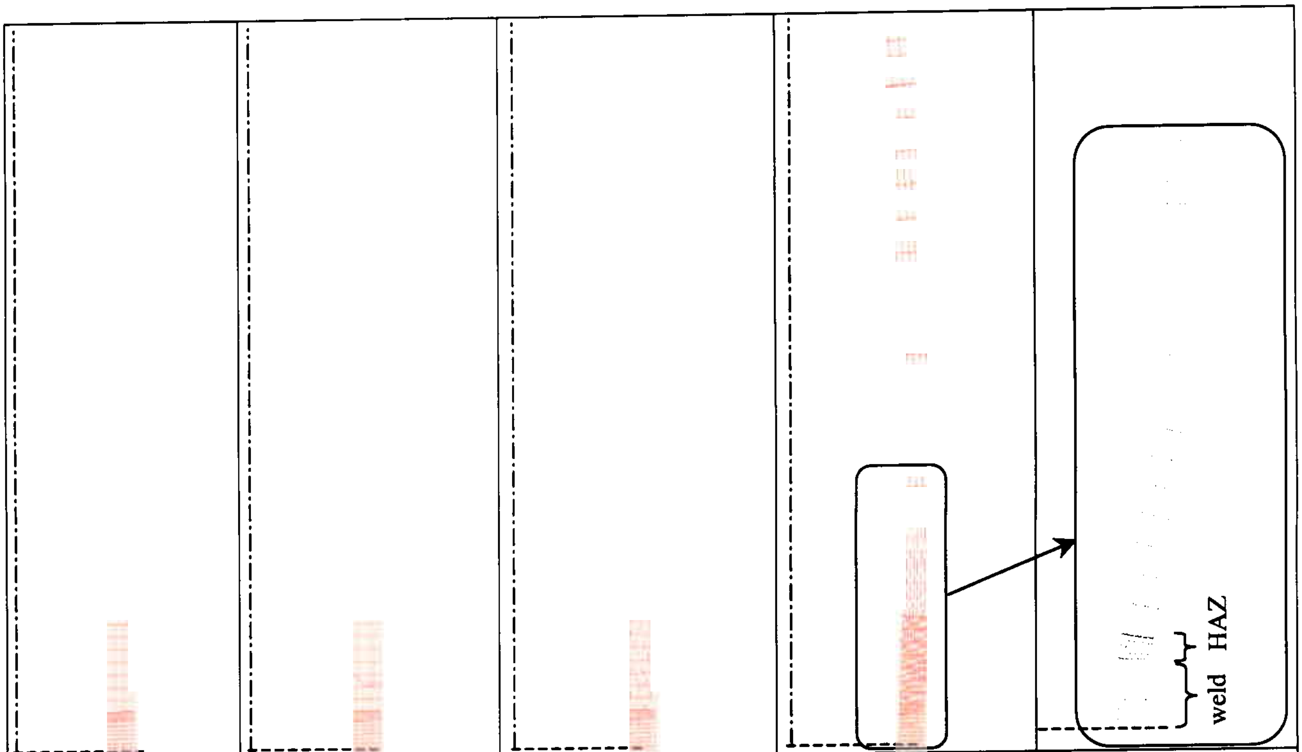

t=0.002h, f_{tot} = 0	t=280h, f_{tot} = 0.01	t=650h, f_{tot} = 0.025	t=1230h, f_{tot} = 0.1	t=1230h, zoom, x5

Figure 27: deformed shape evolution (x1) during LST submitted to internal pressure with axial end effect

The first point concerns the deformed shape, which exhibits a rather interesting behaviour, near to the crack initiation time (figure 27): the radial displacement becomes larger in the Base Metal, far from the weld. Although the difference is small (there is less than 20% between the displacement at the centre and the displacement 168 mm far from the centre, see figure 36), it was not observed on the case 41 and 51 described in 4.3. It is worth to note that this difference can be reduced to 10% by increasing the thickness and the length of the upper stiff tube (crack initiation being unchanged). Also, the behaviour of the weld could play an important role here, to explain the differences between the LST and the high thickness pressure vessel. By the way, the weld is highly creep resistant, so that the following mechanism could apply:

- in the LST, the weld width is of the same order compared to the thickness, thus the behaviour of the weld may have an influence on the surrounding parts;
- in the HTR pressure vessel, the weld width if 5 to 6 times smaller than the thickness, so that the strain is completely controlled by the Base Metal.

This hypothesis works with the same mechanism of the HAZ restraint previously explained. Nevertheless, in the experiments the temperature fields will decrease along the axis of the tube, so that the stiffness of the end will be much higher than at the centre. The present calculation is not representative of the future experiments, it is just a first evaluation, and more accurate simulations will be performed on the experimental temperature fields.

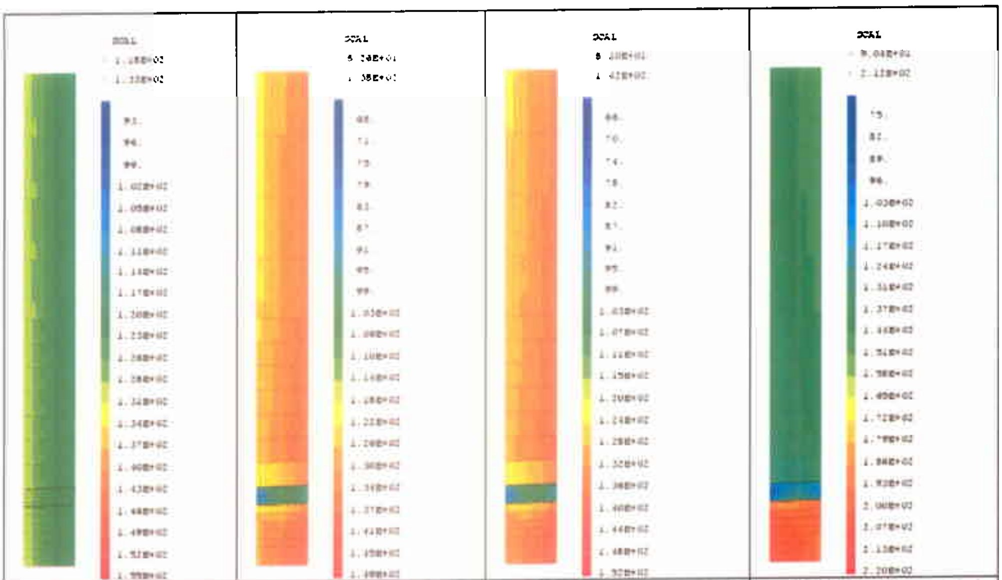

$t=0.002h$, $f_{tot} = 0$	$t=280h$, $f_{tot} = 0.01$	$t=650h$, $f_{tot} = 0.025$	$t=1230h$, $f_{tot} = 0.1$

Figure 28: hoop stress evolution (MPa)

Concerning the stress evolution, a similar decrease of the hoop stress is observed in the HAZ (and increase in the weld) compared to pressure vessel calculations (case 41 to 51).

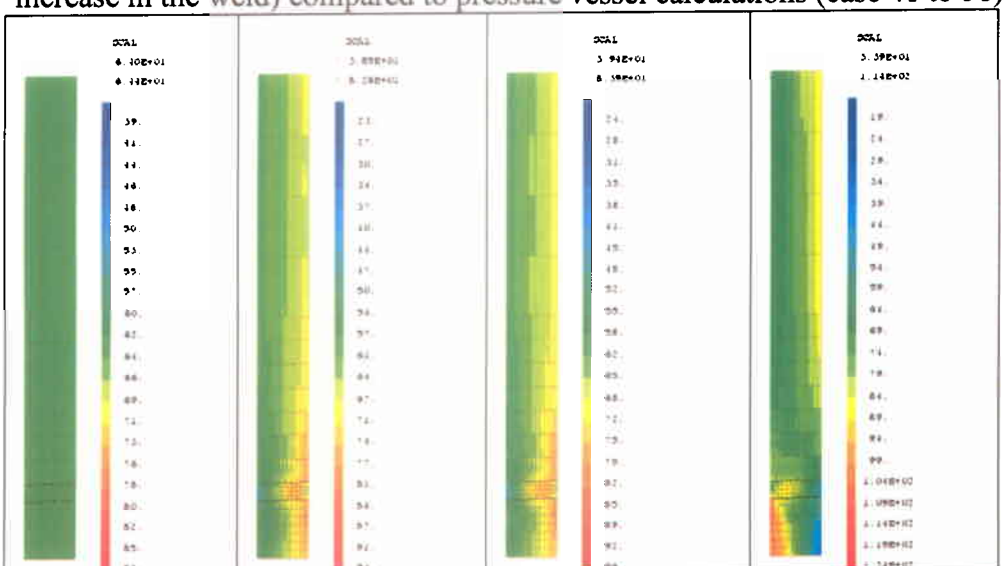

$t=0.002h$, $f_{tot} = 0$	$t=280h$, $f_{tot} = 0.01$	$t=650h$, $f_{tot} = 0.025$	$t=1230h$, $f_{tot} = 0.1$

Figure 29: axial stress evolution (MPa)

The axial stresses (Figure 29) are consistent with the strains, i.e. they are tensile at the outer part (the tube is growing), but at the initiation time they become in compression in the outer part of the weld because of the particular displacements reported above.

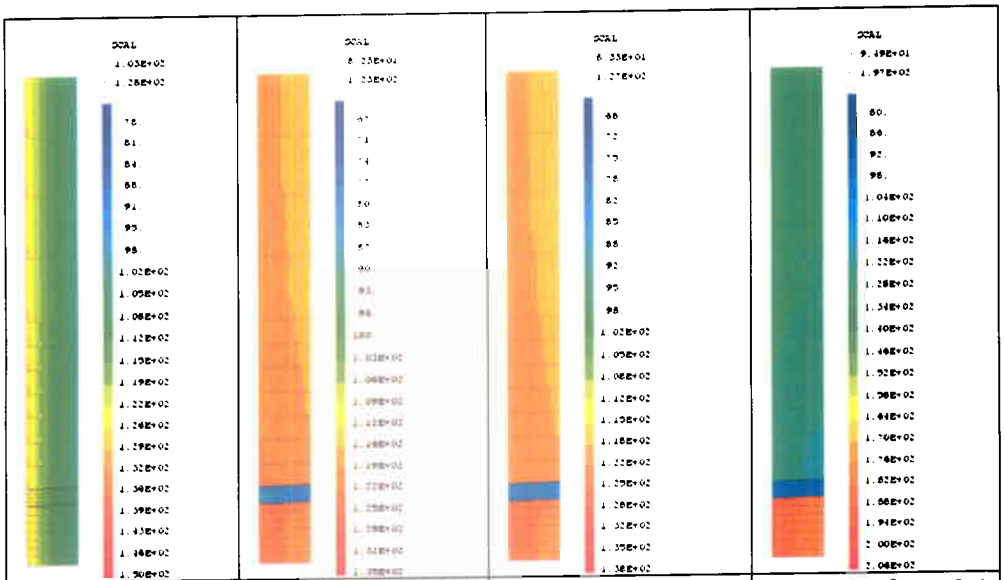

t=0.002h, $f_{tot} = 0$	t=280h, $f_{tot} = 0.01$	t=650h, $f_{tot} = 0.025$	t=1230h, $f_{tot} = 0.1$

Figure 30: Von Mises stress evolution (MPa)

The Von Mises stress (Figure 30) is also very similar to the hoop stress since it tends to decrease in the HAZ due to a very local stress redistribution.

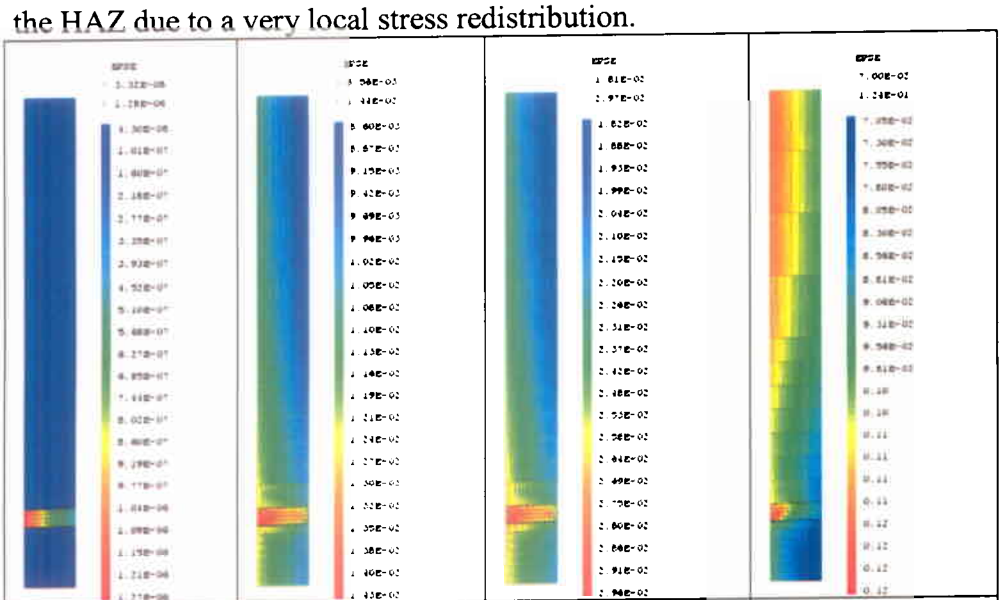

t=0.002h, $f_{tot} = 0$	t=280h, $f_{tot} = 0.01$	t=650h, $f_{tot} = 0.025$	t=1230h, $f_{tot} = 0.1$

Figure 31: cumulated inelastic strain evolution

As explained previously, it seems that the weld metal has a lower cumulated viscoplastic strain than in the Base Metal, in the last step of the calculations (Figure 31). This could be related to the recovery terms, which are not taken into account for the weld (see table 2), this zone being harder. Nevertheless, the maximum of the cumulated viscoplastic strain is still in the HAZ (figures 31 and 34).

Thus the total creep damage is also inside the HAZ as shown on figure 32.

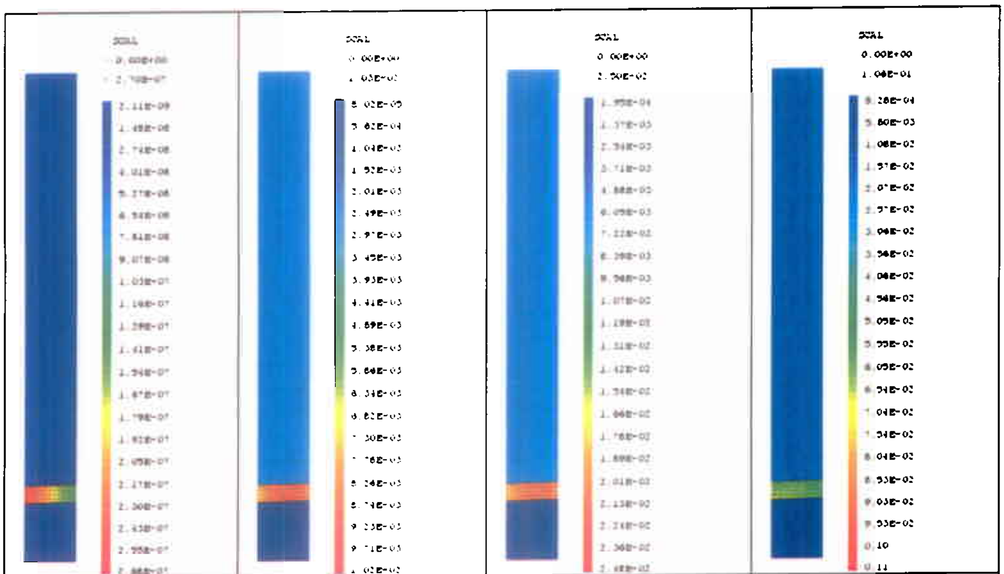

t=0.002h, f_{tot} = 0 | t=280h, f_{tot} = 0.01 | t=650h, f_{tot} = 0.025 | t=1230h, f_{tot} = 0.1

Figure 32: total creep damage evolution

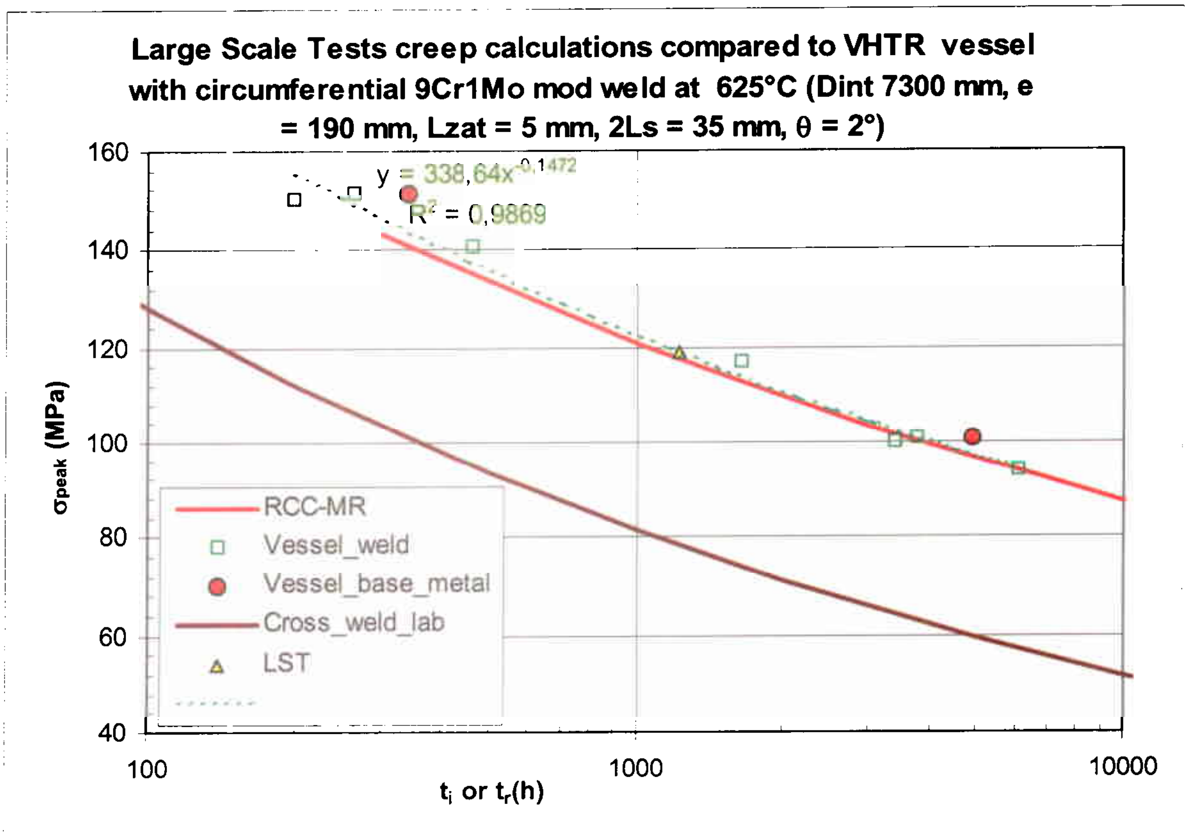

Figure 33: creep initiation time calculated for LST with internal pressure and

The time corresponding to f_{tot}=0.1 (i.e. t=1230h) can be plotted on figure 33. We can compare a calculation done for the main VHTR vessel (green square), to the LST result (yellow triangle), for approximately the same peak stress (117.1 for the first and 119.2 MPa for the second, the differences coming from the different pressure values which modify the Von Mises stress taking into account a mean radial stress). It seems to exist a small creep life reduction, though it is not so easy to confirm this tendency. By the way this creep life reduction would be consistent with the curve on figure 26.

The evolution of maximum cumulated viscoplastic strain in each zone (figure 34) is also very similar to the calculation on a bigger component (figures 21 and 22), due to the constraint effect. At the end of the test we should then reach about 15% of local strain.

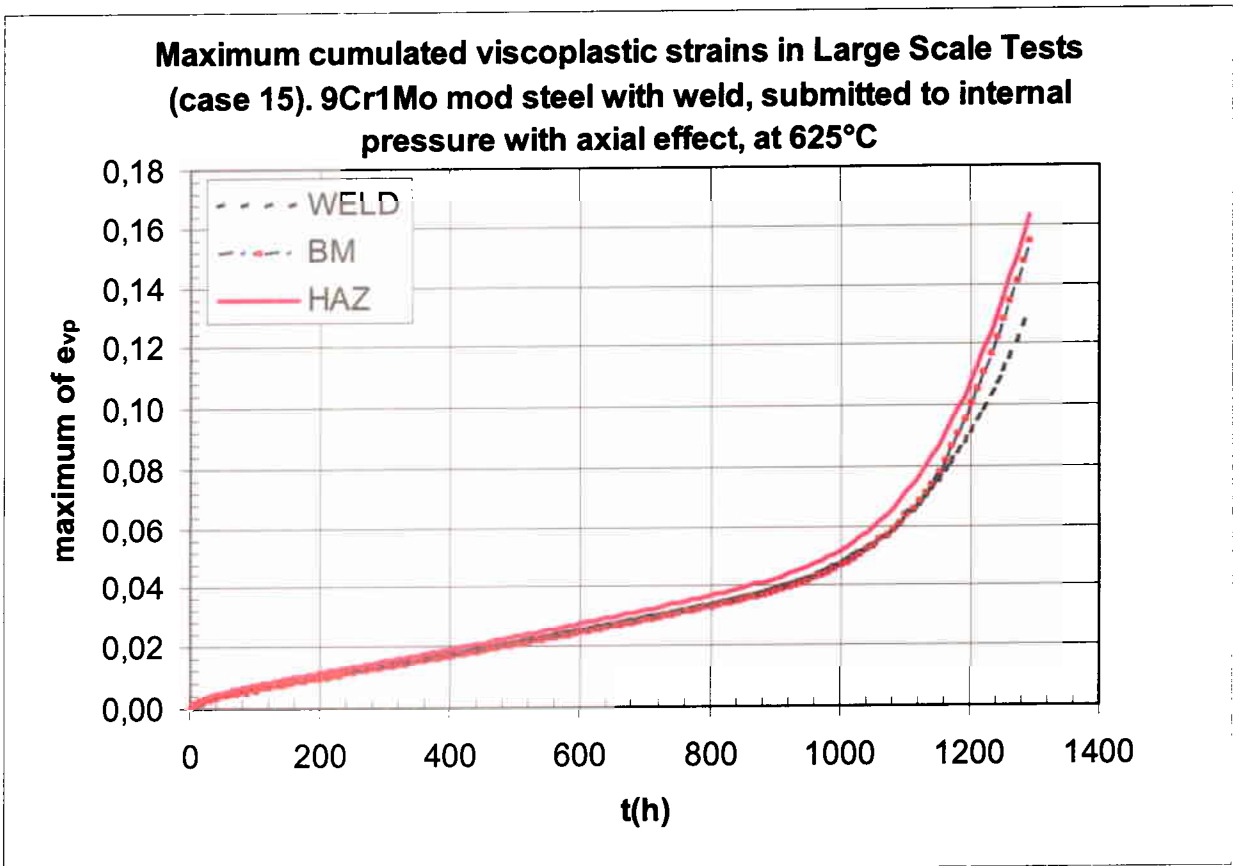

Figure 34: maximum cumulated viscoplastic strain in BM, WM, and HAZ, for Large Scale Test (case 15)

Although the strains are very similar, the total damages are very different, especially in the last creep phase, i.e. after 1000h (figure 35). Before this time, there is a factor 3 between damage in BM and HAZ. But in the tertiary creep phase, the damage rate increases in HAZ. This behaviour is still true for the other previous calculations (figures 23 and 24).

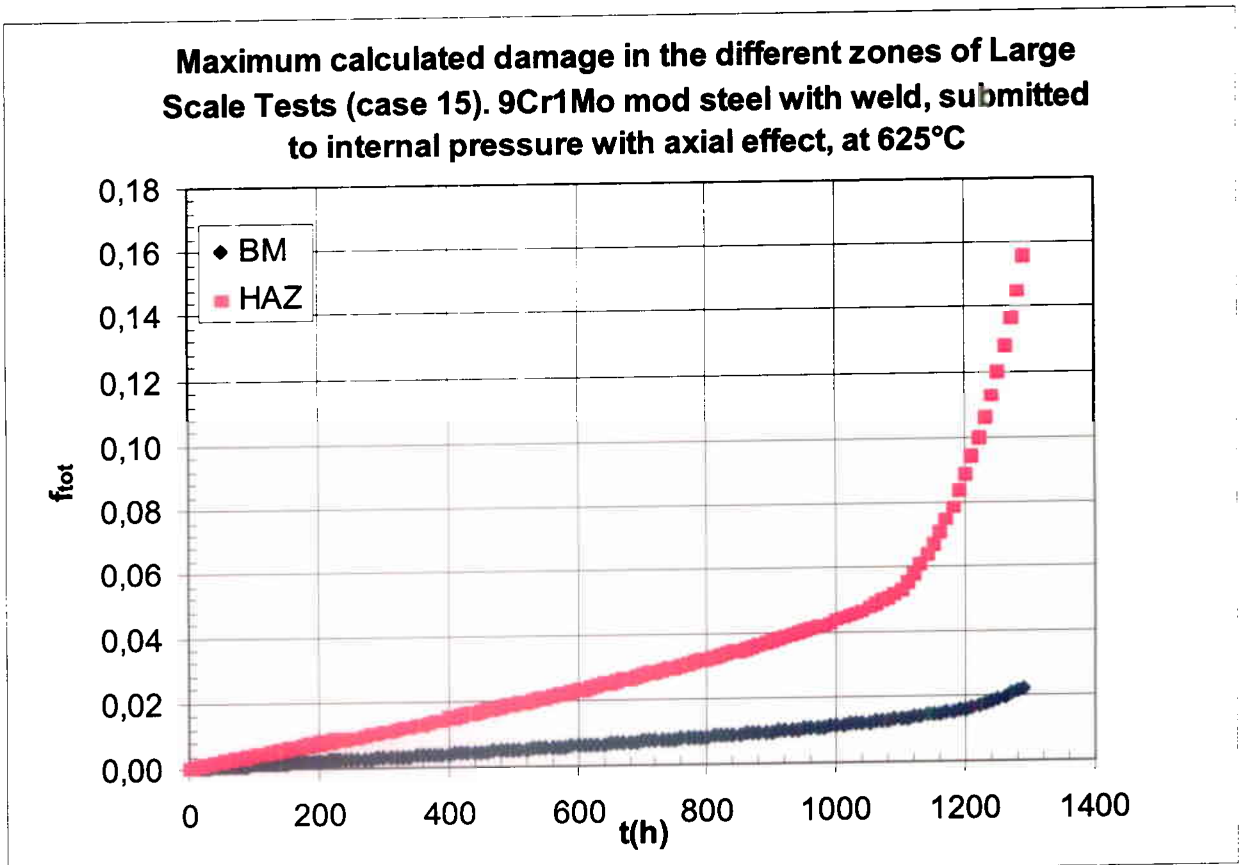

Figure 35: maximum total damage in BM and HAZ, for Large Scale Test (case 15)

At the end of the tests, the specimen should have an increase of about 10 to 12 mm for the radial displacement (figure 36). The particular behaviour of the calculated displacements was already discussed at the beginning of 4.4. Nevertheless, the ratio of the radial displacement to the internal radius is approximately equal to 12.5/125 = 0.1 at the end of the test, which is just a little bit smaller than the local maximum viscoplastic strains.

As reported on 3.3.2 in the experimental set-up, the discussion is still open concerning the definition of the end of the test. Of course, we may have a significant increase of creep life compared to the small laboratory cross weld specimen, which is the result we would like to obtain. But it should be better to plan an arrest before the bursting, which may induce damage to the installation rig; an early stop means also a technological method to detect or measure the creep crack initiation.

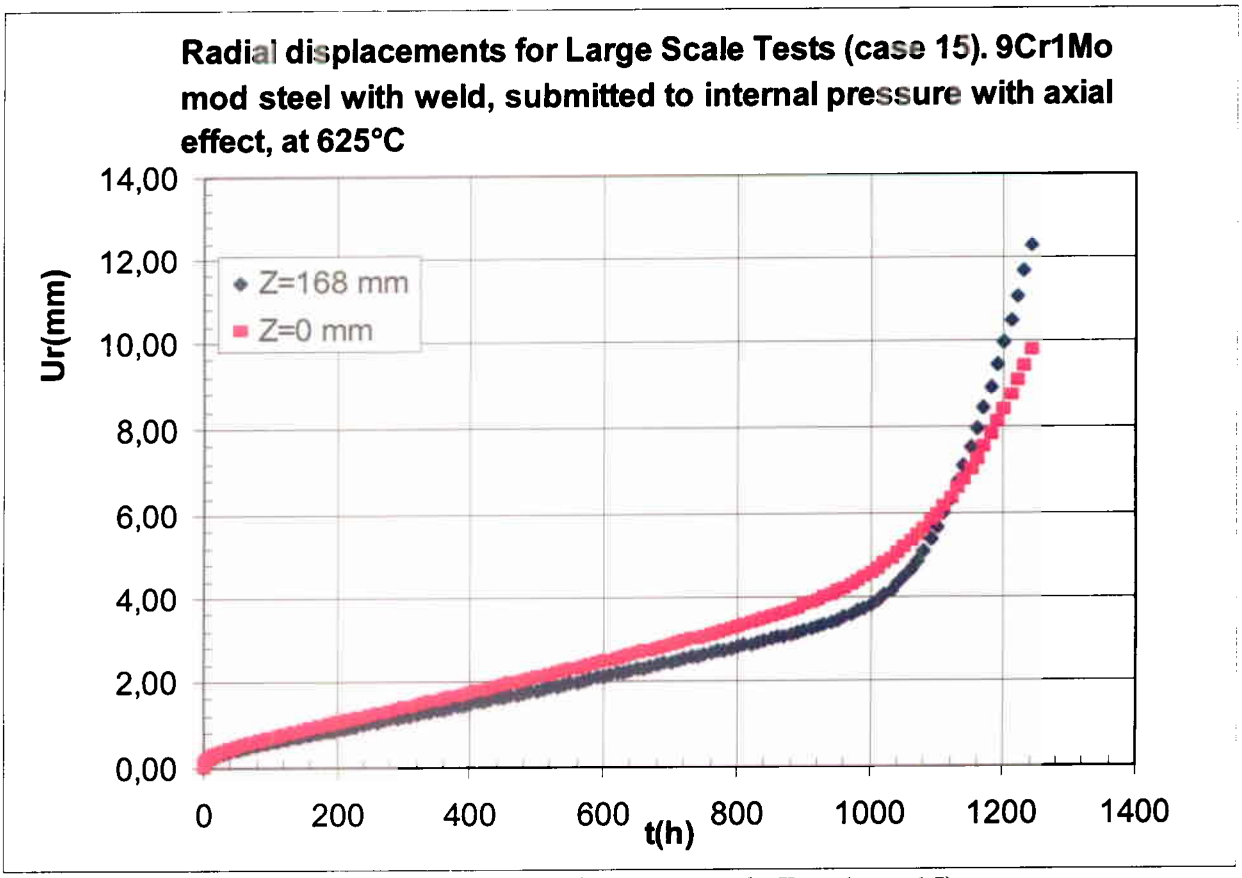

Figure 36: evolution of radial displacement for Large Scale Test (case 15)

4.5 A PROPOSITION TO INCLUDE PLATE GEOMETRIES INSIDE THE MODEL

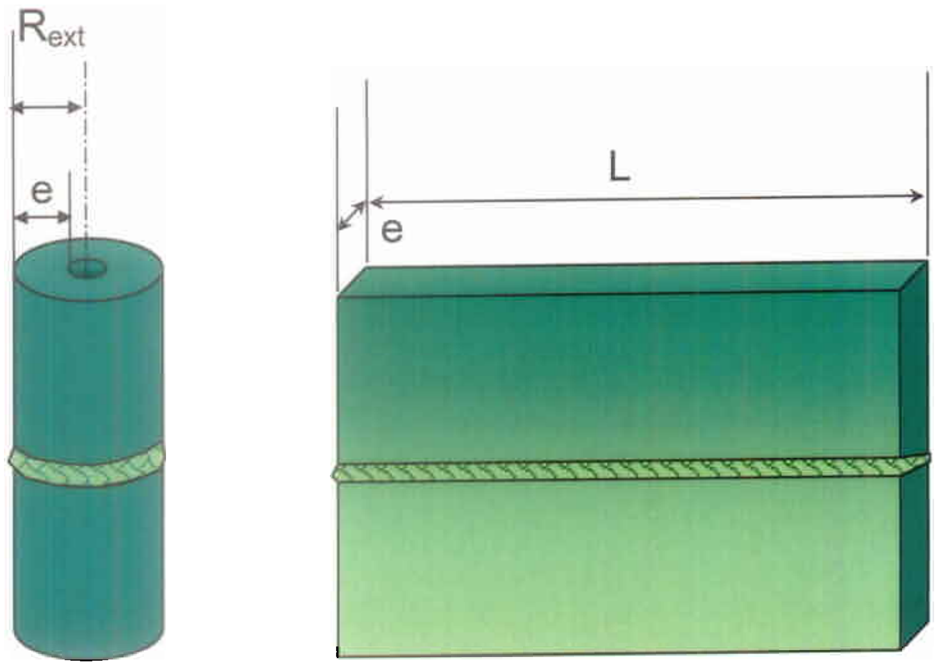

Figure 37: schema of circumferential weld in tube, and plate with weld

As plate geometries may exist inside a reactor, it could be interesting to apply $\beta' = \frac{1}{\sqrt{eR_{ext}}}$ as well as figure 26, for this configuration. From figure 37, it becomes obvious that the length of the plate L should be set equal to the circumference of the tube = 2 π R_{ext}, since we can imagine to enrol the plate around the tube axis, to obtain the same geometry. This is just a pure assumption, which must be discussed and has to be validated by Finite Element calculations and real size tests.

5. CONCLUSION

According to some papers from the literature, the creep flow and damage on Cr-Mo steels and their welds seems to be very dependent on the behaviour of the different zones, i.e. the Parent Metal, the different parts of the Heat Affected Zone, and the Weld Metal. Moreover, for the martensitic steels, which come back to this metallurgical state after welding, the Weld Metal and the Coarse Grain Heat Affected Zone have a very high hardness partly due to an unrelieved microstructural state (for instance the dislocation density is very high). They are thus very creep resistant. At the opposite, the Base Metal and the Inter Critical Heat Affected Zone may relax their internal microscopic stresses by both strain and temperature recovery, since they do not sustain an austenitic phase transformation during welding. These zones have a soft hardness, the ICHAZ being sometimes softer than Parent Metal. The ICHAZ is then the weakest link during a creep loading. This creep mismatch, which exists in 9Cr1Mo mod steel welds, may produce geometry size-effects. They have been particularly studied by means of Finite Elements method, taking into account the different behaviour and damage laws of the welds. Basically, it means that small cross-weld specimens will tend to have the same creep life time than the ICHAZ, and that thick and big components could have a life time close to the Base Metal one. This mechanism is explained by a constrained effect: the high creep resistant zones restrain the deformations of low creep resistant regions. The efficiency of this behaviour is mainly related to the stiffness of the structure.

Nevertheless, there are not a lot of experimental proofs of this peculiar phenomenon, as testing on big specimens is not easy and not cheap. It is proposed to carry out few Large Scale Tests on tubular specimens submitted to creep at high temperature at CEA Cadarache. By means of simplified calculations but also with Finite Element creep flow and damage models identified at the Ecole Nationale Supérieure des Mines de Paris, the main parameters of the tests have been set-up. They are the results of optimization between several different features, like the weight and dimensions of the tube and connecting heads, the required heating power, the maximum possible internal pressure, the creep time life... The following parameters have been chosen:

- internal radius of 125 mm, thickness of 15 mm, total length of at least ~670 mm;
- internal pressure of 150 bar, axial effect due to this pressure;
- mean temperature of 625°C.

According to the simple peak rupture stress criterion, based on a combination of the maximum principal stress and of the Von Mises (see equations 1 and 6), we should obtain a creep life of 1091h (from BM creep rupture curves). Whereas the Finite Element calculations with large displacements assumption, and a pressure always acting along the normal of the surface, gave us 1230h for the time to crack initiation. Such a value for creep damage is more consistent with the Base Metal rupture curve than with the small laboratory Cross-Weld specimens time to rupture (t_R=145h for the same peak rupture stress level).
For the purpose of the demonstration, it is very important to keep the temperature of 625°C, at least for the first tests, because of the large difference between HAZ and BM creep properties at all stress levels. The few characterization test results existing at 550°C seem to show that the difference is very dependent on the stress level, at this temperature.
The Base Metal has been provided by Buhlmann France, in the form of a tubular cylinder of 310 mm of external diameter and 50 mm of thickness; the weld will be realized by Framatome Chalon with the Gas Tungsten Arc Welding process using a Narrow Gap. The upper and lower connecting heads have already been machined, and the ceramics internal bodies have been supplied. The whole installation rig is placed inside the CEA "Airbus" steel vessel facility. Each specimen will be monitored by means of 30 type K thermocouples, and by 10 displacement sensors placed

around the circumference. The pressure will be also controlled in real time. CEA agrees to give the results of all the following future tests:

- thermal specimen specially instrumented in thermocouples, but not submitted to an internal pressure;
- a Base Metal tube with internal pressure, to give the reference life without weld;
- two tubes with circumferential weld.

Concerning the Finite Element calculations, it has been shown that the creep life of the LST is close to the one of a VHTR pressure vessel (with a circumferential weld). A geometry size effect is proposed, based on the initial idea of V. Gaffard [2], and extended to the case of hollow cylinders. The creep life of a component should follow an exponential law function of the $\beta' L_{HAZ} = \frac{L_{HAZ}}{\sqrt{eR_{ext}}}$ parameter (L_{HAZ} is the width of HAZ, e the thickness and R_{ext} the external radius); but the function is very sensitive to the stress level. Additional works are required to understand why, even if it should be related to the strain rate laws: the approach, based on parametric curves, could be used to determine a very accurate creep life reduction factor, for welded structures. It could be interesting to extend the approach to longitudinal welds or plate geometries, as proposed in this document.

The calculations show also that the creep damage will always appear in the HAZ:

- for the small specimens, the strain and damage rates are higher there;
- for the large components, the strains are similar in Base Metal and in HAZ due to the restraint phenomenon, but the damage rates remain higher in HAZ.

Finally, the calculations have confirmed that the initial peak rupture stress is a very attractive equivalent criterion to represent the creep life of welded tubular structures: different calculated stress states compared to an experimental creep curve exhibited a similar slope. This result must be carefully seen, because of the few points investigated (compressive stresses are not possible to include, as they lead to buckling), and due to the important stress redistributions during the calculations. The Von Mises criterion seems not so bad, but gives lower stresses for the internal pressure with axial effect. The worst criterion is the Maximum Strain Energy equivalent stress, very similar to the maximum principal stress one in our case.

REFERENCES

[1] 6th Framework Programme, RAPHAEL-IP, Annex 1 – « Description of Work », Euratom call Nuchtech-2004.3.4.1.1-1

[2] V. Gaffard, « Experimental Study and Modelling of High Temperature Creep Flow and Damage Behaviour of 9Cr1Mo-NbV Steel Weldments », Ph.D Thesis of the Ecole des Mines de Paris, December 13th, 2004

[3] M. Law, W. Payten, « Cross Weld Creep Testing and its Extrapolation to Service Welds», International Journal of Pressure Vessel and Piping, Vol. 74 (1997), pp. 129-133

[4] M. Law, W. Payten, « Weld Performance under Creep using Finite Element Modelling», International Journal of Pressure Vessel and Piping, Vol. 72 (1997), pp. 45-49

[5] J. Storesund, S. Tung Tu, « Geometrical Effect on Creep in Cross Weld Specimens», International Journal of Pressure Vessel and Piping, Vol. 62 (1995), pp. 179-193

[6] P. Segle, J. Storesund, S. Tung Tu, L. A. Samuelson, «Some Issues in Life Assessment of Longitudinal Seam Welds based on Creep Tests with Cross Welds Specimens», International Journal of Pressure Vessel and Piping, Vol. 66 (1996), pp. 199-222

[7] F. R. Hall, D. R. Hayhurst, « Continuum Damage Mechanics Modelling of High Temperature Deformation and Failure in a Pipe Weldment», Proceedings of The Royal Society, London, A, 433 (1991), pp. 383-405.

[8] M. Prager, «Issues in Life Assessment of Chrome-Moly Welds», PVP-Vol.239/MPC-Vol.33, Serviceability of Petroleum, Process, and Power Equipment, ASME, New York, 1992, pp. 253-65.

[9] J. Lemaître, J.L. Chaboche, «Mécanique des matériaux solides», editions Dunod, 1985.

[10] RCC-MR, editions AFCEN, 2003.

[11] L. Kloc, V. Slenicka, «Transition from power law to viscous creep behaviour of P-91 type heat resistant steel», Materials Science and Engineering, A234-236, pp. 962-965.

[12] Y. Lejeail, E. Pluyette, « Définition du programme d'Essais pour la détermination de coefficients de joints soudés en acier T91 dans le domaine du fluage. Précalculs et influence de certains paramètres. », NT CEA/DEN/CAD/DER/SESI/LCSI/NT DO 30 27/09/04

[13] S. Timoshenko, « Théorie des Plaques et des Coques », Librairie Polytechnique Ch. Béranger, Paris et Liège, 1951.

Appendix 1

Experimental creep curves from [5] J. Storesund, S. Tung Tu, « Geometrical Effect on Creep in Cross Weld Specimens», International Journal of Pressure Vessel and Piping, Vol. 62 (1995), pp. 179-193

Creep-Rupture curves for as welded state

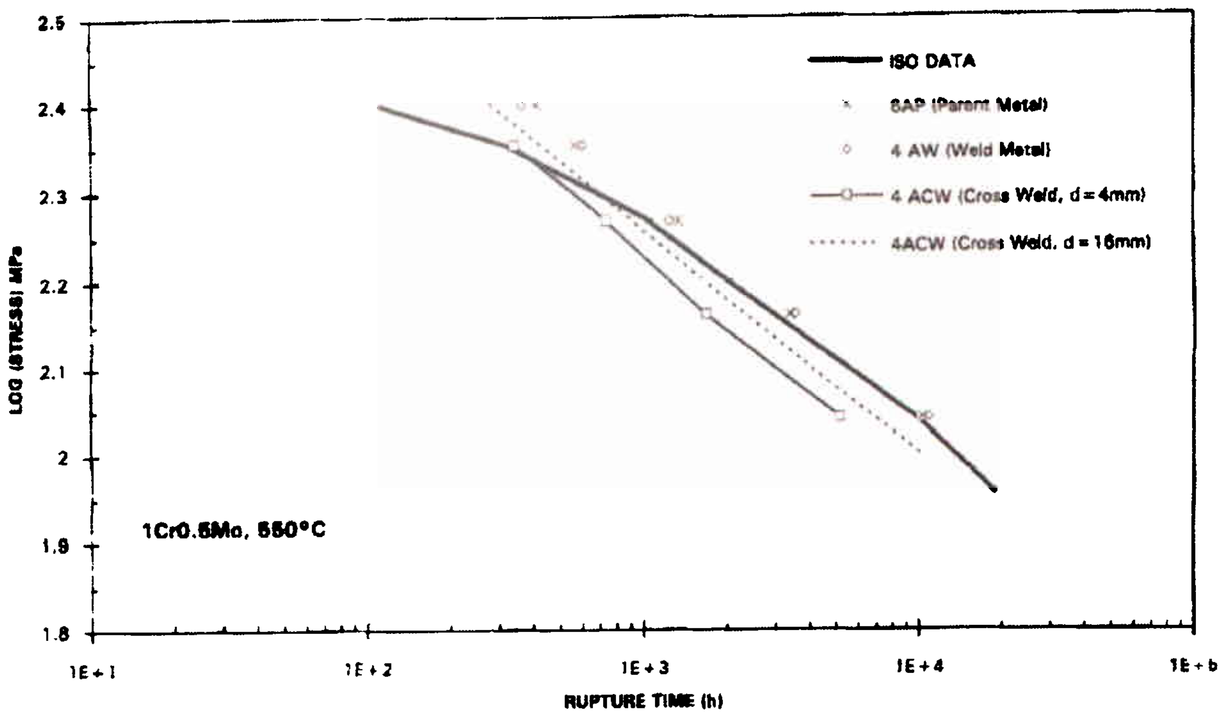

Creep-Rupture curves for PWHT state

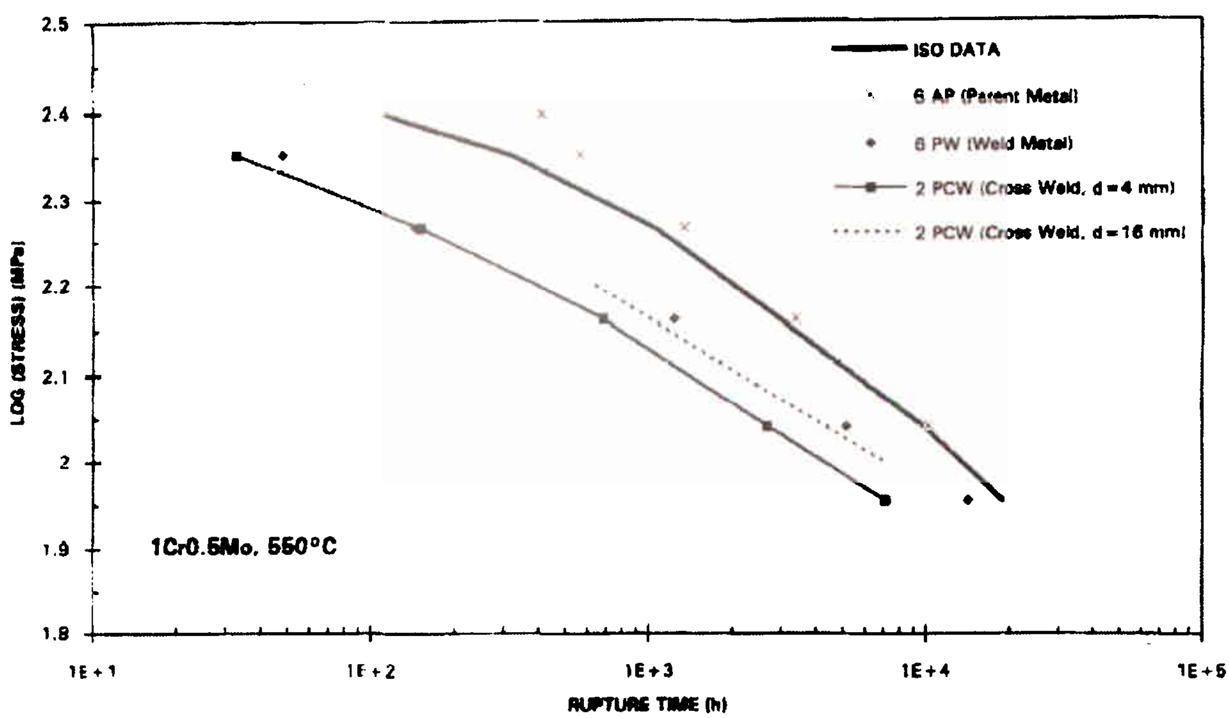

Minimum creep-rate curve